## Contents

## 目录

P. Dona ( ☑)

P. 多纳 ( ☑)

Center for Space, Time and the Quantum, Marseille, France

法国马赛空间、时间与量子中心

Department of Physics and Astronomy, University of Western Ontario, London, ON, Canada

加拿大安大略省伦敦市西安大略大学物理与天文学系

M. Han

韩 M.

Department of Physics, Florida Atlantic University, Boca Raton, FL, USA

美国佛罗里达州博卡拉顿市佛罗里达大西洋大学物理系

Department Physik, Institut für Quantengravitation, Theoretische Physik III, Friedrich-Alexander Universität Erlangen-Nürnberg, Erlangen, Germany

德国埃尔兰根市弗里德里希-亚历山大-埃尔兰根-纽伦堡大学理论物理第三研究所量子引力研究所物理系

e-mail: hanm@fau.edu

邮箱:hanm@fau.edu

H. Liu

刘 H.

Department Physik, Institut für Quantengravitation, Theoretische Physik III, Friedrich-Alexander Universität Erlangen-Nürnberg, Erlangen, Germany

德国埃尔兰根市弗里德里希-亚历山大-埃尔兰根-纽伦堡大学理论物理第三研究所量子引力研究所物理系

e-mail: hongguang.liu@gravity.fau.de

邮箱:hongguang.liu@gravity.fau.de

Numerical methods are a powerful tool for doing calculations in spinfoam theory. We review the major frameworks available, their definition, and various applications. We start from sl2cfoam-next, the state-of-the-art library to efficiently compute EPRL spinfoam amplitudes based on the booster decomposition. We also review two alternative approaches based on the integration representation of the spinfoam amplitude: Firstly, the numerical computations of the complex critical points discover the curved geometries from the spinfoam amplitude and provide important evidence of resolving the flatness problem in the spinfoam theory. Lastly, we review the numerical estimation of observable expectation values based on the Lefschetz thimble and Markov-Chain Monte Carlo method, with the EPRL spinfoam propagator as an example.

数值方法是旋扭理论计算中强有力的工具。本文综述了现有的主要框架、其定义与各类应用。我们从 sl2cfoam-next 开始介绍，这是基于助推分解高效计算 EPRL 旋扭振幅的前沿计算库。我们还综述了另外两种基于旋扭振幅积分表示的方法: 第一，复临界点的数值计算从旋扭振幅中得到了弯曲几何，为解决旋扭理论中的平坦性问题提供了重要依据；最后，我们以 EPRL 旋扭传播子为例，综述了基于莱夫谢茨锚点与马尔可夫链蒙特卡洛方法的可观测量期望值数值估计方法。

## Keywords

## 关键词

Loop quantum gravity - Spinfoam theory - Numerical frameworks - High-performance computing - Booster decomposition - Lefschetz thimble

圈量子引力-自旋泡沫理论-数值框架-高性能计算-助推分解-莱夫谢茨 thimble

## Introduction

## 引言

Spinfoam theory is a covariant formulation of loop quantum gravity. It provides a background-independent and Lorentzian quantum gravity path integral regularized on a fixed triangulation. Spinfoam assigns transition amplitudes to spin network states living on the triangulation's boundary. The state-of-the-art spinfoam model is the EPRL-FK model defined in [1, 2] (for a pedagogical introduction, see [3, 4]).

旋泡沫理论是圈量子引力的协变表述。它给出了定义在固定三角剖分上、不依赖背景背景的洛伦兹量子引力路径积分正则化。旋泡沫为生活在三角剖分边界上的自旋网络态分配跃迁振幅。当前最先进的旋泡沫模型是定义于文献 [1, 2] 的 EPRL-FK 模型 (入门介绍参见文献 [3, 4])。

Computations in spinfoam are very involved, and for a long time, the theory was relegated to a formal proposal, and very few explicit calculations existed. The majority of the results of the approach are obtained in the large spin regime, often identified as semiclassical. The theory shows a remarkable connection to a discrete version of general relativity if the limit is taken simultaneously as the refinement.

旋泡沫的计算十分复杂，长期以来该理论仅停留在形式化提议阶段，极少有显式计算成果。该方法的多数结果都得到于大自旋区，这个区通常被认为是半经典区。当同时取精化极限时，该理论与离散版本的广义相对论存在惊人关联。

Recently, the field has undergone a numerical revolution. The interest of the community in numerical methods grew considerably, while, at the same time, fast technological developments provided simpler access to high-performance computing facilities.

近年来，该领域经历了一场数值革命，学界对数值方法的兴趣大幅增长，与此同时，技术的快速发展也让人们更易获取高性能计算资源。

Many different and complementary approaches were born, providing different tools suitable to solve different problems. We can finally do spinfoam computations and answer some of the theory open questions. In this work, we present a selection of these techniques.

目前已经发展出多种互补的方法，提供了适用于解决不同问题的不同工具。我们终于可以开展旋泡沫计算，回答该理论的一些开放问题。本文将介绍其中一部分技术。

The library sl2cfoam [5] was the first attempt to build a complete library to compute Lorentzian EPRL spinfoam transition amplitudes. It is coded in C and based on a divide-and-conquer paradigm. The amplitude is divided into easier-to-compute components and then reassembled. The library evolved into sl2cfoam-next [6] and is now optimized for high-performance computing. With sl2cfoam-next an interactive Julia interface is provided. This numerical framework is modular (can be used to compute any transition amplitude), scalable (can run on a laptop or a cluster), and user-friendly (a minimal amount of additional code is required). There are two main disadvantages of this approach. The number of resources required increases very rapidly but not exponentially. The numerical evaluation involves an unavoidable approximation (see section "The Necessary Approximation"), and we do not control it entirely.

sl2cfoam 库 [5] 是首个构建完整库来计算洛伦兹 EPRL 旋泡沫跃迁振幅的尝试，它用 C 语言编写，基于分治范式: 将振幅拆分为更易计算的分量后再重新组装。该库现已演变为 sl2cfoam-next[6]，针对高性能计算做了优化，还提供了交互式 Julia 接口。这个数值框架是模块化的 (可用于计算任意跃迁振幅)、可扩展的 (可在笔记本电脑或集群上运行) 且对用户友好 (仅需极少量额外代码)。该方法有两个主要缺点: 所需资源量增长极快 (虽非指数增长)，且数值计算不可避免地涉及近似 (参见章节“必要近似”)，我们无法完全控制该近似。

The method of complex critical points provides a complementary numerical approach for performing computations with the Lorentzian EPRL spinfoam model in the regime where the sl2cfoam-next code becomes computationally expensive is available. This approach is based on the integral expression of the spinfoam model. The main task is to compute oscillatory integrals representing the spinfoam amplitude numerically. This approach closely relates to the stationary phase approximation, one of the main tools for studying the quantum theory in the semiclassical regime. This numerical code focuses on the complex critical points in the semiclassical regime of the spinfoam amplitude. The complex critical points are the key to recovering the curved geometries and the semiclassical gravity dynamics. The results produced by this code provide important pieces of evidence for resolving the confusion in the LQG community known as "the flatness problem" [7-10]. The flatness problem, which claims that the semiclassical geometries in the spinfoam model are all flat, results from mistakenly ignoring the contributions from complex critical points [11-13]. This confusion is clarified by explicitly demonstrating the curved geometry from the spinfoam amplitude with the numerical method.

复临界点方法是一种互补数值方法，适用于在 sl2cfoam-next 代码计算成本过高的区域对洛伦兹 EPRL 旋泡沫模型开展计算。该方法基于旋泡沫模型的积分表达式，核心任务是对代表旋泡沫振幅的振荡积分做数值计算。它与研究半经典区量子理论的核心工具——稳定相位近似密切相关，该数值代码专注于旋泡沫振幅半经典区中的复临界点，而复临界点是得到弯曲几何与半经典引力动力学的关键。该代码得到的结果为解决 LQG 学界所谓的“平坦性问题”争议提供了重要证据 [7-10]。认为旋泡沫模型中的半经典几何全都是平坦的这一平坦性问题，源自错误地忽略了复临界点的贡献 [11-13]。我们通过数值方法从旋泡沫振幅中明确得到了弯曲几何，澄清了这一争议。

From the computation of the spinfoam amplitude integrals beyond the leading order, we can derive the quantum corrections to the semiclassical limit of the theory (The quantum corrections derived from the spinfoam amplitude can also be analyzed numerically evaluating the next-to-leading order in the stationary phase approximation; see [14].). The integrands in the spinfoam amplitude are highly oscillatory. Computing oscillatory integrals used to be numerically expensive, but the recent method based on the Lefschetz thimble makes the computation much more efficient (see [15] for a review). Given any critical point of the integral, the Lefschetz thimble is an integration cycle connected to the critical point, such that the integrand becomes non-oscillatory on the cycle and the original integral is a linear combination of the integrals on the Lefschetz thimbles. We developed a numerical code to compute the spinfoam correlation functions with the Lefschetz thimble and Monte-Carlo methods [16]. Thanks to the non-oscillatory integrand on the Lefschetz thimble, computing the integral with the Monte-Carlo method becomes efficient (The Monte-Carlo method can also be used as a tool for finding critical points in the complexified integration space; see [17].). In addition to reproducing the correct semiclassical behavior of the spinfoam propagator, the numerical results efficiently compute the quantum corrections to the propagator from the spinfoam amplitude.

通过计算超出领头阶的旋泡沫振幅积分，我们可以得到理论半经典极限的量子修正 (旋泡沫振幅导出的量子修正也可以通过数值计算稳定相位近似中的次领头阶来分析；参见 [14])。旋泡沫振幅中的被积函数振荡性极强，计算这类振荡积分过去数值成本很高，但最近基于莱夫谢茨 thimble 的方法大幅提升了计算效率 (综述参见 [15])。对于任意给定的积分临界点，莱夫谢茨 thimble 是连接该临界点的积分周线，被积函数在这个周线上非振荡，且原积分等于各莱夫谢茨 thimble 上积分的线性组合。我们开发了结合莱夫谢茨 thimble 与蒙特卡洛方法计算旋泡沫关联函数的数值代码 [16]。得益于莱夫谢茨 thimble 上被积函数的非振荡性，蒙特卡洛方法计算积分变得十分高效 (蒙特卡洛方法还可用于在复化积分空间中寻找临界点；参见 [17])。除了能重现旋泡沫传播子正确的半经典行为外，该数值方法还可以高效计算旋泡沫振幅给出的传播子量子修正。

In addition to the numerical frameworks presented in this chapter, there exist other numerical codes based on the spinfoam models simplified compared to the EPRL model, such as the effective spinfoam model (see, e.g., [18, 19]), where geometry and the connection with area-angle Regge calculus plays a central role, and the hypercuboid truncated model (see, e.g., [20]), where the spinfoam renormalization is studied. We do not review them here since other chapters focus on these approaches. However, we would like to point out the interesting similarity between our result based on the EPRL model and the result from the effective spinfoam model. From the perspective of the semiclassical analysis, the effective spinfoam model also needs to apply the method of complex critical point and turns out to give qualitatively similar behavior to the result presented in section "Complex Critical Points and Resolution of Flatness Problem," particularly about the dependence of the amplitude on the curvature of the semiclassical geometry. It seems to suggest the close relationship between the effective spinfoam model and the EPRL model in the large- $j$ regime.

除本章介绍的数值框架外，还有其他基于比 EPRL 模型更简化的自旋泡沫模型的数值代码，例如有效自旋泡沫模型 (参见例如文献 [18, 19])——几何与面积-角度里奇微积分的关联在该模型中发挥核心作用，以及超长方体截断模型 (参见例如文献 [20])——该模型研究了自旋泡沫重整化。由于其他章节专门介绍这些方法，我们在此不再赘述。但我们需要指出，我们基于 EPRL 模型得到的结果与有效自旋泡沫模型给出的结果存在值得关注的相似性。从半经典分析的角度来看，有效自旋泡沫模型同样需要应用复临界点方法，且得到的定性行为与“复临界点与平坦性问题的解决”一节给出的结果相似，尤其在振幅对半经典几何曲率的依赖关系上。这似乎表明，有效自旋泡沫模型与 EPRL 模型在大 $j$ 区间关系密切。

The architecture of this chapter is as follows: First, we discuss the library sl2cfoam in section ”Booster Functions and SU(2) Invariants: sl2cfoam.” Section ”Booster Functions and SU(2) Invariants: sl2cfoam” also includes a concise review of the Lorentzian EPRL spinfoam amplitude and the booster function decomposition, which the library is based on. In section ”Complex Critical Points and Resolution of Flatness Problem,” we review the integral representation of the spinfoam amplitude, discuss the algorithm of computing the complex critical points, and demonstrate the curved geometries emergent from the spinfoam amplitude in a few numerical examples. In section ”Spinfoam Propagator and Lefschetz Thimble,” we discuss the algorithm of computing the spinfoam oscillatory integrals on the Lefschetz thimble and the application on the spinfoam propagator.

本章结构如下: 首先，我们在“升压函数与 SU(2) 不变量:sl2cfoam”一节讨论 sl2cfoam 库。“升压函数与 SU(2) 不变量:sl2cfoam”一节还简要回顾了洛伦兹 EPRL 自旋泡沫振幅以及该库所基于的升压函数分解。在“复临界点与平坦性问题的解决”一节，我们回顾了自旋泡沫振幅的积分表示，讨论了计算复临界点的算法，并通过几个数值示例展示了从自旋泡沫振幅中涌现出的弯曲几何。在“自旋泡沫传播子与莱夫谢茨针”一节，我们讨论了计算莱夫谢茨针上自旋泡沫振荡积分的算法，以及该方法在自旋泡沫传播子中的应用。

## Booster Functions and SU(2) Invariants: sl2cfoam

## 助推函数与 SU(2) 不变量:sl2cfoam

In this section, we will review the main ingredients and a few applications of the booster decomposition of the EPRL amplitude and its numerical implementation in sl2cfoam-next. The reader interested in more details can find a recent and pedagogical introduction to this framework in [21].

在本节中，我们将回顾 EPRL 振幅助推分解的核心内容、若干应用及其在 sl2cfoam-next 中的数值实现。想要了解更多细节的读者可以在文献 [21] 中找到该框架最新的教学式介绍。

## The EPRL Transition Amplitude

## EPRL 跃迁振幅

This section briefly introduces the EPRL spinfoam model and fixes our notation. For a comprehensive and more detailed description of the model, its derivation, physical motivation, and connection with LQG, we refer to other chapters of this book, reviews [22], or other monographs [3].

本节简要介绍 EPRL 自旋泡沫模型并确定我们使用的记号。若需全面、详细地了解该模型、其推导、物理动机以及与 LQG 的联系，请参考本书其他章节、综述文献 [22] 或其他专著 [3]。

The EPRL spinfoam theory attempts to quantize gravity with a path integral regularized on a triangulation of the spacetime manifold or, more precisely, its dual 2-complex $\Delta$. It provides dynamics to LQG, assigning a transition amplitude to the states in kinematical Hilbert space living at the boundary of the spinfoam.

EPRL 自旋泡沫理论尝试通过在时空流形的三角剖分 (更准确地说，是其对偶 2-复形 $\Delta$ ) 上正则化路径积分来量子化引力。它为 LQG 提供动力学，给生活在自旋泡沫边界的运动学希尔伯特空间中的态赋予跃迁振幅。

The EPRL transition amplitude $A_\Delta$ is defined in terms of local quantities of the 2- complex $\Delta$ colored with LQG quantum numbers: each face with a spin $j_f$ and each edge with an intertwiner $i_e$ . We have a face amplitude $A_f\left(j_f\right)$ , an edge amplitude $A_e\left(i_e\right)$ , and a vertex amplitude $A_v\left(j_f, i_e\right)$ each assigned to the corresponding component of the 2-complex. We also sum over all possible bulk quantum numbers.

EPRL 跃迁振幅 $A_\Delta$ 由带 LQG 量子数着色的 2-复形 $\Delta$ 的局域量定义: 每个面配一个自旋 $j_f$ ，每条边配一个 intertwinner $i_e$ 。我们有面振幅 $A_f\left(j_f\right)$ 、边振幅 $A_e\left(i_e\right)$ 和顶点振幅 $A_v\left(j_f, i_e\right)$ ，分别对应分配给 2-复形的对应分量，同时还要对所有可能的体量子数求和。

$$A_\Delta=\sum_{j_f, i_e} \prod_f A_f\left(j_f\right) \prod_e A_e\left(i_e\right) \prod_v A_v\left(j_f, i_e\right), \tag{1}$$

The face and edge amplitudes are fixed, requiring the correct convolution property of the path integral at fixed boundary [23] $A_f\left(j_f\right)=2 j_f+1$ and $A_e\left(i_e\right)=2 i_e+1$ . The vertex amplitude is given by

面振幅和边振幅是固定的，要求固定边界下路径积分满足正确的卷积性质 [23] $A_f\left(j_f\right)=2 j_f+1$ 和 $A_e\left(i_e\right)=2 i_e+1$ 。顶点振幅由下式给出:

$$A_v\left(j_f, i_e\right)=\sum_{m_s, m_t} \int \prod_{e \in v} \mathrm{dg}_e \delta\left(\mathrm{g}_{e^{\prime}}\right) \prod_{f \in v} D^{\gamma j_f, j_f}_{j_f m_t, j_f m_s}\left(\mathrm{g}_t^{-1} \mathrm{g}_s\right) \prod_{e \ni f}\binom{j_f}{m_p}^{\left(i_e\right)} .$$

(2)

The $D^{\gamma j_f, j_f}$ are the matrix elements unitary irreducible representations in the principal series of $\mathrm{SL}(2, \mathbb{C})$ labeled by $\rho, k=\gamma j, j$ where $\gamma$ is the Immirzi parameter. The delta function $\delta\left(g_e^{\prime}\right)$ regularizes the amplitude removing a redundant integration as prescribed in [24]. The product of the holonomies $g_t^{-1} g_s$ represents the parallel transport from the source edge of the face $s$ to the target one $t$ . We integrate over all of them. The magnetic indices $m_s$ and $m_t$ are contracted with an intertwiner tensor labeled by a quantum number $i_e$ .

$D^{\gamma j_f, j_f}$ 是由 $\rho, k=\gamma j, j$ 标记的 $\mathrm{SL}(2, \mathbb{C})$ 主系列幺正不可约表示的矩阵元，其中 $\gamma$ 是 Immirzi 参数。$\delta$ 函数 $\delta\left(g_e^{\prime}\right)$ 按照文献 [24] 的要求正则化振幅，消除冗余积分。和乐 $g_t^{-1} g_s$ 的乘积代表从面 $s$ 的源边到目标边 $t$ 的平行移动。我们对所有这些变量积分。磁指标 $m_s$ 和 $m_t$ 与由量子数 $i_e$ 标记的交缠张量缩并。

This expression will be rewritten in a form tailored to each numerical technique in the following sections.

后续章节会将该表达式改写为适配不同数值方法的形式。

## Booster Function Decomposition of the Amplitude

## 振幅的助推函数分解

Each face in the vertex amplitude (2) is decorated with a spin $j_f$ and contributes to the amplitude with a $\gamma$ -simple representation

顶点振幅 (2) 中的每个面都由一个自旋 $j_f$ 标记，且通过 $\gamma$ -单表示对振幅产生贡献

$$D^{\gamma j_f, j_f}_{j_f m_t, j_f m_s}\left(g_t^{-1} g_s\right) = \sum_{l_f=j_f}^{\infty} \sum_{n_f=-l_f}^{l_f} D^{\gamma j_f, j_f}_{j_f m_t, l_f n_f}\left(g_t^{-1}\right) D^{\gamma j_f, j_f}_{l_f n_f, j_f m_s}\left(g_s\right). \tag{3}$$

We used the representation property to separate the contribution of the edge group elements. The sum over $l_f$ is bounded from below by $j_f$ and unbounded from above. General $SL(2,\mathbb{C})$ unitary representations are infinite-dimensional.

我们利用表示性质分离了边群元素的贡献。对 $l_f$ 的求和下限为 $j_f$ ，无上界。一般的 $SL(2,\mathbb{C})$ 幺正表示是无限维的。

The vertex amplitude (2) involves four integrations (one was removed for the regularization) over a six-dimensional non-compact group of highly oscillating functions. Performing brute-force integration is a complex and demanding task.

顶点振幅 (2) 包含四次对六维非紧群上高度振荡函数的积分 (其中一次因正则化被移除)，暴力积分是一项复杂且高要求的任务。

To simplify the integration, we parameterize each group element using the Cartan decomposition of $\mathrm{SL}(2,\mathbb{C})$ . The group element and integration measure decomposes as

为简化积分，我们使用 $\mathrm{SL}(2,\mathbb{C})$ 的嘉当分解对每个群元素参数化。群元素与积分测度可分解为:

$$g = u e^{\frac{r}{2}\sigma_3} v^{-1}, \text{ and } \mathrm{d}g = \frac{1}{4\pi}\sinh^2 r \,\mathrm{d}r\,\mathrm{d}u\,\mathrm{d}v. \tag{4}$$

where $u, v \in SU(2)$ and the rapidity $r \in [0, +\infty)$ . This is analogous to choosing polar coordinates for an integral on the plane $\mathbb{R}^2$ . The integral over two unbounded Cartesian coordinates is mapped in a bounded angular integration and an unbounded radial one. The matrix elements in the unitary representations also decompose nicely with the parametrization (4).

其中 $u, v \in SU(2)$ 和快度 $r \in [0, +\infty)$ 。这类似于将平面 $\mathbb{R}^2$ 上的积分转换为极坐标，原两个无界笛卡尔坐标上的积分被映射为一个有界角积分和一个无界径向积分。幺正表示中的矩阵元也可以通过该参数化 (4) 很好地分解。

$$D^{\gamma j, j}_{ln, jm}(g) = \sum_{p=-j}^{j} D^{l}_{np}(u)\, d^{\gamma j, j}_{ljp}(r)\, D^{j}_{pm}\left(v^{-1}\right), \tag{5}$$

where $d^{\gamma j, j}_{ljp}(r)\,\delta_{pq} = D^{\gamma j, j}_{lp, jq}\left(e^{\frac{r}{2}\sigma_3}\right)$ is the reduced matrix element (see [21, 25, 26] for an expression in terms of hypergeometric functions).

其中 $d^{\gamma j,j}_{ljp}(r)\,\delta_{pq} = D^{\gamma j,j}_{lp,jq}\left(e^{\frac{r}{2}\sigma_3}\right)$ 是约化矩阵元 (参见 [21, 25, 26] ，获取超几何函数表示的表达式)。

Each edge group element contributes to the vertex amplitude with four matrix elements. The prototype of this contribution is

每个边群元素对顶点振幅的贡献都包含四个矩阵元，该贡献的原型为:

$$\int \mathrm{d}g_e \prod_{f\ni a} D^{\gamma j_f,j_f}_{l_f n_f j_f m_f}(g_e) = \int \mathrm{d}g_e \prod_{f\ni e}\sum_{p_f} D^{l_f}_{n_f p_f}(u_e)\, d^{\gamma j_f,j_f}_{l_f j_f p_f}(r_e)\, D^{j_f}_{p_f m_f}\left(v_e^{-1}\right),$$

(6)

where $f$ labels the faces in the edge $e$ . We perform the $SU(2)$ integrals in terms of (4 jm) Wigner symbols to obtain

其中 $f$ 标记边 $e$ 上的面。我们利用 (4j) 维格纳符号计算 $SU(2)$ 积分，得到:

$$\begin{aligned}&\int \mathrm{d}g_e \prod_{f\ni e} D^{\gamma j_f,j_f}_{l_f n_f j_f m_f}(g_e)\\ &= \sum_{i_e,k_e} (2i_e+1)(2k_e+1)\begin{pmatrix} l_f \\ p_f\end{pmatrix}^{(k_e)} B^{\gamma}_4(l_f, j_f; i_e, k_e)\begin{pmatrix} j_f \\ p_f\end{pmatrix}^{(i_e)},\end{aligned} \tag{7}$$

where we defined the booster function as the one-dimensional integral

其中我们将助推函数定义为如下一维积分:

$$B^{\gamma}_4(l_f, j_f; i_e, k_e) = \sum_{p_f}\begin{pmatrix} l_f \\ p_f\end{pmatrix}^{(k_e)}\left(\int_0^{\infty}\mathrm{d}r\frac{1}{4\pi}\sinh^2 r\prod_{f\in e} d^{\gamma j_f,j_f}_{l_f j_f p_f}(r)\right)\begin{pmatrix} j_f \\ p_f\end{pmatrix}^{(i_e)}.$$

(8)

Introduced in [25], the booster functions $B^{\gamma}_4$ are related to the Clebsh-Gordan coefficients of $\mathrm{SL}(2,\mathbb{C})$ and can be evaluated in terms of complex gamma functions [27,28], can be numerically computed with very high precision [5,6], and possess an interesting geometrical interpretation in terms of boosted tetrahedra [29]. The booster functions depend on the Immirzi parameter $\gamma$ and encode the quantum simplicity constraints for the EPRL model. The (4jm) symbols involving the $l_f$ spins contract among themselves, forming a $\{15j\}$ symbols, a higher-order $SU(2)$ invariant. The other $(4jm)$ symbols contract with the corresponding $(4jm)$ symbols in the definition of the vertex amplitude (2).

助推函数 $B^{\gamma}_4$ 最早引入于文献 [25]，它与 $\mathrm{SL}(2,\mathbb{C})$ 的克莱布希-高登系数相关，可以用复伽马函数表示 [27,28]，能以极高精度数值计算 [5,6]，且在助推四面体框架下拥有有趣的几何诠释 [29]。助推函数依赖于 Immirzi 参数 $\gamma$ ，编码了 EPRL 模型的量子简单性约束。含 $l_f$ 自旋的 (4jm) 符号相互缩并，形成一个 $\{15j\}$ 符号，即一个高阶 $SU(2)$ 不变量。其余的 $(4jm)$ 符号与顶点振幅 (2) 定义中对应的 $(4jm)$ 符号缩并。

In summary, we can rewrite the EPRL vertex amplitude (2) into a linear combination of $\{15j\}$ symbols weighted by booster functions

综上，我们可将 EPRL 顶点振幅 (2) 改写为助推函数加权的 $\{15j\}$ 符号线性组合:

$$A_v(j_f, i_e) = \sum_{l_f=j_f}^{\infty} \{15j\}(j_f, l_f) \prod_{e=2}^{5} B_4^{\gamma}(l_f, j_f; i_e, k_e). \tag{9}$$

We reduced the problem of performing high-dimensional oscillatory integrals to computing a series of one-dimensional integrals, $SU(2)$ invariants, and summing all the elements. The expression (9) for the vertex amplitude in the spin-intertwiner representation is particularly convenient for a numerical calculation since it consists of simpler and repeatable tasks. The library sl2cfoam-next provides a numerical implementation of the vertex amplitude computing booster functions and $\{15j\}$ symbols and summing them together in the most time- and memory-efficient way.

我们将原本的高维振荡积分问题约化为计算一系列一维积分、$SU(2)$ 不变量并对所有项求和。自旋-缠结表示下顶点振幅的表达式 (9) 对于数值计算格外方便，因为它由简单且可重复的任务构成。库 sl2cfoam-next 提供了顶点振幅的数值实现，它以最高的时间与内存效率计算助推函数和 $\{15j\}$ 符号并完成求和。

## SU(2) Invariants

## SU(2) 不变量

The computation of SU(2) invariants can be very resource-intensive. Computing the $\{15j\}$ symbol as a contraction of $(4jm)$ symbols is inefficient in terms of memory usage and computational time. In sl2cfoam-next we compute the $\{15j\}$ symbol of the first kind [30] expressing it as a finite sum of $\{6j\}$ symbols. The optimized calculation of $SU(2)$ invariants is an important topic also in other scientific fields (spectroscopy, nuclear physics, or chemistry). We did not reinvent the wheel and use the very performant libraries WIGXJPF and FASTWIGXJ [31] to compute the $\{6j\}$ symbols we need.

SU(2) 不变量的计算可能会非常消耗资源。将 $\{15j\}$ 符号计算为 $(4jm)$ 符号的收缩，在内存占用和计算时间方面效率都很低。在 sl2cfoam-next 中，我们计算第一类 $\{15j\}$ 符号 [30] 时，将其表示为 $\{6j\}$ 符号的有限和。$SU(2)$ 不变量的优化计算在其他科学领域 (光谱学、核物理或化学) 也是重要课题。我们没有重复造轮子，而是使用性能优异的 WIGXJPF 和 FASTWIGXJ 库 [31] 来计算我们所需的 $\{6j\}$ 符号。

## Booster Functions

## 助推函数

One of the main advantages of the booster decomposition (9) is reducing the group integrals to one-dimensional ones. Furthermore, it is possible to recast the reduced matrix elements of $\mathrm{SL}(2,\mathbb{C})$ to finite sums

of exponentials [5] and with a change of variable $r \mapsto e^{-r}$ map the unbounded integral to the unit interval $(0, 1]$ . The drawback is dealing with highly oscillatory integrands. To evaluate the integral with high enough accuracy, we divide the interval $(0, 1]$ into several subintervals depending on the spins in the booster function, the Immirzi parameter, and an optional accuracy parameter of the library. The subdivision is finer around the origin, where the integrand oscillates more. Finally, the integral over each subinterval is done using the Gauss-Kronrod quadrature method in double or quadruple precision.

助推分解 (9) 的核心优势之一是将群积分约化为一维积分。此外，我们可以将 $\mathrm{SL}(2,\mathbb{C})$ 的约化矩阵元改写为有限指数和 [5]，并通过变量替换 $r \mapsto e^{-r}$ 将无界积分映射到单位区间 $(0, 1]$ 。该方法的缺点是需要处理高度振荡的被积函数。为了足够高精度地计算积分，我们根据助推函数中的自旋、伊米尔齐参数以及库提供的可选精度参数，将区间 $(0, 1]$ 划分为多个子区间。在原点附近被积函数振荡更剧烈，因此划分更精细。最后，每个子区间上的积分采用高斯-克罗罗德求积法，以双精度或四精度计算。

## The Necessary Approximation

## 必要近似

A remnant of the non-compactness of the group in (9) hides in the sums over the spins $l_f$ . They are bounded from below by $j_f$ but not from above. Since the amplitude is finite [24], the unbounded sums are convergent. To evaluate the amplitude numerically, we need to approximate the unbounded sums by truncating them. In sl2cfoam-next we choose to truncate all the summations homogeneously with the same parameter $\Delta l$ , effectively replacing

(9) 中群非紧致性的残留影响隐藏在对自旋 $l_f$ 的求和中。这些求和仅存在下界 $j_f$ ，不存在上界。由于振幅是有限的 [24]，无界求和是收敛的。为了对振幅进行数值计算，我们需要通过截断来近似无界求和。在 sl2cfoam-next 中，我们选择对所有求和采用统一截断，使用同一个参数 $\Delta l$ ，实际替换为

$$\sum_{l_f=j_f}^{\infty} \to \sum_{l_f=j_f}^{j_f+\Delta l} \tag{10}$$

Unfortunately, we do not know how to estimate the error we are committing by truncating with a given $\Delta l$ . Recently [21,32], we proposed to use convergence acceleration techniques to improve our approximation of the amplitude and reduce the dependence on the truncation parameter. Using Aitken's delta squared method, the vertex amplitude is well approximated by

遗憾的是，我们目前尚不清楚如何估计给定 $\Delta l$ 截断带来的误差。近期研究 [21,32] 中，我们提出使用收敛加速技术来改进振幅的近似结果，降低对截断参数的依赖。利用艾特肯 $\delta$ 平方方法，顶点振幅可以很好地近似为

$$A_v \approx \frac{A_v(\Delta l)\,A_v(\Delta l-2) - A_v^2(\Delta l-1)}{A_v(\Delta l) - 2A_v(\Delta l-1) + A_v(\Delta l-2)}. \tag{11}$$

The dependence of the result on other convergence techniques and the associated error is currently under investigation.

其他收敛技术对结果的影响以及相关误差目前仍在研究中。

## Assembling the Amplitude

## 组装振幅

To compute any EPRL transition amplitude, we perform many products (among invariants, booster functions, vertex amplitudes) and sums (spins, magnetic indices, intertwiners). For acceptable performances, we have to deal with them efficiently. The problem is similar to matrix multiplication in computer science, which is solved using specialized routines for contractions of multidimensional arrays and parallelization.

要计算任意 EPRL 跃迁振幅，我们需要进行多次乘积运算 (涉及不变量、booster 函数、顶点振幅) 与求和运算 (自旋、磁指标、缠结子)。为获得可接受的计算性能，必须高效处理这些运算。该问题与计算机科学中的矩阵乘法类似，可通过多维数组收缩专用程序和并行化方法解决。

To compute the vertex amplitude, we build a multidimensional array with the $\{15j\}$ symbols and another with the booster functions for varying spins $l_f$ and intertwiners. We calculate the vertex amplitude contracting the two tensors using basic linear algebra subprograms (BLAS) routines. The library is parallelized considerably using a hybrid OpenMP-MPI scheme. The calculation of booster tensor and vertex tensors for different $l_f$ is distributed on many MPI nodes, and every node parallelizes the necessary operations across its CPUs using OpenMP. The vertex amplitude is also stored in a multidimensional array, and the contraction of many vertices to form a transition amplitude can be parallelized. For increased performance, tensor contractions can be parallelized using GPU cores with the julia module SL2CfoamGPU.

计算顶点振幅时，我们会用 $\{15j\}$ 符号构建一个多维数组，再用对应不同自旋 $l_f$ 和缠结子的 booster 函数构建另一个多维数组。我们借助基础线性代数子程序 (BLAS) 对两个张量做收缩来计算顶点振幅。该程序库通过 OpenMP-MPI 混合方案实现了高度并行化。针对不同 $l_f$ 的 booster 张量和顶点张量计算被分发到多个 MPI 节点处理，每个节点再通过 OpenMP 在自身 CPU 间并行完成必要运算。顶点振幅也存储在多维数组中，因此收缩多个顶点形成跃迁振幅的过程也可并行化。为提升性能，张量收缩还可借助 julia 模块 SL2CfoamGPU 通过 GPU 核心并行完成。

## Applications

## 应用

We used sl2cfoam and sl2cfoam-next to compute numerous transition amplitudes. In this section, we review some of the main results.

我们使用 sl2cfoam 和 sl2cfoam-next 计算了大量跃迁振幅。本节我们将回顾其中部分主要成果。

## Quickstart

## 快速入门

We start with a showcase of how user-friendly the library is. We need a few lines of code to compute one vertex amplitude using the julia interface. In Fig. 1 we show how to import and initialize the library.

我们首先展示这个库的易用性。仅需几行代码，即可通过 Julia 接口计算一个顶点振幅。图 1 展示了如何导入并初始化该库。

We specify the value of the Immirzi parameter (set to 1.2 in this example) and a folder where the library stores and retrieves the FASTWIGXJ tables of invariants and the computed amplitudes. Saving the value of known amplitudes and avoiding recalculations save a lot of computational time in the long run in exchange of disk space. In Listing 2, we compute the vertex amplitude.

我们指定 Immirzi 参数的值 (本示例中设为 1.2)，以及一个用于该库存储和读取 FASTWIGXJ 不变量表与已计算振幅的文件夹。保存已知振幅、避免重复计算，从长远来看能以磁盘空间为代价节省大量计算时间。在代码清单 2 中，我们计算了顶点振幅。

We set the ten boundary spins (in this example, all equal to 1) and the value of the truncation parameter (in this example $\Delta l = 15$ ). Finally, we compute the vertex amplitude and store it in an array with five indices, one per intertwiner.

我们设置十个边界自旋 (本示例中全部等于 1) 和截断参数的值 (本示例中为 $\Delta l = 15$ )。最后，我们计算顶点振幅并将其存储在一个带有五个索引的数组中，每个索引对应一个 intertwinner。

## Single Vertex Asymptotic

## 单顶点渐近行为

The most celebrated result of the EPRL spinfoam model is its connection with the Regge action in the large spin limit with coherent boundary data [33-35].

EPRL 自旋泡沫模型最广为人知的结果，就是它在大自旋极限下、相干边界条件中与里奇作用量的联系 [33-35]。

$$A_v\left(j_f, \mathbf{n}_f\right) = \sum_{i_e} A_v\left(j_f, i_e\right) \prod_e c_{i_e}\left(\mathbf{n}_f\right). \tag{12}$$

The vertex amplitude (9) is contracted with Livine-Speziale coherent intertwiners $c_{i_e}\left(\mathbf{n}_f\right)$ [36] representing the spacelike boundary of a Lorentzian 4-simplex. When the spins are homogeneously large, i.e., under a rescaling $j_f \to \lambda j_f$ with $\lambda \gg 1$ , the amplitude (12) takes the asymptotic form

顶点振幅 (9) 与 Livine-Speziale 相干 intertwiner $c_{i_e}(\mathbf{n}_f)$ [36] 缩并，后者描述洛伦兹 4 单形的类空边界。当自旋均匀增大时，即在标度变换 $j_f \to \lambda j_f$ (满足 $\lambda \gg 1$ ) 下，振幅 (12) 具有如下渐近形式

$$A_v(\lambda j_f, \mathbf{n}_f) = \frac{1}{\lambda^{12}}\left(N_1 e^{i\lambda S_R} + N_2 e^{-i\lambda S_R}\right) + O\left(\lambda^{-13}\right), \tag{13}$$

---

```
using SL2Cfoam
    Immirzi = 1.2
    data_folder = ”path/to/data/folder”
configuration = SL2Cfoam.Config(VerbosityOff, VeryHighAccuracy, 100, 0)
    SL2Cfoam.cinit(data_folder, Immirzi, configuration)
```

---

Fig. 1 Initialization of sl2cfoam-next

图 1 sl2cfoam-next 初始化

---

```
spins = ones(10)
D1 = 15
Av = vertex_compute(spins, D1)
```

---

Fig. 2 Computation of a vertex amplitude with sl2cfoam-next

图 2 使用 sl2cfoam-next 计算顶点振幅

where $S_R$ is the Regge action of the 4-simplex

其中 $S_R$ 是该 4 单形的里奇作用量

$$S_R = \sum_f \gamma \theta_f(\mathbf{n}_f)\, j_f, \tag{14}$$

with $\gamma$ is the Immirzi parameter and $\theta_f$ is the dihedral angles of the 4-simplex. The coefficients $N_s$ can be computed exactly, but a simple closed formula in terms of the 4-simplex geometry does not exist [14,35].

式中 $\gamma$ 为伊米尔齐参数，$\theta_f$ 是 4 单形的二面角。系数 $N_s$ 可以精确计算，但目前还没有用 4 单形几何表示的简洁闭合公式 [14,35]。

The path toward the numerical verification of the formula (13) started in [35] with sl2cfoam and was completed in [6] with sl2cfoam-next. This was the perfect testing ground for the library since it is one of the few analytic results in the theory.

对公式 (13) 的数值验证工作始于文献 [35] 使用 sl2cfoam 的研究，最终由文献 [6] 使用 sl2cfoam-next 完成。由于它是该理论少有的解析结果，因此是测试该程序库的绝佳场景。

We use boundary data representing a very symmetric isosceles Lorentzian 4- simplex (see [35] for a detailed description of the boundary data). We focus on the Immirzi parameter $\gamma = 2.0$ , scales up to $\lambda = 30$ with a truncation $\Delta l = 8$ .

我们采用描述高度对称的等腰洛伦兹 4 单形的边界数据 (边界数据的详细描述见 [35])，我们聚焦于伊米尔齐参数 $\gamma = 2.0$ ，将标度提升至 $\lambda = 30$ ，并采用截断 $\Delta l = 8$ 。

We summarize the results in Fig. 3. The numerical evaluation and the asymptotic formula are in excellent qualitative and quantitative agreement, even at relatively small scales.

我们将结果总结在图 3 中。即使在相对较小的标度下，数值计算结果与渐近公式在定性和定量上都高度吻合。

This analysis consecrated sl2cfoam-next as a priceless tool to study the EPRL spinfoam model. However, it also highlights one of the limitations of the framework. The larger the scale of the boundary spins $\lambda$ , the larger truncation $\Delta l$ is needed to approximate the amplitude. This agreement was possible only thanks to the optimizations introduced in s12cfoam-next. A similar calculation performed in [35] using sl2cfoam was limited to $\Delta l = 1$ , and only the order of magnitude of the numerical data and the asymptotic formula agreed.

这一分析确立了 sl2cfoam-next 是研究 EPRL 自旋泡沫模型的宝贵工具，但也暴露了该框架的一项局限：边界自旋 $\lambda$ 的标度越大，近似振幅所需的截断 $\Delta l$ 就越大。这种高精度的吻合只有依靠 sl2cfoam-next 引入的优化才能实现。文献 [35] 使用 sl2cfoam 完成的类似计算只能达到 $\Delta l = 1$ ，且仅数值结果与渐近公式在量级上一致。

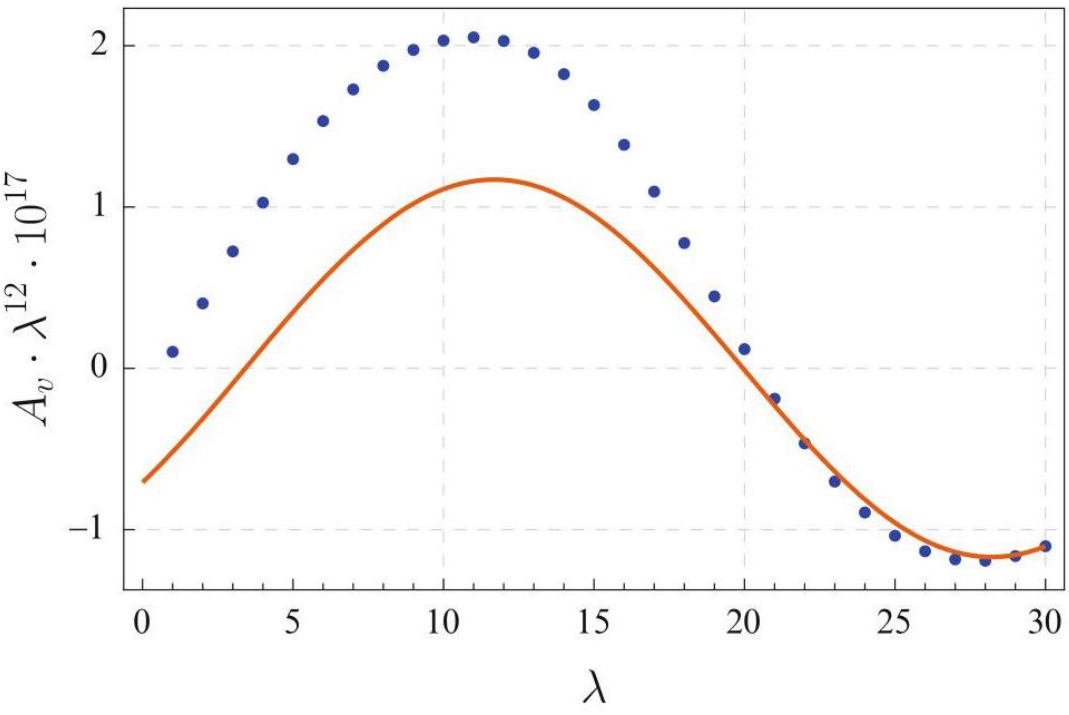

Fig. 3 Plot of the rescaled coherent vertex amplitude (12) as function of the scale $\lambda$ . The numerical evaluation uses $\gamma = 2$ and $\Delta l = 8$ and boundary data corresponding to a Lorentzian isosceles 4- simplex. The asymptotic expression (13) with $N_1 = \bar{N}_2 = 5.85 \cdot 10^{-18} \cdot e^{i2.22}$ and $S_R = -0.19$ is plotted as a red continuous line. The data was kindly shared by the authors of [6]

图 3 重标度后的相干顶点振幅 (12) 关于标度 $\lambda$ 的函数图。数值计算使用 $\gamma = 2$ 和 $\Delta l = 8$ ，边界数据对应洛伦兹等腰 4 单形。带有 $N_1 = \bar{N}_2 = 5.85 \cdot 10^{-18} \cdot e^{i2.22}$ 和 $S_R = -0.19$ 的渐近表达式 (13) 以红色实线绘制。数据由文献 [6] 的作者友好提供

For other asymptotic behaviors of (9), a similar analysis was already performed in [35] using sl2cfoam obtaining already a good qualitative and quantitative match.

对于 (9) 的其他渐近行为，文献 [35] 已经使用 sl2cfoam 完成了类似分析，得到了良好的定性与定量匹配。

## Many Vertices and the Flatness Problem

## 多顶点与平坦性问题

The regime of the EPRL spinfoam theory in which we can recover (discrete) general relatively is still under study. The presence of the Regge action in the large spin limit of a single vertex amplitude is not enough. We must explore extended triangulations to find if we can also extract the Regge equation of motion. The community agrees that a double scaling limit of low energies and refined triangulation (corresponding to large spins and many vertices) is the best candidate [12, 13, 18, 37, 38] .

EPRL 自旋泡沫理论中可以恢复 (离散) 广义相对论的区域仍在研究中。单个顶点振幅的大自旋极限存在 Regge 作用量并不足够。我们必须探究扩展三角剖分，确认能否从中提取出 Regge 运动方程。学界普遍认为，低能量加精细三角剖分 (对应大自旋与多顶点) 的双标度极限是最佳候选 [12, 13, 18, 37, 38] 。

Numerical calculations played an essential role in confirming the so-called flatness problem of the EPRL model [7, 9, 13, 39, 40] . For a path integral formulation of a quantum theory, the amplitude is exponentially suppressed if and only if the boundary data is inconsistent with the classical equation of motions. The flatness problem claims that, at fixed triangulation, the amplitude is dominated in the large spin limit by flat geometries. It was interpreted as a signal that the EPRL model apparently cannot recover non-flat solutions of Einstein's equations. The problem disappears if a refinement of the triangulation is taken into account at the same time as the large spin limit (see section "Asymptotics of $A(\Delta_3)$ " for a complementary discussion).

数值计算在证实 EPRL 模型所谓的平坦性问题中起到了关键作用 [7, 9, 13, 39, 40] 。对于量子理论的路径积分表述，当且仅当边界数据不满足经典运动方程时，振幅会发生指数抑制。平坦性问题指出，在固定三角剖分下，大自旋极限中的振幅由平坦几何主导。这曾被解读为 EPRL 模型显然无法恢复爱因斯坦方程的非平坦解的信号。如果在取大自旋极限的同时考虑三角剖分精细化，该问题就会消失 (补充讨论见“$A(\Delta_3)$ 的渐近行为”章节)。

It is possible to verify numerically that the Lorentzian EPRL transition amplitude with coherent boundary data compatible only with a curved geometry exponentially decreases when the boundary spins are rescaled homogeneously. We tested it with the simplest triangulation $\Delta_3$ consisting of three 4-simplices sharing a tetrahedron and all sharing one triangle dual to the only bulk face (see Fig. 4).

我们可以通过数值验证: 洛伦兹 EPRL 跃迁振幅中，若相干边界数据仅与弯曲几何相容，当边界自旋被均匀缩放时，振幅会指数衰减。我们在最简单的三角剖分 $\Delta_3$ 上完成了测试，该三角剖分由三个 4 单形共享一个四面体，且所有 4 单形共享一个三角形，该三角形对偶于唯一的体块面 (见图 4)。

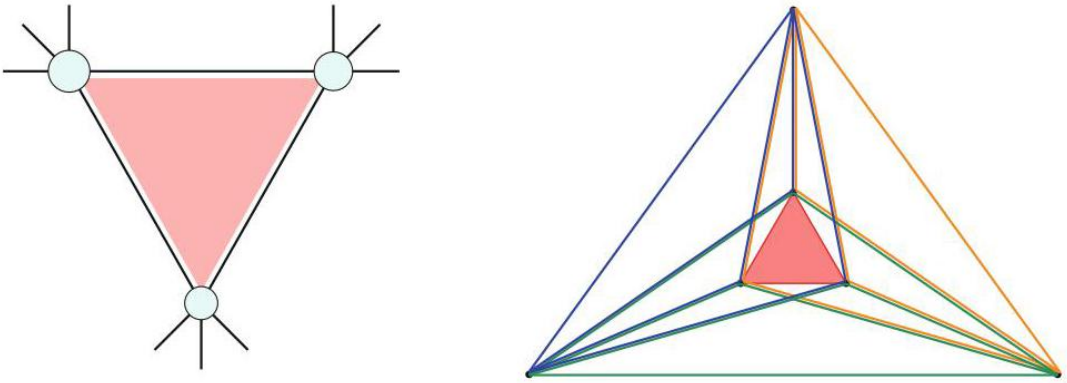

Fig. 4 Left panel: The spinfoam diagram associated to the $\Delta_3$ triangulation. We highlighted in red the face dual to the bulk triangle. Right panel: The $\Delta_3$ triangulation. We highlighted in red the bulk triangle and colored the three 4-simplices for a simpler visualization

图 4 左图: 对应 $\Delta_3$ 三角剖分的自旋泡沫图，我们将对偶于体块三角形的面用红色标出。右图: $\Delta_3$ 三角剖分，我们将体块三角形用红色标出，并为三个 4 单形分别着色以便于观察

The amplitude associated with the $\Delta_3$ triangulation is

$\Delta_3$ 三角剖分对应的振幅为

$$A_{\Delta_3}\left(j_f,\mathbf{n}_f\right)=\sum_{i_e}\sum_{i_h}\sum_{j_h}(2j_h+1)A_{v_1}\left(j_f,i_e;j_h,i_{h_1},i_{h_2}\right)A_{v_2}\left(j_f,i_e;j_h,i_{h_2},i_{h_3}\right)$$

$$\times A_{v_3}\left(j_f,i_e;j_h,i_{h_3},i_{h_1}\right)\prod_e c_{i_e}\left(\mathbf{n}_f\right), \tag{15}$$

where we denoted with $h$ the face dual to the bulk triangle (highlighted in red in Fig. 4), with $j_h$ the associated spin, with $h_1,h_2,h_3$ the three bulk edges, with $i_{h_1},i_{h_2},i_{h_3}$ the associated intertwiners, and with $c_{i_e}$ the boundary coherent states representing a classical curved geometry.

其中我们用 $h$ 表示对偶于体块三角形的面 (图 4 中红色标出部分)，用 $j_h$ 表示其对应的自旋，用 $h_1,h_2,h_3$ 表示三个体块边，用 $i_{h_1},i_{h_2},i_{h_3}$ 表示对应的交缠子，用 $c_{i_e}$ 表示表示经典弯曲几何的边界相干态。

For simplicity, we considered highly symmetric boundary data with all the spins equal $j_f=j$. The rate of exponential decrease at large spins is related to the curvature of the geometry: the more curved the

geometry is, the fastest the amplitude decreases. We constructed boundary data corresponding to a Euclidean curved geometry with the largest possible (discrete) curvature compatible with the symmetry (see [41] for a detailed description of the boundary data).

为简化起见，我们考虑高度对称的边界数据，所有自旋都相等 $j_f = j$。大自旋下的指数衰减速率与几何曲率相关: 几何曲率越大，振幅衰减越快。我们构造了对应欧几里得弯曲几何的边界数据，其具有对称性允许的最大 (离散) 曲率 (边界数据的详细描述见文献 [41])。

In Fig. 5, we plot the EPRL transition amplitude for the $\Delta_3$ triangulation with Immirzi parameter $\gamma = 2$ , truncation parameter $\Delta l = 2$ , and rescaling the boundary spins homogeneously with scale $\lambda$ from 1 to 30 . The exponential decrease in the amplitude is apparent. Thus we confirm that just taking large spins is not a good semiclassical limit of the theory.

在图 5 中，我们绘制了 $\Delta_3$ 三角剖分下的 EPRL 跃迁振幅，Immirzi 参数为 $\gamma = 2$ ，截断参数为 $\Delta l = 2$ ，边界自旋以标度 $\lambda$ 从 1 到 30 均匀缩放。振幅的指数衰减十分明显。因此我们证实，仅取大自旋并不是该理论良好的半经典极限。

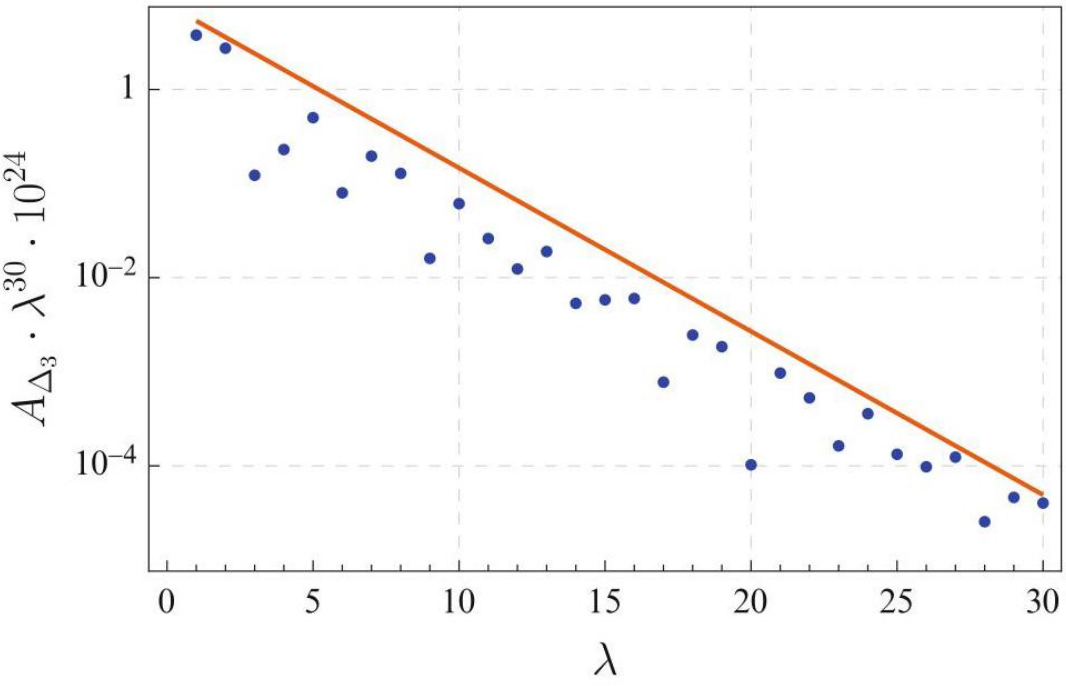


Fig. 5 Log-linear plot of the absolute value of the $A_{\Delta_3}$ EPRL amplitude for different boundary spins scale $\lambda$ . The calculation is done with Immirzi parameter $\gamma = 2$ and small truncation parameter $\Delta l = 2$ . We plot the function $8e^{-4\lambda/10}$ with a continuous blue line. This function is just a visual guide highlighting the amplitude's exponential decrease. It is not the result of a fit, and we do not have enough data points to disentangle the exponential behavior from the oscillations. The data was kindly shared by the authors of [6]

图 5 不同边界自旋标度 $\lambda$ 下，$A_{\Delta_3}$ EPRL 振幅绝对值的对数-线性图。计算采用 Immirzi 参数 $\gamma = 2$ 和小截断参数 $\Delta l = 2$ 。我们用蓝色实线绘制函数 $8e^{-4\lambda/10}$ ，该函数仅用于直观指示振幅的指数衰减，并非拟合结果，而且我们没有足够的数据点从振荡中分离出指数行为。数据由文献 [6] 的作者友好提供。

## Radiative Corrections

## 辐射修正

Spinfoams are ultraviolet finite. However, in the case of a vanishing cosmological constant, they are affected by infrared divergences. Divergences arise due to unbounded summation over the spin labels on bulk faces. They require some renormalization procedure, and in general, their study and understanding are essential in defining the continuum limit.

自旋泡沫是紫外有限的。但在宇宙常数为零的情况下，它会受到红外发散的影响。发散源于对体块面自旋标记的无界求和，这需要引入重整化流程，总体而言，研究并理解这类发散对定义连续极限至关重要。

The divergences of the Lorentzian EPRL model have been studied analytically using asymptotic techniques in [42], with a hybrid numerical and analytical analysis in [43], and very recently numerically using sl2cfoam-next with a massive computational effort in [32].

洛伦兹 EPRL 模型的发散已经通过渐近技术在文献 [42] 中得到解析研究，在文献 [43] 中完成了解析与数值混合分析，最近更是借助 sl2cfoam-next 通过大量计算在文献 [32] 中得到数值研究。

We focus on the computation of the radiative corrections to the EPRL spinfoam edge. The amplitude comprises two vertices glued along four edges, with six internal and four boundary faces. We sum over the spins of the internal faces $j_h$ , and we fix the spins to the boundary faces $j_f$ . Similarly, we sum over the bulk intertwiners associated with the internal edges $i_{h_e}$ , and we fix the boundary ones $i_e$ . We regularize the two vertex amplitudes removing the same integration over the boundary edge. The result is two identical vertex amplitudes, and the radiative correction amplitude is given by

我们聚焦于计算 EPRL 自旋泡沫边界棱的辐射修正。该振幅包含沿四条棱粘合的两个顶点，拥有六个内部面和四个边界面。我们对内部面的自旋 $j_h$ 求和，固定边界面的自旋 $j_f$ 。同理，我们对与内部棱关联的体块交缠子 $i_{h_e}$ 求和，固定边界交缠子 $i_e$ 。我们对两个顶点振幅做正则化处理，移除对边界棱的相同积分，最终得到两个相同的顶点振幅，辐射修正振幅可表示为

$$A_{rc} = \sum_{j_h} \left( \prod_{f \in h} (2j_f + 1) \right) \sum_{i_{h_e}} \left( \prod_{h_e} (2i_{h_e} + 1) \right) A_v^2 \left( j_h, j_f, i_{h_e}, i_e \right). \tag{16}$$

The sums over $j_h$ are unbounded and can cause the amplitude to diverge. We introduce a homogeneous cutoff $K$ and study the value of the amplitude as a function of $K$ . The nature of this cutoff is utterly different from the truncation $\Delta l$ , introduced as a tool to approximate the convergent sums over the virtual spins $l_f$ and the vertex amplitudes $A_v$ .

对 $j_h$ 的求和是无界的，会导致振幅发散。我们引入均匀截断 $K$ ，将振幅作为 $K$ 的函数研究其取值。该截断的性质与截断 $\Delta l$ 完全不同，后者是用于近似对虚自旋 $l_f$ 和顶点振幅 $A_v$ 的收敛求和的工具。

We numerically evaluate the amplitude (16) for values of the cutoff $K$ from $\frac{1}{2}$ to 10 at half-integer steps. We fix the boundary spins to $j_f = \frac{1}{2}$ and the boundary intertwiners to $i_e = 0$ . For each $K$ we fix $\Delta l = 20$ , and

we approximate the amplitude using the convergence acceleration formula (11). In this calculation, we use $\gamma = 0.1$ . We summarize the results in Fig. 6.

我们对截断 $K$ 从 $\frac{1}{2}$ 到 10、步长为半整数的取值, 数值计算了振幅 (16)。我们将边界自旋固定为 $j_f = \frac{1}{2}$ ，边界交缠子固定为 $i_e = 0$ 。对每个 $K$ 我们固定 $\Delta l = 20$ ，利用收敛加速公式 (11) 近似计算振幅。本次计算我们使用 $\gamma = 0.1$ ，结果总结在图 6 中。

We fit the amplitude with a function $a + bK^c$ and find $c = 1.06$ . We confidently claim that also the amplitude is scaling linearly. For completeness we report also the values of $a = -5.31 \cdot 10^{-6}$ and $b = 7.18 \cdot 10^{-6}$ .

我们用函数 $a + bK^c$ 拟合振幅，得到 $c = 1.06$ 。我们可以确定地说，该振幅也满足线性标度。为完整起见，我们也给出 $a = -5.31 \cdot 10^{-6}$ 和 $b = 7.18 \cdot 10^{-6}$ 的数值结果。

Recently, in [44], other potentially divergent contributions of the radiative corrections to the EPRL propagator have been studied. All the contributions of diagrams with four or two bulk faces are indeed convergent. The results with different boundary data and Immirzi parameters are incredibly stable.

近期，文献 [44] 研究了 EPRL 传播子辐射修正中其他可能发散的贡献。所有含两个或四个体块面的图的贡献实际都是收敛的，不同边界数据和 Immirzi 参数下的结果都极为稳定。

## Other Applications and Future Developments

## 其他应用与未来发展

The numerical framework sl2cfoam-next is mainly used in phenomenological applications: studying the early universe, quantum tunneling of a black hole to a white hole, and exploring the continuum limit.

数值框架 sl2cfoam-next 主要用于唯象学应用: 研究早期宇宙、黑洞到白洞的量子隧穿，以及探索连续极限。

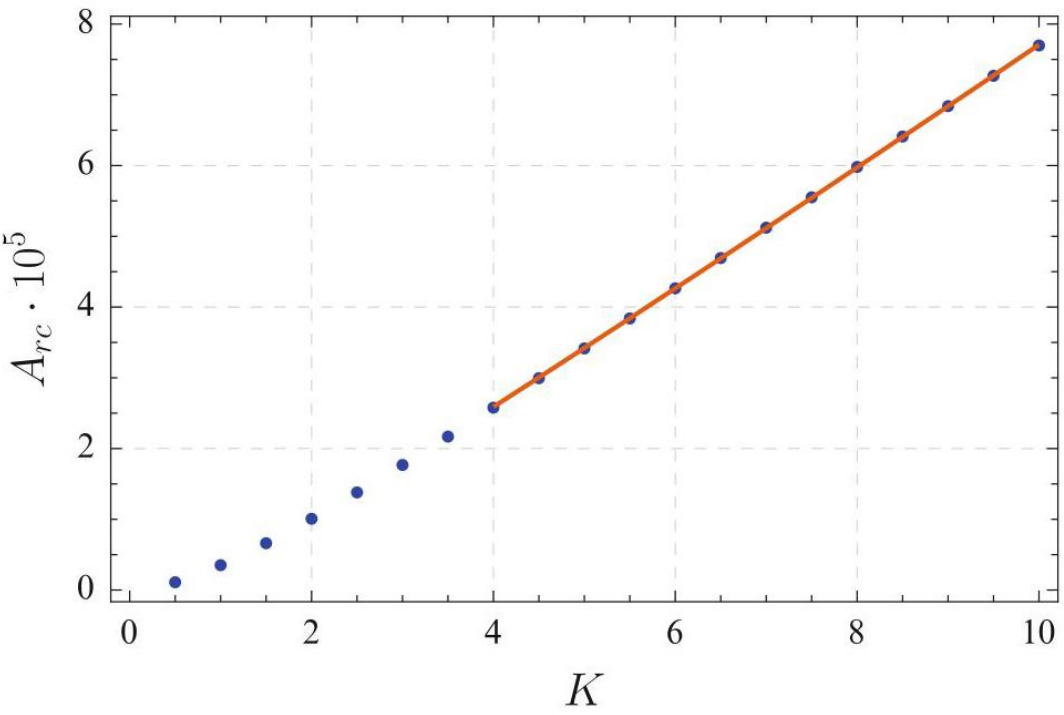


Fig. 6 Plot of the radiative correction amplitude $A_{rc} \times 10^5$ as a function of the cutoff $K$ in halfinteger steps. The numerical evaluation uses $\gamma = 0.1$ and $\Delta l = 20$ . The data was kindly shared by the authors of [32]

图 6 辐射修正振幅 $A_{rc} \times 10^5$ 随截断 $K$ 变化的图，步长为半整数。数值计算采用 $\gamma = 0.1$ 和 $\Delta l = 20$ 。数据由文献 [32] 的作者善意分享

Some preliminary results are available [45, 46]. In this section, we would like to mention some innovative techniques used to overcome the issue of sl2cfoam-next of being very resource-intensive on large triangulations.

目前已有一些初步结果 [45, 46]。在本节中，我们将介绍一些用于克服 sl2cfoam-next 在大三角剖分下资源消耗过大问题的创新技术。

For example, to calculate the expectation value of a geometrical operator $O\left(j_f, i_e\right)$ at fixed boundary spins $j_f$ , it is necessary to compute the spinfoam amplitude for every value of the boundary intertwiners $i_e$ . With 20 boundary tetrahedra, all boundary spins equal $j$ , and the computation of one expectation value requires the evaluation of $(2j+1)^{20}$ amplitudes. Even in the small spins regime $j = 2$ , and with the most optimistic estimate of $1\mu s$ of CPU time per amplitude, the computation of one expectation value would take $5^{20}\mu s \approx 3$ years.

例如，要计算固定边界自旋 $j_f$ 下几何算符 $O\left(j_f, i_e\right)$ 的期望值，需要对边界相交子 $i_e$ 的每个取值计算自旋泡沫振幅。当存在 20 个边界四面体，且所有边界自旋均等于 $j$ 时，计算一个期望值就需要对 $(2j+1)^{20}$ 个振幅进行求值。即使在小自旋区域 $j = 2$ ，且按最乐观估计每个振幅消耗 $1\mu s$ CPU 时间，计算一个期望值也需要 $5^{20}\mu s \approx 3$ 年。

The proposed solution to this problem uses statistical methods like Markov chain Monte Carlo techniques

to evaluate the many sums and efficiently sample the space of possible amplitudes.

针对该问题，目前提出的解决方案是利用马尔可夫链蒙特卡洛等统计方法计算多求和问题，并对可能的振幅空间进行高效采样。

A similar issue also arises when we want to compute a spinfoam transition amplitude with many bulk faces. The amplitude calculation must be repeated for many values of the bulk variables, and the CPU time needed piles up rapidly.

当我们需要计算包含大量体块面的自旋泡沫跃迁振幅时，也会遇到类似问题。必须对体变量的多个取值重复计算振幅，所需 CPU 时间会迅速累积。

Another actively developed direction is the reduction of the dependence on the numerical result from the truncation parameters. Other convergence acceleration techniques and a systematic way to estimate the error in the amplitude are being studied.

另一个活跃发展的方向是降低数值结果对截断参数的依赖。目前正在研究其他收敛加速技术，以及系统估计振幅误差的方法。

## Complex Critical Points and Resolution of Flatness Problem

## 复临界点与平坦性问题的解决

The semiclassical consistency is an important requirement in quantum physics, as any satisfactory quantum theory must reproduce the corresponding classical theory in the approximation of small $-h$ . In particular, the role of semiclassical analysis is crucial in quantum gravity, as it is the zero-th order test of the consistency with general relativity. Moreover the semiclassical expansion provides a method of computing quantum effect perturbatively and connects the non-pertubative formulation of LQG to the perturbative regime. In spinfoam models, the semiclassical regime relates to the large- $j$ regime. As mentioned above, the numerical framework sl2cfoam-next is very resource-intensive for computing the spinfoam amplitude in the large- $j$ regime and for large triangulations. Therefore, we look for the alternative strategies toward the semiclassical analysis of spinfoam models. In this section, we introduce the numerical method based on the stationary phase approximation of the spinfoam amplitude, and in particular, we discuss the method of complex critical point, which is crucial for obtaining curved geometries from the large- $j$ spinfoam amplitude. The discussion of this section is mostly based on the recent result in [47]. Some earlier literature on the stationary phase analysis of spinfoam amplitude are [33,48-54].

半经典自洽性是量子物理中一项重要要求，因为任何合格的量子理论都必须在小 $-h$ 近似下还原出对应的经典理论。半经典分析对量子引力而言尤其关键，它是检验理论与广义相对论自洽性的零阶检验。此外，半经典展开提供了微扰计算量子效应的方法，还将 LQG 的非微扰表述与微扰区域连接起来。在自旋泡沫模型中，半经典区域对应大 $j$ 区域。如前文所述，对大 $j$ 区域以及大三角剖分情形计算自旋泡沫振幅时，数值框架 sl2cfoam-next 的资源消耗极大。因此我们需要寻找替代方案来开展自旋泡沫模型的半经典分析。本节我们介绍基于自旋泡沫振幅平稳相位近似的数值方法，尤其会重点讨论复临界点方法——该方法对从大 $j$ 自旋泡沫振幅得到弯曲几何至关重要。本节讨论主要基于文献 [47] 的最新研究结果。关于自旋泡沫振幅平稳相位分析的早期研究可参见 [33,48-54]。

## Spinfoam Amplitude and Complex Critical Points

## 旋泡沫振幅与复临界点

## Integral Representation of Spinfoam Amplitude

## 自旋泡沫振幅的积分表示

The four-dimensional triangulation $\Delta$ is made by 4-simplices $v$, tetrahedra $e$, triangles $f$, line segments, and points. Here we denote the internal triangle by $h$ and the boundary triangle by $b$ ( $f$ is either $h$ or $b$ ) and assign the SU(2) spins $j_h, j_b \in \mathbb{N}_0/2$ to $h, b$. The Lorentzian EPRL spinfoam amplitude on $\Delta$ sums over internal spins $\{j_h\}$ and has the following integral expression in analogy with path integral:

四维三角剖分 $\Delta$ 由 4-单形 $v$、四面体 $e$、三角形 $f$、线段和点构成。此处我们将内部三角形记为 $h$，边界三角形记为 $b$ ( $f$ 要么是 $h$ 要么是 $b$ )，并为 $h, b$ 分配 SU(2) 自旋 $j_h, j_b \in \mathbb{N}_0/2$。$\Delta$ 上的洛伦兹 EPRL 自旋泡沫振幅对内部自旋 $\{j_h\}$ 求和，具有如下类比路径积分的积分表达式:

$$A(\Delta) = \sum_{\{j_h\}}^{j^{\max}} \prod_h d_{j_h} \int [\mathrm{dg}\, \mathrm{d}\mathbf{z}]\, e^{S\left(j_h, g_{ve}, \mathbf{z}_{vf}; j_b, \xi_{eb}\right)}. \tag{17}$$

$\mathbf{d}_{j_h} = 2j_h + 1$ is the dimension of SU (2) irreducible representation. The boundary states of $A(\Delta)$ are the SU (2) coherent states $|j_b, \xi_{eb}\rangle$, where $j_b, \xi_{eb}$ determines the area and the 3-normal of $b$ in the boundary tetrahedra $e$. The summed/integrated variables are $g_{ve} \in \mathrm{SL}(2,\mathbb{C})$, $\mathbf{z}_{vf} \in \mathbb{CP}^1$, and $j_h$, while the boundary $j_b, \xi_{eb}$ is not summed/integrated. The integration measure is $[\mathrm{dg}\, \mathrm{d}\mathbf{z}] = \prod_{(v,e)} \mathrm{dg}_{ve} \prod_{(v,f)} \mathrm{d}\Omega_{\mathbf{z}_{vf}}$, where $\mathrm{dg}_{ve}$ is the SL $(2,\mathbb{C})$ Haar measure and $\mathrm{d}\Omega_{\mathbf{z}_{vf}}$ is a scaling invariant measure on $\mathbb{CP}^1$. We truncate the sum over internal $j_h \in \mathbb{N}_0/2$ at $j^{\max}$. $j^{\max}$ is determined by boundary spins $j_b$ via the triangle inequality for some internal triangles; otherwise $j^{\max}$ is an IR cut-off. The spinfoam action $S$ is complex and linear to the spins $j_h, j_b$. Here we imply the action $S$ derived in [50], so that there is no internal $\xi_{eh}$ appearing in the integral of $A(\Delta)$ (this version of integral expression of $A(\Delta)$ turns out to avoid some degeneracy of the Hessian). We skip the detailed expression of $S$ but refer the reader to [50] (see also [47]).

$\mathbf{d}_{j_h} = 2j_h + 1$ 是 SU(2) 不可约表示的维数。$A(\Delta)$ 的边界态是 SU(2) 相干态 $|j_b, \xi_{eb}\rangle$，其中 $j_b, \xi_{eb}$ 确定了边界四面体 $e$ 中 $b$ 的面积和 3-法向量。求和/积分变量为 $g_{ve} \in \mathrm{SL}(2,\mathbb{C})$, $\mathbf{z}_{vf} \in \mathbb{CP}^1$ 和 $j_h$，边界 $j_b, \xi_{eb}$ 不参与求和/积分。积分测度为 $[\mathrm{dg}\,\mathrm{d}\mathbf{z}] = \prod_{(v,e)} \mathrm{dg}_{ve} \prod_{(v,f)} \mathrm{d}\Omega_{\mathbf{z}_{vf}}$，其中 $\mathrm{dg}_{ve}$ 是 $\mathrm{SL}(2,\mathbb{C})$ 哈尔测度，$\mathrm{d}\Omega_{\mathbf{z}_{vf}}$ 是 $\mathbb{CP}^1$ 上的标度不变测度。我们对内部 $j_h \in \mathbb{N}_0/2$ 的求和在 $j^{\max}.j^{\max}$ 处截断，$j^{\max}.j^{\max}$ 由边界自旋 $j_b$ 通过部分内部三角形的三角不等式确定；否则 $j^{\max}$ 是红外截断。自旋泡沫作用量 $S$ 是复的，且对自旋 $j_h, j_b$ 是线性的。此处我们采用文献 [50] 中推导的作用量 $S$，因此 $A(\Delta)$ 的积分中不会出现内部 $\xi_{eh}$ (该版本的 $A(\Delta)$ 积分表达式可以避免黑塞矩阵的一些简并问题)。我们略去 $S$ 的具体表达式，读者可参考 [50](也可参见 [47])。

We apply the Poisson summation formula to change the sum over $j_h$ to the integral, as a preparation for the stationary phase analysis. Indeed, we firstly replace each $\mathbf{d}_{j_h}$ by a smooth compact support function $\tau_{[-\varepsilon, j^{\max}+\varepsilon]}(j_h)$ satisfying

我们应用泊松求和公式将对 $j_h$ 的求和转换为积分，作为平稳相位分析的准备。首先，我们确实将每个 $\mathbf{d}_{j_h}$ 替换为满足如下条件的光滑紧支撑函数 $\tau_{[-\varepsilon, j^{\max}+\varepsilon]}(j_h)$

$$\tau_{[-\varepsilon, j^{\max}+\varepsilon]}(j_h) = \mathbf{d}_{j_h},\ j_h \in [0, j^{\max}] \ \text{ and } \ \tau_{[-\varepsilon, j^{\max}+\varepsilon]}(j_h) = 0,$$

$$j_h \notin [-\varepsilon, j^{\max} + \varepsilon], \tag{18}$$

for any $0 < \varepsilon < 1/2$. This replacement does not change the value of the amplitude $A(\Delta)$, but now the summand of $\sum_{j_h}$ is smooth and compact support in $j_h$. We apply the Poisson summation formula

对任意 $0 < \varepsilon < 1/2$ 成立。该替换不会改变振幅 $A(\Delta)$ 的值，但此时 $\sum_{j_h}$ 的被加项在 $j_h$ 上是光滑紧支撑的。我们应用泊松求和公式

$$\sum_{n\in\mathbb{Z}} f(n) = \sum_{k\in\mathbb{Z}} \int_{\mathbb{R}} \mathrm{d}n f(n) e^{2\pi i k n}$$

to the spinfoam amplitude. The discrete sum over $j_h$ in $A(\Delta)$ becomes the integral,

针对自旋泡沫振幅。$j_h$ 在 $A(\Delta)$ 中的离散求和变为积分:

$$A(\Delta) = \sum_{\{k_h\in\mathbb{Z}\}} \int_{\mathbb{R}} \prod_h \mathrm{d}j_h \prod_h 2\tau_{[-\varepsilon, j^{\max}+\varepsilon]}(j_h) \int [\mathrm{dg}\,\mathrm{d}\mathbf{z}]\, e^{S^{(k)}},$$

$$S^{(k)} = S + 4\pi i \sum_h j_h k_h \tag{19}$$

By the area spectrum of LQG $\mathfrak{a}_f = 8\pi\gamma G - k\sqrt{j_f(j_f+1)}$, the classical area $\mathfrak{a}_f$ and small $-h$ imply the large spin $j_f \gg 1$. This motivates to understand the large- $j$ regime as the semiclassical regime of the spinfoam model. To probe the semiclassical regime, we scale uniformly the boundary spins $j_b \to \lambda j_b$ with any $\lambda \gg 1$ and make the change of variables for the internal spins $j_h \to \lambda j_h$; at the same time, we also scale $j^{\max}$ by $j^{\max} \to \lambda j^{\max}$. The resulting $A(\Delta)$ is given by

根据 LQG $\mathfrak{a}_f = 8\pi\gamma G - k\sqrt{j_f\left(j_f+1\right)}$ 的面积谱，经典面积 $\mathfrak{a}_f$ 与小 $-h$ 对应大自旋 $j_f \gg 1$。这说明可以将大 $j$ 区域理解为自旋泡沫模型的半经典区域。为探究半经典区域，我们将边界自旋 $j_b \to \lambda j_b$ 按任意 $\lambda \gg 1$ 做均匀标度，对内部自旋 $j_h \to \lambda j_h$ 做变量替换；同时我们也将 $j^{\max}$ 按 $j^{\max} \to \lambda j^{\max}$ 做标度，得到的 $A(\Delta)$ 表示如下:

$$A(\Delta) = \sum_{\{k_h \in \mathbb{Z}\}} \int_{\mathbb{R}} \prod_h \mathrm{d}j_h \prod_h 2\lambda\tau_{[-\varepsilon,\lambda j^{\max}+\varepsilon]}(\lambda j_h) \int [\mathrm{dg}\ \mathrm{d}\mathbf{z}]\, e^{\lambda S^{(k)}},$$

$$S^{(k)} = S + 4\pi i \sum_h j_h k_h \tag{20}$$

where $j_h$ is real and continuous. Each term in $A(\Delta)$ at fixed $\{k_h\}$ is cast into a standard form ready for the stationary phase approximation, in order to explore its semiclassical behavior as $\lambda \gg 1$ .

其中 $j_h$ 为实连续变量。为探究 $\lambda \gg 1$ 下的半经典行为，固定 $\{k_h\}$ 后 $A(\Delta)$ 中的每一项都被改写为适用于稳相近似的标准形式。

## The Flatness Problem

## 平坦性问题

By the stationary phase approximation, each integral in (20) with $\lambda \gg 1$ receives the dominant contributions from solutions of the critical equations

根据稳相近似，式 (20) 中每个含 $\lambda \gg 1$ 的积分的主导贡献来自临界方程的解

$$\mathrm{Re}(S) = \partial_{g_{ve}} S = \partial_{\mathbf{z}_{vf}} S = 0, \tag{21}$$

$$\partial_{j_h} S = 4\pi i k_h,\ k_h \in \mathbb{Z}. \tag{22}$$

We view the integration domain as a real manifold, and the solution inside the integration domain, denoted by $\left\{\mathring{j}_h, \mathring{g}_{ve}, \mathring{\mathbf{z}}_{vf}\right\}$, is refered to as the real critical point.

我们将积分域视为实流形，积分域内的解记为 $\left\{\mathring{j}_h, \mathring{g}_{ve}, \mathring{\mathbf{z}}_{vf}\right\}$，称为实临界点。

Every real solution satisfying the part (21) and a nondegeneracy condition endows a Regge geometry to $\Delta$ [33, 48 − 50] . However, further imposing (22) to these Regge geometries gives the accidental flatness constraint to every deficit angle $\delta_h$ hinged by the internal triangle $h$ [9, 55]

所有满足式 (21) 部分条件和非退化条件的实解都会为 $\Delta$ [33, 48 − 50] 赋予一个里奇几何。然而，对这些里奇几何进一步施加条件 (22) 后，会为内三角形 $h$ [9, 55] 所连接的每个亏缺角 $\delta_h$ 带来额外的平坦性约束

$$\gamma\delta_h = 4\pi k_h,\ k_h \in \mathbb{Z}. \tag{23}$$

The Barbero-Immirzi parameter $\gamma \neq 0$ is finite. When $k_h = 0, \delta_h$ at every internal triangle is zero, so the Regge geometry endowed by the real critical point is flat. If the dominant contribution to $A(\Delta)$ with $\lambda \gg 1$ only came from real critical points, Eq. (23) would imply that only the flat geometry and geometries with $\gamma\delta_h = \pm 4\pi\mathbb{Z}_+$ could contribute dominantly to $A(\Delta)$ , whereas the contributions from generic curved geometries were suppressed. Then the semiclassical behavior of $A(\Delta)$ would fail to be consistent with GR. By the argument in [11,12] and confirmed recently by [47], the resolution of this flatness problem requires to analytically extend the equations (21) and (22) to the complexified variables and solve for the complex critical points, which turn out to encode curved geometries.

巴贝罗-伊 mmirzi 参数 $\gamma \neq 0$ 是有限的。当每个内三角形对应的 $k_h = 0, \delta_h$ 都为零时，实临界点赋予的里奇几何就是平坦的。若带 $\lambda \gg 1$ 的 $A(\Delta)$ 的主导贡献仅来自实临界点，式 (23) 将表明只有平坦几何和带 $\gamma\delta_h = \pm 4\pi\mathbb{Z}_+$ 的几何能对 $A(\Delta)$ 产生主导贡献，一般弯曲几何的贡献会被压低。此时 $A(\Delta)$ 的半经典行为将无法与广义相对论一致。根据文献 [11,12] 的论证，且近期文献 [47] 也证实，该平坦性问题的解决方案需要将方程 (21)(22) 解析延拓到复变量，求解复临界点，而这类临界点恰好能编码弯曲几何。

Before coming to the details about complex critical point, we would like to mention that a generic $\left\{j_h, \mathring{g}_{ve}, \dot{\mathbf{z}}_{vf}\right\}$ can endow discontinuous 4 d orientation to $\Delta$ , i.e., the orientation flips between 4-simplices. Then generally (23) may become $\gamma \sum_{v\in h} s_v \Theta_h(v) = 4\pi k_h$ where $s_v = \pm 1$ labels two possible orientations at each 4-simplex $v$.$\Theta_h(v)$ is the dihedral angle hinged by $h$ in $v$ .

在详细讨论复临界点之前，我们需要指出，一般的 $\left\{j_h, \mathring{g}_{ve}, \dot{\mathbf{z}}_{vf}\right\}$ 可以为 $\Delta$ 赋予不连续的 4 d 定向，即定向在 4-单形之间发生翻转。因此一般来说式 (23) 可写为 $\gamma \sum_{v\in h} s_v \Theta_h(v) = 4\pi k_h$ ，其中 $s_v = \pm 1$ 标记每个 4-单形的两种可能定向，$v.\Theta_h(v)$ 是 $v$ 中由 $h$ 连接的二面角。

## Complex Critical Points

## 复临界点

The argument toward the flatness problem assumes all the dominant contribution to the spinfoam amplitude comes from the real critical point. However, as we will show, the large- $\lambda$ spinfoam amplitude does receive dominant contributions from the complex critical point away from the real integration domain. The complex critical points encode the curved geometries missing in the above argument. Demonstrating this property requires a more refined stationary phase analysis: We come back to the amplitude (20) and separate $M$ internal areas $j_{h_o}$ $(h_o = 1, \cdots, M)$ from other $j_{\bar{h}}$ $\left(\bar{h} = 1, \cdots, F - M\right)$.$F$ is the total number of internal triangles in $\Delta$.$M$ equals to number of internal segments $I$ . The areas $\left\{j_{h_o}\right\}$ are suitably chosen such that we can change variables from the areas $\left\{j_{h_o}\right\}_{h_o=1}^{M}$ to the internal segment-lengths $\{l_I\}_{I=1}^{M}$ (by inverting Heron' s formula (We relate the chosen $M$ areas $\left\{j_{h_o}\right\}$ to $M$ segment-lengths $\{l_I\}$ by Heron' s formula as in the Regge geometry. Inverting the relation between $\left\{j_{h_o}\right\}_{h_o=1}^{M}$ and $\{l_I\}_{I=1}^{M}$ defines the local change of variables $\left(j_{h_o}, j_{\bar{h}}\right) \to (l_I, j_{\bar{h}})$ in a neighborhood of the real critical point. This procedure is just changing variables and

does not impose any restriction.)) in a neighborhood of $\{j_{h_o}\}$ of a real critical point $\left\{\mathring{j}_h, \mathring{g}_{ve}, \mathring{\mathbf{z}}_{vf}\right\}$, and we have $\mathrm{d}^{M+N} j_h = \mathcal{J}_l \, \mathrm{d}^M l_I \, \mathrm{d}^{F-M} j_{\bar{h}}$ where $\mathcal{J}_l$ is the Jacobian.

平直性问题的论证假定，旋度网振幅的所有主导贡献都来自实临界点。但正如我们将要展示的，大 $\lambda$ 旋度网振幅确实会从远离实积分域的复临界点获得主导贡献。复临界点编码了上述论证中遗漏的弯曲几何。要证明这一性质需要更精细的稳相分析: 我们回到振幅 (20)，将 $M$ 个内面积 $j_{h_o}\,(h_o = 1, \cdots, M)$ 与其他面积分离，$j_{\bar{h}}\ \left(\bar{h} = 1, \cdots, F - M\right)$.$F$ 是 $\Delta.M$ 中内三角形的总数，等于内线段的数量 $I$。合理选择面积 $\{j_{h_o}\}$ 后，我们可以通过逆海伦公式将变量从面积 $\{j_{h_o}\}_{h_o=1}^{M}$ 换为内线段长度 $\{l_I\}_{I=1}^{M}$，就像里奇几何中那样，我们通过海伦公式将选定的 $M$ 个面积 $\{j_{h_o}\}$ 与 $M$ 个线段长度 $\{l_I\}$ 关联起来。对 $\{j_{h_o}\}_{h_o=1}^{M}$ 与 $\{l_I\}_{I=1}^{M}$ 的关系求逆，即可在实临界点的邻域内定义局部变量替换 $\left(j_{h_o}, j_{\bar{h}}\right) \to \left(l_I, j_{\bar{h}}\right)$，这个过程只是变量替换，不附加任何限制。该操作可在实临界点 $\left\{\mathring{j}_h, \mathring{g}_{ve}, \mathring{\mathbf{z}}_{vf}\right\}$ 的 $\{j_{h_o}\}$ 邻域内完成，我们得到 $\mathrm{d}^{M+N} j_h = \mathcal{J}_l \, \mathrm{d}^M l_I \, \mathrm{d}^{F-M} j_{\bar{h}}$，其中 $\mathcal{J}_l$ 是雅可比行列式。

$$A(\Delta) = \sum_{\{k_h\}} \int \prod_{I=1}^{M} \mathrm{d}l_I \mathcal{Z}_{\Delta}^{\{k_h\}}(l_I), \tag{24}$$

$$\mathcal{Z}_{\Delta}^{\{k_h\}}(l_I) = \int \prod_{\bar{h}} \mathrm{d}j_{\bar{h}} \prod_{h} \left(2\lambda d_{\lambda j_h}\right) \int [\mathrm{dg}\ \mathrm{d}\mathbf{z}]\, e^{\lambda S^{(k)}} \mathcal{J}_l, \tag{25}$$

The partial amplitude $\mathcal{L}_{\Delta}^{\{k_h\}}$ has the external parameters $r \equiv \{l_I, j_b, \xi_{eb}\}$ including not only the boundary data $j_b, \xi_{eb}$ but also internal segment-lengths $l_I$ . Then we apply the stationary phase analysis for the complex action with parameters [56,57] (The literature [56,57] uses the semi-analytic machinery, since they deal with more generic situation with $S$ being smooth instead of being analytic.) to $\mathcal{L}_{\Delta}^{\{k_h\}}$ : Consider the large- $\lambda$ integral $\int_K e^{\lambda S(r,x)} \mathrm{d}^N x$ and regard $r$ as the external parameter. $S(r,x)$ is an analytic function of $r \in U \subset \mathbb{R}^k, x \in K \subset \mathbb{R}^N$.$U \times K$ is a neighborhood of $\left(\mathring{r}, \mathring{x}\right)$, where $\mathring{x}$ is a real critical point of $S\left(\mathring{r}, x\right)$. We denote by $\mathcal{S}(r,z), z = x + iy \in \mathbb{C}^N$, the analytic extension of $S(r,x)$ to a complex neighborhood of $\mathring{x}$. The complex critical equation is given by $\partial_z \mathcal{S} = 0$, which contains $N$ holomorphic equations for $N$ complex variables. The complex critical equation is solved by $z = Z(r)$ where $Z(r)$ is analytic in $r$ in the neighborhood $U$. When $r = \mathring{r}, Z\left(\mathring{r}\right) = \mathring{x}$ reduces to the real critical point. When $r$ deviates away from $\mathring{r}, Z(r) \in \mathbb{C}^N$ can move away from the real plane $\mathbb{R}^N$, and thus generally $Z(r)$ is called the complex critical point (see Fig. 7b). We have the following large- $\lambda$ asymptotic expansion for the integral

偏振幅 $\mathcal{L}_{\Delta}^{\{k_h\}}$ 的外部参数为 $r \equiv \{l_I, j_b, \xi_{eb}\}$，不仅包含边界数据 $j_b, \xi_{eb}$，还包含内部分段长度 $l_I$。随后我们对带参数复作用量应用稳相分析 [56,57](文献 [56,57] 采用半解析方法，因为它们处理更一般的情形，其中 $S$ 是光滑而非解析的)，分析对象为 $\mathcal{L}_{\Delta}^{\{k_h\}}$ : 考虑大- $\lambda$ 积分 $\int_K e^{\lambda S(r,x)} \mathrm{d}^N x$，将 $r$ 视为外部参数。在 $\left(\mathring{r}, \mathring{x}\right)$ 的邻域内，$S(r,x)$ 是 $r \in U \subset \mathbb{R}^k, x \in K \subset \mathbb{R}^N$.$U \times K$ 的解析函数，其中 $\mathring{x}$ 是 $S\left(\mathring{r}, x\right)$ 的实临界点。我们将 $S(r,x)$ 解析延拓到 $\mathring{x}$ 的复邻域，记为 $\mathcal{S}(r,z), z = x + iy \in \mathbb{C}^N$。复临界方程由 $\partial_z \mathcal{S} = 0$ 给出，它包含 $N$ 个全纯方程对应 $N$ 个复变量，该方程由 $z = Z(r)$ 求解，其中在邻域 $U$ 内 $Z(r)$ 关于 $r$ 解析。当 $r = \mathring{r}, Z\left(\mathring{r}\right) = \mathring{x}$ 时，退化为实临界点。当 $r$ 偏离 $\mathring{r}, Z(r) \in \mathbb{C}^N$ 时，解会偏离实平面 $\mathbb{R}^N$，因此通常将 $Z(r)$ 称为复临界点 (见图 7b)。我们得到该积分如下的大- $\lambda$ 渐近展开

$$\int_K e^{\lambda S(r,x)} \mathrm{d}^N x = \left(\frac{1}{\lambda}\right)^{\frac{N}{2}} \frac{e^{\lambda \mathcal{S}(r, Z(r))}}{\sqrt{\det\left(-\delta_{z,z}^2 \mathcal{S}\left(r, Z(r)\right)/2\pi\right)}} \left[1 + O(1/\lambda)\right] \tag{26}$$

where $\mathcal{S}(r, Z(r))$ and $\delta^2_{z,z}\mathcal{S}(r, Z(r))$ are the action and Hessian at the complex critical point.

其中 $\mathcal{S}(r, Z(r))$ 和 $\delta^2_{z,z}\mathcal{S}(r, Z(r))$ 分别是复临界点处的作用量与黑塞矩阵。

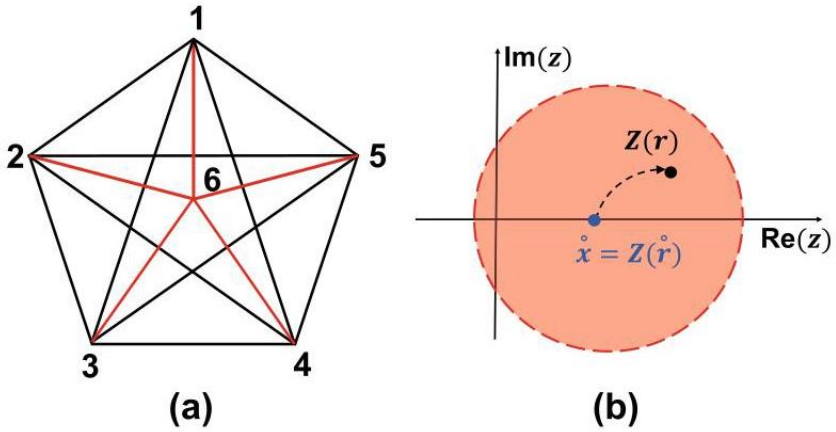


Fig. 7 (a) The triangulation $\sigma_{1-5}$ made by the 1-5 Pachner move dividing a 4-simplex into five 4-simplices. $\sigma_{1-5}$ has ten internal triangles and five internal segments $I = 1, \cdots, 5$ (red). (b) The real and complex critical points $\mathring{x}$ and $Z(r)$ .$\mathcal{S}(r, z)$ is analytic extended from the real axis to the complex neighborhood illustrated by the red disk

图 7 (a) 由 1-5 帕赫纳移动将一个 4-单形划分为五个 4-单形得到的三角剖分 $\sigma_{1-5}$。$\sigma_{1-5}$ 有 10 个内部三角形和 5 条内部分段 $I = 1, \cdots, 5$ (红色)。(b) 实临界点与复临界点 $\mathring{x}$ 和 $Z(r)$ .$\mathcal{S}(r, z)$ 从实轴解析延拓到红盘所示的复邻域

The importance of (26) is that the integral can receive the dominant contribution from the complex critical point away from the real plane. This fact has been overlooked by the argument of the flatness problem. Moreover, Eq. (26) reduces $A(\Delta)$ to the integral

(26) 式的重要性在于，积分可以接收偏离实平面的复临界点的主导贡献。这一事实被平坦性问题的原有论证忽略了。此外，(26) 式将 $A(\Delta)$ 约化为如下积分

$$\left(\frac{1}{\lambda}\right)^{\frac{N}{2}} \int \prod_{I=1}^{M} \mathrm{d}l_I \mathcal{N}_l e^{\lambda \mathcal{S}(r, Z(r))} \left[1 + O(1/\lambda)\right] \tag{27}$$

at each $k_h$.$\mathcal{N}_l \propto \prod_h (4j_h)\, \mathcal{J}_l \left[\det\left(-\delta^2_{z,z}\mathcal{S}/2\pi\right)\right]^{-1/2}$ at $Z(r)$ . Given that $\{l_I\}$ determines the Regge geometry on $\Delta$ , Eq. (27) is a path integral of Regge geometries with the complex effective action $\mathcal{S}$ . The path integral sums over curved geometries. In the following, we make the above general analysis concrete by considering the amplitudes on $\Delta = \Delta_3, \sigma_{1-5}$ , and we compute numerically the complex critical points, which demonstrate the curved geometries in the spinfoam amplitude.

在 $k_h.\mathcal{N}_l \propto \prod_h (4j_h)\,\mathcal{J}_l\left[\det\left(-\delta^2_{z,z}\mathcal{S}/2\pi\right)\right]^{-1/2}$ 的每一处 $Z(r)$。已知 $\{l_I\}$ 决定了 $\Delta$ 上的里奇几何，式 (27) 是带复有效作用量 $\mathcal{S}$ 的里奇几何路径积分。该路径积分对所有弯曲几何求和。在下文中，我们通过考虑 $\Delta = \Delta_3, \sigma_{1-5}$ 上的振幅将上述通用分析具体化，并对复临界点进行数值计算，以此证明自旋泡沫振幅中存在弯曲几何。

## Applications

## 应用

## Asymptotics of $A(\Delta_3)$

## $A(\Delta_3)$ 的渐近行为

The simplicial complex $\Delta_3$ contains three 4-simplices and a single internal triangle $h$. All line segments of $\Delta_3$ are boundary, so $M = 0$ in (24). The Regge geometry $\mathbf{g}$ on $\Delta_3$ is completely fixed by the (Regge-like) boundary data $\{j_b, \xi_{eb}\}$ that uniquely corresponds to the boundary segment-lengths.

单纯复形 $\Delta_3$ 包含三个 4 单形和一个内部三角形 $h$。$\Delta_3$ 的所有线段均在边界上，因此满足 (24) 中的 $M = 0$。$\Delta_3$ 上的里奇几何 $\mathbf{g}$ 完全由 (类里奇的) 边界数据 $\{j_b, \xi_{eb}\}$ 确定，该边界数据与边界边长一一对应。

Following the above general scheme, $r = \{j_b, \xi_{eb}\}$ is the boundary data. $\mathring{r} = \left\{\mathring{j}_b, \mathring{\xi}_{eb}\right\}$ determines the flat geometry, denoted by $\mathbf{g}(\mathring{r})$, with $\delta_h = 0.\mathring{x} = \left\{j_h, \mathring{g}_{ve}, \dot{\mathbf{z}}_{vf}\right\}$ is the real critical point associated to $\mathring{r}$, and it endows the orientations $s_v = +1$ to all 4-simplices. $\mathring{r}, \mathbf{g}\left(\mathring{r}\right)$, and $\mathring{x}$ are computed numerically in [47].

遵循上述一般框架，$r = \{j_b, \xi_{eb}\}$ 为边界数据。$\mathring{r} = \left\{\mathring{j}_b, \mathring{\xi}_{eb}\right\}$ 确定了平坦几何，记为 $\mathbf{g}(\mathring{r})$，其中 $\delta_h = 0.\mathring{x} = \left\{j_h, \mathring{g}_{ve}, \dot{\mathbf{z}}_{vf}\right\}$ 是与 $\mathring{r}$ 关联的实临界点，它为所有 4 单形赋予了定向 $s_v = +1$。文献 [47] 对 $\mathring{r}, \mathbf{g}\left(\mathring{r}\right)$ 和 $\mathring{x}$ 进行了数值计算。

The integration domain of $A(\Delta_3)$ is 124 real dimensional. The local coordinates $x \in \mathbb{R}^{124}$ cover the neighborhood of $\mathring{x}$ inside the integration domain. $S(r, x)$ is the spinfoam action and is analytic in the neighborhood of $\left(\mathring{r}, \mathring{x}\right).z \in \mathbb{C}^{124}$ complexifies $x.\mathcal{S}(r, z)$ extends holomorphically $S(r, x)$ to a complex neighborhood of $\mathring{x}$. Here we only complexify $x$ but do not complexify $r$. We focus on $k_h = 0$, since the integrals with $k_h \neq 0$ have no real critical point when $r = \mathring{r}$ and are still suppressed even when taking into account complex critical points, as far as $\delta_h$ is not close to $4\pi k_h$.

$A(\Delta_3)$ 的积分域是 124 实维的。局部坐标 $x \in \mathbb{R}^{124}$ 覆盖了积分域内 $\mathring{x}$ 的邻域。$S(r, x)$ 是自旋泡沫作用量，在 $\left(\mathring{r}, \mathring{x}\right).z \in \mathbb{C}^{124}$ 邻域内解析，复化 $x.\mathcal{S}(r, z)$ 将 $S(r, x)$ 全纯延拓到 $\mathring{x}$ 的复邻域。此处我们仅对 $x$ 复化，不对 $r$ 复化。我们聚焦于 $k_h = 0$，因为当 $r = \mathring{r}$ 时，带 $k_h \neq 0$ 的积分不存在实临界点，且只要 $\delta_h$ 不接近 $4\pi k_h$，即使考虑复临界点，这类积分依旧被压低。

We deform the boundary data $r = \mathring{r} + \delta r$ to obtain the curved geometries $\mathbf{g}(r)$ with $\delta_h \neq 0$. In practice, we vary the length $l_{26}$ of the line segment connecting the points 2 and 6, while leaving other segment lengths unchanged. A family of (Regge-like) boundary data $r$ parametrized by $l_{26}$ can be constructed numerically and give the family of curved geometries.

我们对边界数据 $r = \mathring{r} + \delta r$ 做形变，得到带 $\delta_h \neq 0$ 的弯曲几何 $\mathbf{g}(r)$。实际操作中，我们改变连接点 2 和点 6 的线段长度 $l_{26}$，保持其他边长不变。我们可以数值构造出由 $l_{26}$ 参数化的一族 (类里奇) 边界数据 $r$，得到弯曲几何族。

At each $r \neq \mathring{r}$, the real critical point is absent. But we are able to find the complex critical point $z = Z(r)$ satisfying $\partial_z \mathcal{S}(r, z) = 0$ with the high-precision numerics. The details about the numerical solution and error analysis are given in [47]. We insert $Z(r)$ into $\mathcal{S}(r, z)$, and we compute numerically the difference between $\mathcal{S}(r, Z(r))$ and the Regge action $\mathcal{I}_R$ of the curved geometry $\mathbf{g}(r)$:

在每个 $r \neq \mathring{r}$ 处，不存在实临界点。但我们通过高精度数值计算找到了满足 $\partial_z \mathcal{S}(r, z) = 0$ 的复临界点 $z = Z(r)$。数值解与误差分析的细节参见文献 [47]。我们将 $Z(r)$ 代入 $\mathcal{S}(r, z)$，通过数值计算得到 $\mathcal{S}(r, Z(r))$ 与弯曲几何 $\mathbf{g}(r)$ 的里奇作用量 $\mathcal{I}_R$ 之间的差值:

$$\delta\mathcal{I}(r) = \mathcal{S}(r, Z(r)) - i\mathcal{I}_R[\mathbf{g}(r)], \tag{28}$$

$$\text{where } \mathcal{I}_R[\mathbf{g}(r)] = \mathfrak{a}_h(r)\,\delta_h(r) + \sum_b \mathfrak{a}_b(r)\,\Theta_b(r)\ . \tag{29}$$

The areas $\mathfrak{a}_h(r), \mathfrak{a}_b(r)$ and deficit/dihedral angles $\delta_h(r), \Theta_b(r)$ are computed from $\mathbf{g}(r)$.

面积 $\mathfrak{a}_h(r), \mathfrak{a}_b(r)$ 与亏缺/二面角 $\delta_h(r), \Theta_b(r)$ 由 $\mathbf{g}(r)$ 计算得到。

We repeat the computation for many $r$'s from varying the length $l_{26}$. The computations give a family of $\delta\mathcal{I}(r)$ with many $r$'s. By the asymptotic formula (26), the dominant contribution from $Z(r)$ to $A(\Delta_3)$ is proportional to $\left|e^{i\lambda\mathcal{S}}\right| = e^{\lambda\,\mathrm{Re}(\mathcal{S})} \leq 1$. As shown in Fig. 8a, c, given any finite $\lambda \gg 1$, there are the curved geometries with small nonzero $|\delta_h|$, such that $|A(\Delta_3)|$ is the same order of magnitude as $|A(\Delta_3)|$ at the flat geometry. The range of allowed $\delta_h$ for nonsuppressed $A(\Delta_3)$ is nonvanishing as far as $\lambda$ is finite. The range of allowed $\delta_h$ is enlarged when $\gamma$ is small, shown in Fig. 8d. The qualitative behavior is similar to the result from the effective spinfoam model in [58]. Moreover, motivated by relating $\delta\mathcal{I}$ to higher curvature terms [11], we find the best polynomial fit of $\delta\mathcal{I}$ in terms of $\delta_h$ (the blue curve in Fig. 8a)

我们对改变长度 $l_{26}$ 得到的多个 $r$ 重复了计算，得到了对应多个 $r$ 的一族 $\delta\mathcal{I}(r)$。根据渐近公式 (26)，$Z(r)$ 对 $A(\Delta_3)$ 的主导贡献与 $\left|e^{i\lambda\mathcal{S}}\right| = e^{\lambda\,\mathrm{Re}(\mathcal{S})} \leq 1$ 成正比。如图 8a、8c 所示，给定任意有限的 $\lambda \gg 1$，存在非零小 $|\delta_h|$ 的弯曲几何，使得 $|A(\Delta_3)|$ 与平坦几何处的 $|A(\Delta_3)|$ 数量级相同。只要 $\lambda$ 有限，未被压制的 $A(\Delta_3)$ 所允许的 $\delta_h$ 取值范围就非零。如图 8d 所示，当 $\gamma$ 较小时，允许的 $\delta_h$ 范围会扩大，其定性行为与文献 [58] 中有效自旋泡沫模型的结果相似。此外，受将 $\delta\mathcal{I}$ 与高阶曲率项关联的启发 [11]，我们得到了 $\delta\mathcal{I}$ 关于 $\delta_h$ 的最佳多项式拟合 (图 8a 中的蓝色曲线)

$$\delta\mathcal{I} = a_2(\gamma)\,\delta_h^2 + a_3(\gamma)\,\delta_h^3 + a_4(\gamma)\,\delta_h^4 + O\left(\delta_h^5\right), \tag{30}$$

For example, at $\gamma = 0.1$ , the best fit coefficient $a_i\,(i = 2, 3, 4)$ and the corresponding fitting errors are $a_2 = -0.00016_{\pm 10^{-17}} - 0.00083_{\pm 10^{-16}} i, a_3 = -0.0071_{\pm 10^{-13}} - 0.011_{\pm 10^{-12}} i, a_4 = -0.059_{\pm 10^{-9}} + 0.070_{\pm 10^{-8}} i$ .

例如，在 $\gamma = 0.1$ 处，最佳拟合系数 $a_i\,(i = 2, 3, 4)$ 和对应的拟合误差为 $a_2 = -0.00016_{\pm 10^{-17}} - 0.00083_{\pm 10^{-16}} i, a_3 = -0.0071_{\pm 10^{-13}} - 0.011_{\pm 10^{-12}} i, a_4 = -0.059_{\pm 10^{-9}} + 0.070_{\pm 10^{-8}} i$ 。

So far we have considered the complex critical point near $\mathring{x}$ with all $s_v = +1$ . Given the boundary data $\mathring{r}$ , there are exactly two real critical points $\mathring{x}$ and $\mathring{x}'$ , where $\mathring{x}'$ corresponds to the same flat geometry but with all orientations $s_v = -1$ . Other six discontinuous orientations (two 4-simplices has plus/minus and the other has minus/plus) do not lead to any real critical point, because they violate the flatness constraint $\gamma\delta_h^s = \gamma \sum_v s_v \Theta_h(v) = 0$ , and $|\delta_h^s|$ is not small for the discontinuous orientation, as it can be checked numerically. Their contribution to $A(\Delta_3)$ is suppressed even when considering the complex critical point. Therefore we only need to focus on the integrals over two real neighborhoods $K, K'$ of $\mathring{x}, \mathring{x}'$ , while the integral outside $K \cup K'$ only gives suppressed contribution to $A(\Delta_3)$ for large $\lambda$ . We carry out a similar analysis as the above for the integral over $K'$ , and we obtain the following asymptotic formula of $A(\Delta_3)$ with $r = \mathring{r} + \delta r$

到目前为止，我们研究了 $\mathring{x}$ 附近所有 $s_v = +1$ 的复临界点。给定边界数据 $\mathring{r}$ ，恰好存在两个实临界点 $\mathring{x}$ 和 $\mathring{x}'$ ，其中 $\mathring{x}'$ 对应相同的平坦几何，但所有取向都为 $s_v = -1$ 。其余六种不连续取向 (两个 4 单形分别为正负/负正组合) 不会产生任何实临界点: 因为它们违反了平坦约束 $\gamma\delta_h^s = \gamma \sum_v s_v \Theta_h(v) = 0$ ，且对于不连续取向，$|\delta_h^s|$ 并不小，这一点可通过数值验证得到。即便考虑复临界点，它们对 $A(\Delta_3)$ 的贡献也是被压低的。因此我们仅需重点关注 $\mathring{x}, \mathring{x}'$ 的两个实邻域 $K, K'$ 上的积分，对大 $\lambda$ 而言，$K \cup K'$ 以外区域的积分对 $A(\Delta_3)$ 仅给出被压低的贡献。我们对 $K'$ 上的积分采用与上文类似的分析，最终得到了含 $r = \mathring{r} + \delta r$ 的 $A(\Delta_3)$ 的如下渐近公式

$$A(\Delta_3) = \left(\frac{1}{\lambda}\right)^{60} e^{i\varphi} \left[\mathcal{N}_+ e^{i\lambda \mathcal{I}_R[\mathbf{g}(r)] + \lambda \delta \mathcal{I}(r)} + \mathcal{N}_- e^{-i\lambda \mathcal{I}_R[\mathbf{g}(r)] + \lambda \delta \mathcal{I}'(r)}\right]$$

$$[1 + O(1/\lambda)] \tag{31}$$

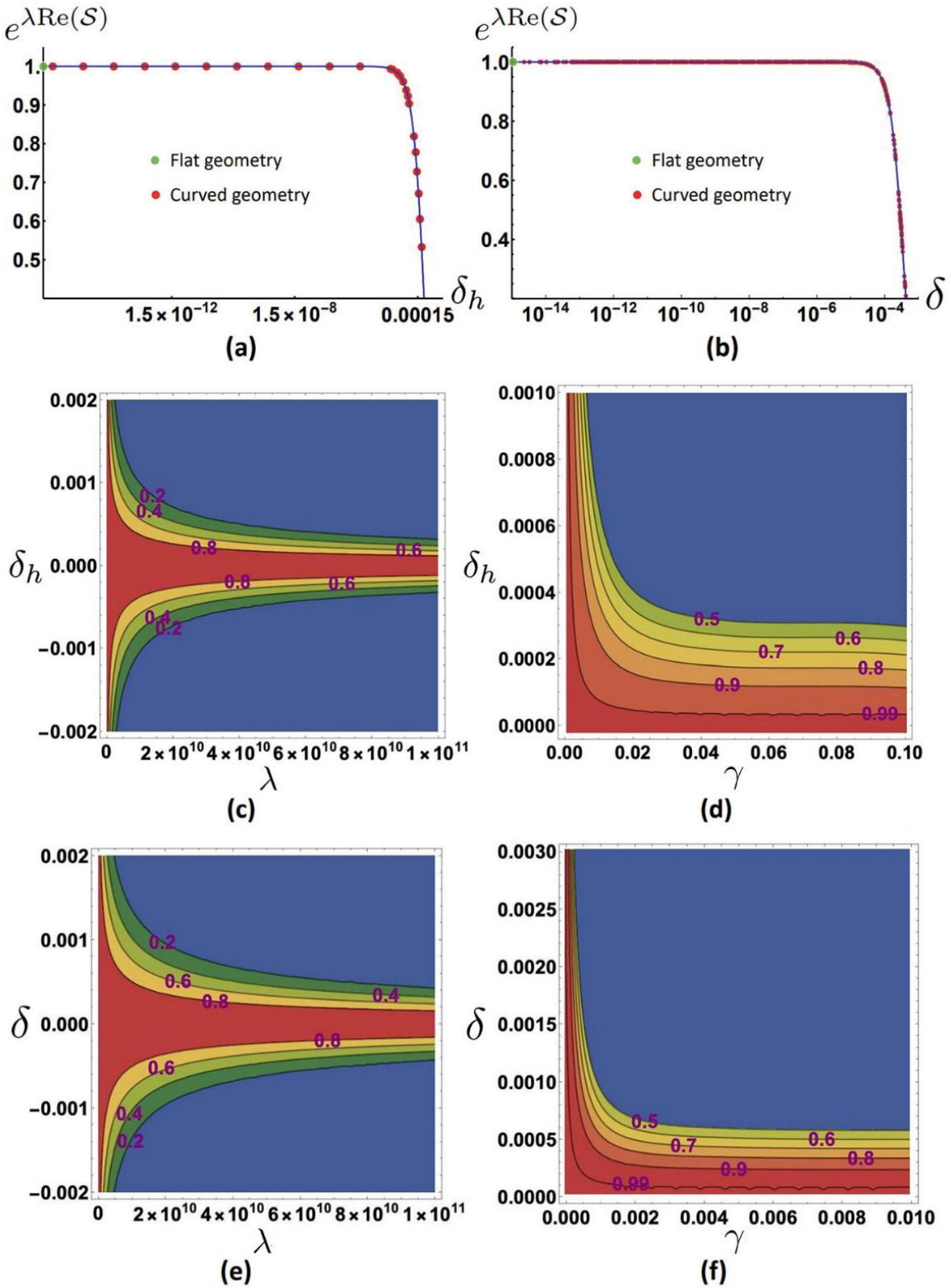


Fig. 8 (a) Plots $e^{\lambda\,\mathrm{Re}(\mathcal{S})}$ versus the deficit angle $\delta_h$ at $\lambda = 10^{11}$ and $\gamma = 0.1$ in $A(\Delta_3)$ and (b) plots $e^{\lambda\,\mathrm{Re}(\mathcal{S})}$ versus the deficit angle $\delta = \sqrt{\frac{1}{10}\sum_{h=1}^{10}\delta_h^2}$ at $\lambda = 10^{11}$ and $\gamma = 1$ in $\mathcal{Z}_{\sigma_{1-5}}$. These two plots show the numerical data of curved geometries (red points) and the best fits (30) and (33) (blue curve). (c) and (d) are the contour

plots of $e^{\lambda\,\mathrm{Re}(\mathcal{S})}$ as functions of $(\lambda,\delta_h)$ at $\gamma=0.1$ and of $(\gamma,\delta_h)$ at $\lambda=5\times10^{10}$ in $A(\Delta_3)$. (e) and (f) are the contour plots of $e^{\lambda\,\mathrm{Re}(\mathcal{S})}$ as functions of $(\lambda,\delta)$ at $\gamma=1$ and of $(\gamma,\delta)$ at $\lambda=5\times10^{10}$ in $\mathcal{Z}_{\sigma_{1-5}}$. They demonstrate the (non-blue) regime of curved geometries where the spinfoam amplitude is not suppressed

图 8 (a) 为 $A(\Delta_3)$ 中 $\lambda=10^{11}$、$\gamma=0.1$ 处 $e^{\lambda\,\mathrm{Re}(\mathcal{S})}$ 相对亏角 $\delta_h$ 的图，(b) 为 $\mathcal{Z}_{\sigma_{1-5}}$ 中 $\lambda=10^{11}$、$\gamma=1$ 处 $e^{\lambda\,\mathrm{Re}(\mathcal{S})}$ 相对亏角 $\delta=\sqrt{\frac{1}{10}\sum_{h=1}^{10}\delta_h^2}$ 的图。这两张图展示了弯曲几何的数值数据 (红点) 以及式 (30) 和 (33) 的最佳拟合 (蓝线)。(c) 和 (d) 分别是 $A(\Delta_3)$ 中 $\gamma=0.1$ 处 $e^{\lambda\,\mathrm{Re}(\mathcal{S})}$ 作为 $(\lambda,\delta_h)$ 的函数、以及 $\lambda=5\times10^{10}$ 处 $e^{\lambda\,\mathrm{Re}(\mathcal{S})}$ 作为 $(\gamma,\delta_h)$ 的函数的等高线图。(e) 和 (f) 分别是 $\mathcal{Z}_{\sigma_{1-5}}$ 中 $\gamma=1$ 处 $e^{\lambda\,\mathrm{Re}(\mathcal{S})}$ 作为 $(\lambda,\delta)$ 的函数、以及 $\lambda=5\times10^{10}$ 处 $e^{\lambda\,\mathrm{Re}(\mathcal{S})}$ 作为 $(\gamma,\delta)$ 的函数的等高线图。它们展示了自旋泡沫振幅不被压低的弯曲几何 (非蓝色) 区域

where $\varphi$ is the overall phase. Two complex critical points near $\mathring{x},\mathring{x}'$, respectively, contribute two terms, with phase plus or minus the Regge action of $\mathbf{g}(r)$ corrected by $\delta\mathcal{I}(r)$ and $\delta\mathcal{I}'(r)=\delta\mathcal{I}(r)^*|_{\delta_h\to-\delta_h}$. $\mathcal{N}_\pm$ is proportional to $\left[\det\left(-\delta^2_{z,z}\mathcal{S}/2\pi\right)\right]^{-1/2}$ evaluated at these two complex critical points.

其中 $\varphi$ 为整体相位。两个分别靠近 $\mathring{x},\mathring{x}'$ 的复临界点贡献两项，相位为经 $\delta\mathcal{I}(r)$ 修正后的 $\mathbf{g}(r)$ 里奇作用量的正负值，且 $\delta\mathcal{I}'(r)=\delta\mathcal{I}(r)^*|_{\delta_h\to-\delta_h}$。$\mathcal{N}_\pm$ 正比于这两个复临界点处求值得到的 $\left[\det\left(-\delta^2_{z,z}\mathcal{S}/2\pi\right)\right]^{-1/2}$。

Known as the cosine problem, there has been the naive guess $A(\Delta_3)\sim\left(\mathcal{N}_1e^{i\lambda\mathcal{I}_R}+\mathcal{N}_2e^{-i\lambda\mathcal{I}_R}\right)^3$ (each factor is from the vertex amplitude), whose expansion gave eight terms corresponding to all possible orientations (see, e.g., [41]). But Eq. (31) demonstrates that $A(\Delta_3)$ only contains two terms corresponding to the continuous orientations.

这就是所谓的余弦问题，此前一直有观点推测 $A(\Delta_3)\sim\left(\mathcal{N}_1e^{i\lambda\mathcal{I}_R}+\mathcal{N}_2e^{-i\lambda\mathcal{I}_R}\right)^3$ (每个因子都来自顶点振幅)，展开后得到对应所有可能定向的八项 (例如参见文献 [41])。但式 (31) 表明，$A(\Delta_3)$ 仅包含对应连续定向的两项。

## 1-5 Pachner Move

## 1-5 帕克纳移动

$\sigma_{1-5}$ is the complex of the 1-5 Pachner move for refining one 4-simplex into five 4-simplices. $\sigma_{1-5}$ has five internal segments (see Fig.7a), so $M=5$ in (24), in contrast to $\Delta_3$, where all segments are on the boundary. There are ten internal triangles $h$ in $\sigma_{1-5}$. The integrals in the partial amplitude $\mathcal{L}_{\sigma_{1-5}}$ have the external parameters $r\equiv\{l_I,j_b,\xi_{eb}\}$ including not only the boundary data $j_b,\xi_{eb}$ but also internal segment-lengths $l_I\,(I=1,\cdots,5)$. We set $\mathring{r}\equiv\{l_I,j_b,\xi_{eb}\}$ determining all internal and boundary segment-lengths of the flat geometry $\mathbf{g}\left(\mathring{r}\right)$ on $\sigma_{1-5}$. Here we still focus on $k_h=0$, and we find in $\mathcal{L}_{\sigma_{1-5}}$ the non-degenerate real critical point $\mathring{x}=\left\{\mathring{j}_{\bar{h}},\mathring{g}_{ve},\mathring{\mathbf{z}}_{vf}\right\}$ corresponding to the flat geometry with all $s_v=1$.

$\sigma_{1-5}$ 是将 1 个 4 单形细分为 5 个 4 单形的 1-5 帕克纳移动复形。$\sigma_{1-5}$ 包含 5 条内边 (见图 7a)，因此对应 (24) 式中的 $M=5$，这与所有边都在边界上的 $\Delta_3$ 不同。$\sigma_{1-5}$ 中存在 10 个内部三角形 $h$。偏振幅 $\mathcal{L}_{\sigma_{1-5}}$ 中的积分带有外部参数 $r\equiv\{l_I,j_b,\xi_{eb}\}$，这些参数不仅包含边界数据 $j_b,\xi_{eb}$，还包含内部边长 $l_I\,(I=1,\cdots,5)$。我们设定 $\mathring{r}\equiv\{l_I,j_b,\xi_{eb}\}$，确定出 $\sigma_{1-5}$ 上平直几何 $\mathbf{g}\left(\mathring{r}\right)$ 的所有内部和边界边长。本文我们仍聚焦于 $k_h=0$，并在 $\mathcal{L}_{\sigma_{1-5}}$ 中找到了对应所有满足条件的 $s_v=1$ 构成的平直几何的非简并实临界点 $\mathring{x}=\left\{\mathring{j}_{\bar{h}},\mathring{g}_{ve},\mathring{\mathbf{z}}_{vf}\right\}$。

There are the local coordinates $x\in\mathbb{R}^N$ covering the neighborhood $K$ of $\mathring{x}$. We analytically continue the spinfoam action $S(r,x)$ to $\mathcal{S}(r,z)$, where $z\in\mathbb{C}^N$, and we fix the boundary data and deform the internal lengths $l_I=\dot{l}_I+\delta l_I$, so that $r=\left\{l_I,\dot{j}_b,\dot{\xi}_{eb}\right\}\equiv r_l$ give curved geometries $\mathbf{g}(r_l)$. As in (26), the dominant contribution to $A(\sigma_{1-5})$ from the complex critical point $Z(r_l)$ is given by

存在局部坐标 $x\in\mathbb{R}^N$ 覆盖 $\mathring{x}$ 的邻域 $K$。我们将自旋泡沫作用量 $S(r,x)$ 解析延拓到 $\mathcal{S}(r,z)$ (其中 $z\in\mathbb{C}^N$)，接着固定边界数据，对内部边长 $l_I=\dot{l}_I+\delta l_I$ 做形变，从而让 $r=\left\{l_I,\dot{j}_b,\dot{\xi}_{eb}\right\}\equiv r_l$ 对应弯曲几何 $\mathbf{g}(r_l)$。和 (26) 式一样，复临界点 $Z(r_l)$ 对 $A(\sigma_{1-5})$ 的主导贡献由下式给出:

$$\left(\frac{1}{\lambda}\right)^{\frac{155}{2}}\int\prod_{I=1}^{5}\mathrm{d}l_I\mathcal{M}e^{\lambda\mathcal{S}(r_l,Z(r_l))}\left[1+O(1/\lambda)\right]. \tag{32}$$

This formula reduces $A(\sigma_{1-5})$ to the integral over Regge geometries $\mathbf{g}(r_l)$. $\mathcal{M}_1$ is proportional to $\prod_h(4j_h)\mathcal{J}_l\left[\det\left(-\delta^2_{z,z}\mathcal{S}/2\pi\right)\right.$ at $Z(r_l)$. The numerical result of $\left|e^{i\lambda\mathcal{S}}\right|=e^{\lambda\,\mathrm{Re}(\mathcal{S})}$ is presented in Fig. 8b, e, f, which demonstrate curved geometries with small $|\delta_h|$ do not lead to the suppression of $\mathcal{Z}_{\sigma_{1-5}}(l_I)$. Moreover $\mathcal{S}(r_l,Z(r_l))$ in (32) is numerically fit by

该公式将 $A(\sigma_{1-5})$ 约化为对雷杰几何的积分，$\mathbf{g}(r_l)$. $\mathcal{M}_1$ 在 $Z(r_l)$ 处与 $\prod_h(4j_h)\mathcal{J}_l\left[\det\left(-\delta^2_{z,z}\mathcal{S}/2\pi\right)\right]^{-1/2}$ 成正比。$\left|e^{i\lambda\mathcal{S}}\right|=e^{\lambda\,\mathrm{Re}(\mathcal{S})}$ 的数值结果展示在图 8b、e、f 中，结果表明小 $|\delta_h|$ 的弯曲几何不会导致 $\mathcal{Z}_{\sigma_{1-5}}(l_I)$ 被压低。此外，(32) 式中的 $\mathcal{S}(r_l,Z(r_l))$ 可通过数值拟合为

$$\mathcal{S}(r_l,Z(r_l))=-i\mathcal{I}_R\left[\mathbf{g}(r_l)\right]-a_2(\gamma)\,\delta(r_l)^2+O\left(\delta^3\right), \tag{33}$$

where $\delta(r_l)=\sqrt{\frac{1}{10}\sum_{h=1}^{10}\delta_h(r_l)^2}$ and $a_2=8.88\times10^{-5}_{\pm10^{-12}}-i0.033_{\pm10^{-10}}$ at $\gamma=1.\mathcal{I}_R\left[\mathbf{g}(r_l)\right]$ is the Regge action of $\mathbf{g}(r_l)$. Some more detailed analysis is given in [47].

其中 $\delta(r_l)=\sqrt{\frac{1}{10}\sum_{h=1}^{10}\delta_h(r_l)^2}$ 和 $a_2=8.88\times10^{-5}_{\pm10^{-12}}-i0.033_{\pm10^{-10}}$ 在 $\gamma=1.\mathcal{I}_R\left[\mathbf{g}(r_l)\right]$ 处的作用量就是 $\mathbf{g}(r_l)$ 的里奇作用量。更多详细分析参见文献 [47]。

## Spinfoam Propagator and Lefschetz Thimble

## 自旋泡沫传播子与莱夫谢茨 thimble

## The Lefschetz Thimble and Algorithm

## 莱夫谢茨流形与算法

As shown in section "Integral Representation of Spinfoam Amplitude," the spin-foam action $S$ is complex valued. As a result, the integrands in (19) are highly oscillatory, especially when $\lambda$ is large. This fact plagues the attempts to use the conventional Monte Carlo method to compute the amplitude and observables in spin-foam. In this section, we review how to use Picard-Lefschetz theory to transform these types of integrals with complex actions to non-oscillatory integrals (see, e.g., [15,59]) for detailed reviews). We summarize the framework presented in [16] that combines the thimble and Markov-Chain Monte Carlo (MCMC) methods which can compute the expectation value of observables when the action is complex valued.

正如“自旋泡沫振幅的积分表示”一节所示，自旋泡沫作用量 $S$ 是复值的。因此，式 (19) 中的被积函数存在高度振荡性，当 $\lambda$ 较大时尤为明显。这一问题阻碍了人们使用传统蒙特卡洛方法计算自旋泡沫中的振幅和可观测量。本节中，我们将回顾如何利用皮卡-莱夫谢茨理论将这类带复作用量的积分转化为非振荡积分 (详细综述参见例如文献 [15,59])。我们总结文献 [16] 提出的框架，该框架结合了流形方法与马尔可夫链蒙特卡洛 (MCMC) 方法，可在作用量为复值时计算可观测量的期望值。

## Picard-Lefschetz Theory and Lefschetz Thimbles

## 皮卡德-勒施切茨理论与勒施切茨 thimble

The Lefschetz thimble method is a high-dimensional generalization of the saddle point integration along the steepest descent (SD) paths. We start from a multidimensional integral, which takes the general form

勒施切茨 thimble 方法是最速下降 (SD) 路径鞍点积分的高维推广。我们从具有如下一般形式的多维积分出发

$$A = \int \mathrm{d}^n x f(\mathbf{x}) \, \mathrm{e}^{-S(\mathbf{x})}, \tag{34}$$

with $S(\mathbf{x})$ complex valued. The starting point is to analytically continue both $f(\mathbf{x})$ and $S(\mathbf{x})$ to holomorphic functions $\widehat{f}(\mathbf{z})$ and $\hat{S}(\mathbf{z})$ . Equation (34) becomes an integral of analytic functions $\widehat{f}(\mathbf{z})$ and $\hat{S}(\mathbf{z})$ of complex variables on the real domain

其中 $S(\mathbf{x})$ 为复值。第一步是将 $f(\mathbf{x})$ 和 $S(\mathbf{x})$ 都解析延拓为全纯函数 $\widehat{f}(\mathbf{z})$ 和 $\hat{S}(\mathbf{z})$ 。式 (34) 变为实定义域上复变量解析函数 $\widehat{f}(\mathbf{z})$ 和 $\hat{S}(\mathbf{z})$ 的积分

$$A = \int_{\mathbb{R}^n} \mathrm{d}^n z \widehat{f}(\mathbf{z}) \, \mathrm{e}^{-\widehat{S}(\mathbf{z})}, \tag{35}$$

where $\mathrm{d}^n z \widehat{f}(\mathbf{z}) \, \mathrm{e}^{-\widehat{S}(\mathbf{z})}$ is a holomorphic $n$ -form restricted on $\mathbb{R}^n$ .

其中 $\mathrm{d}^n z \widehat{f}(\mathbf{z}) \, \mathrm{e}^{-\widehat{S}(\mathbf{z})}$ 是限制在 $\mathbb{R}^n$ 上的全纯 $n$ -形式。

The Picard-Lefschetz theory shows that the integral $A$ can be decomposed into a linear combination of integrals over real $n$ -dimensional integral cycles $\mathcal{J}_\sigma, \sigma = 1, 2, 3, \cdots$ on the complex domain

皮卡德-勒施切茨理论表明，积分 $A$ 可以分解为复定义域上实 $n$ 维积分圈 $\mathcal{J}_\sigma, \sigma = 1, 2, 3, \cdots$ 上积分的线性组合

$$\int_{\mathbb{R}^n} \mathrm{d}^n z \widehat{f}(\mathbf{z}) \mathrm{e}^{-\widehat{S}(\mathbf{z})} = \sum_\sigma n_\sigma \int_{\mathcal{J}_\sigma} \mathrm{d}^n z \widehat{f}(\mathbf{z}) \mathrm{e}^{-\widehat{S}(\mathbf{z})}, \tag{36}$$

where $\sum_\sigma n_\sigma \mathcal{J}_\sigma$ with weights $n_\sigma$ is homologically equivalent to $\mathbb{R}^n$ . The $n$ - dimensional real sub-manifolds $\{\mathcal{J}_\sigma\}$ , called Lefschetz thimbles, present a good basis of relative homology group for the integral (34) [60]. Each $\mathcal{J}_\sigma$ is attached to a critical point $p_\sigma$ satisfying $\partial_z \hat{S}(p_\sigma) = 0$ in the complex space (We do not impose $\mathrm{Re}\left(\hat{S}\right) = 0$ for critical points in the complex space.), as a union of SD paths that are solutions to the SD equations

其中带权 $n_\sigma$ 的 $\sum_\sigma n_\sigma \mathcal{J}_\sigma$ 与 $\mathbb{R}^n$ 同调等价。$n$ 维实子流形 $\{\mathcal{J}_\sigma\}$ 被称为勒施切茨 thimble，它为积分 (34) 提供了相对同调群的一组好基 [60]。每个 $\mathcal{J}_\sigma$ 都对应复空间中满足 $\partial_z \hat{S}(p_\sigma) = 0$ 的临界点 $p_\sigma$ (我们不对复空间中的临界点强加 $\mathrm{Re}\left(\hat{S}\right) = 0$ )，它是最速下降方程的解即所有最速下降路径的并

$$\frac{\mathrm{d}z^a}{\mathrm{d}t} = -\frac{\overline{\partial \hat{S}(\mathbf{z})}}{\partial \overline{z^a}}. \tag{37}$$

Here we call $t$ the flow time. Any points on the thimble will fall to the critical point $p_\sigma$ after flowing for infinitely long time. Following (37), $\mathrm{Re}\left(\hat{S}\right)$ monotonically decreases along each SD path and approaches its minimum at the critical point $p_\sigma$ in the limit $t \to \infty$ , while $\mathrm{Im}\left(\hat{S}\right)$ is a constant along the path. Thus, on each thimble $\mathcal{J}_\sigma$ , the original integral becomes a non-oscillatory integral times a constant phase $\mathrm{e}^{-i\,\mathrm{Im}\left(\widehat{S}(p_\sigma)\right)}$,

我们在此称 $t$ 为流时间。thimble 上任意点经过无穷长时间流后都会落到临界点 $p_\sigma$ 。根据式 (37), $\mathrm{Re}\left(\hat{S}\right)$ 沿每条最速下降路径单调递减，在 $t \to \infty$ 极限下于临界点 $p_\sigma$ 处达到最小值，同时 $\mathrm{Im}\left(\hat{S}\right)$ 沿路径保持常数。因此，在每个 thimble $\mathcal{J}_\sigma$ 上，原积分变为非振荡积分乘以常数相位 $\mathrm{e}^{-i\,\mathrm{Im}\left(\widehat{S}(p_\sigma)\right)}$,

$$\int_{\mathcal{J}_\sigma} \mathrm{d}^n z \widehat{f}(\mathbf{z}) \mathrm{e}^{-\widehat{S}(\mathbf{z})} = \mathrm{e}^{-i\,\mathrm{Im}\left(\widehat{S}(p_\sigma)\right)} \int_{\mathcal{J}_\sigma} \mathrm{d}^n z \widehat{f}(\mathbf{z}) \mathrm{e}^{-\,\mathrm{Re}\left(\widehat{S}(\mathbf{z})\right)}. \tag{38}$$

On each thimble $\mathcal{J}_\sigma, \mathrm{Re}\left(\hat{S}\right)$ grows when moving far away from the critical point, so the integrand is exponentially suppressed at infinity.

在每个 thimble 上，当远离临界点时 $\mathcal{J}_\sigma, \mathrm{Re}\left(\hat{S}\right)$ 增长，因此被积函数在无穷远被指数压制。

Using the Lefschetz thimble basis $\{\mathcal{J}_\sigma\}$ , the integral (36) is valid for a specific set $\{n_\sigma\}$ of the weights of the thimbles. Consider $\widehat{f}$ as an observable. The expectation value $\langle f \rangle$ is given by

利用勒施切茨 thimble 基 $\{\mathcal{J}_\sigma\}$，积分 (36) 对一组特定的 thimble 权集合 $\{n_\sigma\}$ 成立。将 $\widehat{f}$ 视为一个可观测量，其期望值 $\langle f \rangle$ 由下式给出

$$\langle f\rangle = \frac{\int_{\mathbb{R}^n} \mathrm{d}^n z \widehat{f}(\mathbf{z})\, \mathrm{e}^{-\widehat{S}(\mathbf{z})}}{\int_{\mathbb{R}^n} \mathrm{d}^n z \mathrm{e}^{-\widehat{S}(\mathbf{z})}} = \frac{\sum_\sigma n_\sigma \int_{\mathcal{J}_\sigma} \mathrm{d}^n z \widehat{f}(\mathbf{z})\, \mathrm{e}^{-\widehat{S}(\mathbf{z})}}{\sum_\sigma n_\sigma \int_{\mathcal{J}_\sigma} \mathrm{d}^n z \mathrm{e}^{-\widehat{S}(\mathbf{z})}}. \tag{39}$$

A weight $n_\sigma$ is the intersection number between the original integration cycle $\mathbb{R}^n$ and the manifold of the steepest ascent (SA) paths which are solutions to the SA equations

权 $n_\sigma$ 是原积分圈 $\mathbb{R}^n$ 与最速上升 (SA) 方程的解即最速上升路径流形之间的相交数

$$\frac{\mathrm{d}z^a}{\mathrm{d}t} = \overline{\frac{\partial \hat{S}(\mathbf{z})}{\partial \overline{z^a}}}. \tag{40}$$

Contrary to the SD path, along each SA path, $\mathrm{Re}\left(\hat{S}\right)$ monotonically increases and approaches the maximum at the critical point when $t \to \infty$, with $\mathrm{Im}\left(\hat{S}\right)$ being conserved. Computing these weights is challenging in general (see, e.g., [61,62] for some recent progresses). Nevertheless, in the case where one of the thimbles $\mathcal{J}_{\sigma'}$ dominates the integral, we may neglect the contribution of other thimbles and re-express (39) as

与最速下降路径不同，沿每条最速上升路径，$\mathrm{Re}\left(\hat{S}\right)$ 单调递增，并在临界点达到最大值，此时满足 $t \to \infty$，且 $\mathrm{Im}\left(\hat{S}\right)$ 守恒。一般而言计算这些权重颇具挑战性 (相关最新进展参见例如文献 [61,62])。但如果其中一个留霍夫特纤维 $\mathcal{J}_{\sigma'}$ 主导积分，我们可以忽略其他留霍夫特纤维的贡献，将式 (39) 重新写为

$$\langle f\rangle \simeq \frac{n_{\sigma'} \mathrm{e}^{-\mathrm{i}\,\mathrm{Im}(S(p_{\sigma'}))} \int_{\mathcal{J}_{\sigma'}} \mathrm{d}^n z \widehat{f}(\mathbf{z})\, \mathrm{e}^{-\mathrm{Re}\left(\widehat{S}(\mathbf{z})\right)}}{n_{\sigma'} \mathrm{e}^{-\mathrm{i}\,\mathrm{Im}(S(p_{\sigma'}))} \int_{\mathcal{J}_{\sigma'}} \mathrm{d}^n z \mathrm{e}^{-\mathrm{Re}\left(\widehat{S}(\mathbf{z})\right)}} = \frac{\int_{\mathcal{J}_{\sigma'}} \mathrm{d}^n z \widehat{f}(\mathbf{z})\, \mathrm{e}^{-\mathrm{Re}\left(\widehat{S}(\mathbf{z})\right)}}{\int_{\mathcal{J}_{\sigma'}} \mathrm{d}^n z \mathrm{e}^{-\mathrm{Re}\left(\widehat{S}(\mathbf{z})\right)}}, \tag{, 41}$$

which can be considered as a mean value under a sampling on the thimble $\mathcal{J}_{\sigma'}$ with a Boltzmann factor $\mathrm{e}^{-\mathrm{Re}\left(\widehat{S}(\mathbf{z})\right)}$. Then, it is possible to use the MCMC method to numerically compute $\langle f\rangle$ in such case.

该式可理解为在留霍夫特纤维 $\mathcal{J}_{\sigma'}$ 上以玻尔兹曼因子 $\mathrm{e}^{-\mathrm{Re}\left(\widehat{S}(\mathbf{z})\right)}$ 采样得到的平均值，这种情况下就可以使用马尔可夫链蒙特卡洛方法对 $\langle f\rangle$ 进行数值计算。

## Thimbles Generated by Flows

## 由流生成的临界点套

As the first step to applying the above Lefschetz thimble technique, we need to identify the Lefschetz thimble $\mathcal{J}_\sigma$ associated with a given critical point $p_\sigma$ (Fig. 9a). By definition, one might try to decide if a point is on the thimble by checking if it falls to $p_\sigma$ at $t \to \infty$ under the SD equation. However, it is really hard in practice due to the infinite flow time. It is also problematic to use the SA equation with $p_\sigma$ as the initial point to generate the thimble since $p_\sigma$ is a fixed point of the SA equation.

作为应用上述莱夫谢茨套技术的第一步，我们需要确定与给定临界点 $p_\sigma$ 关联的莱夫谢茨套 $\mathcal{J}_\sigma$ (图 9a)。根据定义，人们可以尝试通过检查该点是否满足最速下降 (SD) 方程，在 $t \to \infty$ 时流向 $p_\sigma$ ，来判断它是否位于该套上。但由于流时间是无穷大，这在实际操作中十分困难。而以 $p_\sigma$ 为初始点通过最速上升 (SA) 方程生成套的方案也存在问题，因为 $p_\sigma$ 是 SA 方程的不动点。

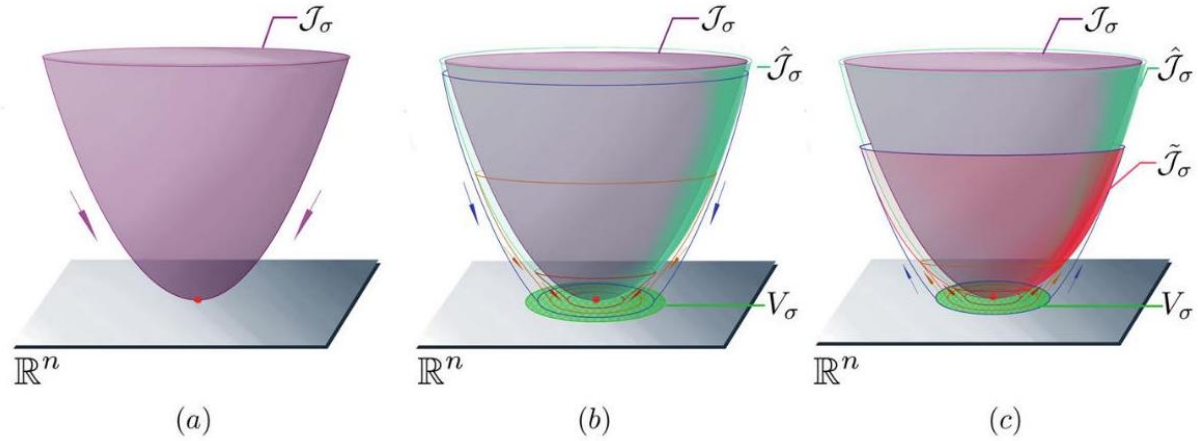


Fig. 9 (a) A Lefschetz thimble $\mathcal{J}_\sigma$ (purple surface) is the union of all the SD paths falling to the critical point $p_\sigma$ (red dot) when $t \to \infty$ . (b) $\hat{\mathcal{J}}_\sigma$ (green transparent surface) is defined as the union of points that flow to $V_\sigma$ (green disk at the bottom) by the SD equation when $t \to \infty$ . The cross-sections of $\widehat{\mathcal{J}_\sigma}$ (illustrated by the blue, yellow, and red circles in $\widehat{\mathcal{J}_\sigma}$ ) flow to the cross-sections in $V_\sigma$ (blue, yellow, and red circles in the green disk). (c) $\tilde{\mathcal{J}}_\sigma$ (red transparent surface) is generated by upward flows from each point in $V_\sigma$ with a finite time by the SA equation. The cross-sections in $V_\sigma$ (blue, yellow, and red circles in the green disk) flow upward to the cross-sections in $\widetilde{\mathcal{L}_\sigma}$ (blue, yellow, and red circles in $\tilde{\mathcal{J}}_\sigma$ )

图 9 (a) 莱夫谢茨套 $\mathcal{J}_\sigma$ (紫色曲面) 是所有在 $t \to \infty$ 时流向临界点 $p_\sigma$ (红点) 的 SD 路径的并集。(b) $\hat{\mathcal{J}}_\sigma$ (绿色透明曲面) 定义为满足 SD 方程，在 $t \to \infty$ 时流向 $V_\sigma$ (底部绿色圆盘) 的所有点的并集。$\widehat{\mathcal{J}_\sigma}$ 的截面 (图中 $\widehat{\mathcal{J}_\sigma}$ 内的蓝、黄、红圆) 流向 $V_\sigma$ 内的截面 (绿色圆盘内的蓝、黄、红圆)。(c) $\tilde{\mathcal{J}}_\sigma$ (红色透明曲面) 由 SA 方程在有限时间内对 $V_\sigma$ 中每个点做向上流生成。$V_\sigma$ 内的截面 (绿色圆盘内的蓝、黄、红圆) 向上流向 $\widetilde{\mathcal{L}_\sigma}$ 内的截面 ( $\tilde{\mathcal{J}}_\sigma$ 内的蓝、黄、红圆)

We follow the method reviewed in [15] to bypass the difficulty of generating the thimble $\mathcal{J}_\sigma$ numerically. The trick is, instead of $p_\sigma$ itself, we consider a small real $n$ -dimensional neighborhood $V_\sigma$ of $p_\sigma$ and a slightly different integration cycle denoted by $\widehat{\mathcal{J}_\sigma}$ (Fig. 9b), which is the union of solutions to the SD equations (37) falling to $V_\sigma$ at $t \to \infty$.$\widetilde{\mathcal{L}_\sigma}$ is a good approximation of the true thimble $\mathcal{J}_\sigma$ when the size of $V_\sigma$ is small enough, and it approaches $\mathcal{J}_\sigma$ when $V_\sigma$ shrinks to the critical point $p_\sigma$ . Since the integrand is analytic, and $\widehat{\mathcal{J}_\sigma}$ is a deformation of $\mathcal{J}_\sigma$ , the integral

我们采用文献 [15] 中回顾的方法来绕过数值生成顶针 $\mathcal{J}_\sigma$ 的困难。诀窍在于，我们不考虑 $p_\sigma$ 本身，而是考虑 $p_\sigma$ 的一个小的实 $n$ 维邻域 $V_\sigma$ 以及一个稍有不同的积分循环，记为 $\widehat{\mathcal{J}_\sigma}$ (图 9b)，它是在 $t \to \infty$.$\widetilde{\mathcal{L}_\sigma}$ 处落入 $V_\sigma$ 的 SD 方程 (37) 的解的并集。当 $V_\sigma$ 的尺寸足够小时，它是真实顶针 $\mathcal{J}_\sigma$ 的一个很好的近似，并且当 $V_\sigma$ 收缩到临界点 $p_\sigma$ 时，它趋近于 $\mathcal{J}_\sigma$ 。由于被积函数是解析的，且 $\widehat{\mathcal{J}_\sigma}$ 是 $\mathcal{J}_\sigma$ 的一个形变，所以积分

$$\int_{\widehat{\mathcal{J}_\sigma}} d^n z f(\mathbf{z}) e^{-\widehat{S}(\mathbf{z})} \tag{42}$$

is the same as (38). However, in this case the above integral becomes oscillatory in contrast to the integral on $\mathcal{J}_\sigma$, as $\mathrm{Im}(\hat{S})$ is no longer constant in $\widehat{\mathcal{J}_\sigma}$. If $V_\sigma$ is small enough, we can control the fluctuation of the $\mathrm{Im}(\hat{S})$ on $\widehat{\mathcal{L}_\sigma}$, such that it is still small and the oscillation of the integral is weak enough to keep the Monte Carlo method accurate.

与式 (38) 相等。但在此情形下，因为 $\mathrm{Im}(\hat{S})$ 在 $\widehat{\mathcal{J}_\sigma}$ 中不再是常数，该积分和 $\mathcal{J}_\sigma$ 上的积分不同，会出现振荡。如果 $V_\sigma$ 足够小，我们可以控制 $\widehat{\mathcal{L}_\sigma}$ 上 $\mathrm{Im}(\hat{S})$ 的涨落，使其涨落仍然很小，积分的振荡足够弱，从而保证蒙特卡罗方法的精度。

Since infinite time evolution is involved, finding the entire $\widehat{\mathcal{L}_\sigma}$ is still not numerically practical. A practical integral cycle $\tilde{\mathcal{J}}_\sigma$ is the union of the paths which are solutions to the SD equations (37) falling to $V_\sigma$ at some finite but sufficiently long flow time $T$. The thimble $\tilde{\mathcal{J}}_\sigma$ approaches $\hat{\mathcal{J}}_\sigma$ in the limit $T \to \infty$. Similar to the method in [61], we can find the approximation $\tilde{\mathcal{J}}_\sigma$ as an inverse process using SA flows. We firstly choose a small real $n$-dimensional neighborhood $V_\sigma$ of the critical point $p_\sigma$ and then generate the upward flows from $V_\sigma$ according to the SA equation with a finite time $T$. The endpoints of these flows form the real $n$ - dimensional manifold $\tilde{\mathcal{J}}_\sigma$ (Fig.9c). Due to the finite flow time, the thimble $\tilde{\mathcal{J}}_\sigma$ does not reach the infinity of the Lefschetz thimble $\mathcal{J}_\sigma$. Its size depends on the choice of flow time $T$.

由于涉及无穷时间演化，在数值上求出完整的 $\widehat{\mathcal{L}_\sigma}$ 仍然不可行。一个实用的积分周线 $\tilde{\mathcal{J}}_\sigma$ 是最速下降方程 (37) 的解路径的并集，这些路径在有限但足够长的流时间 $T$ 下汇聚到 $V_\sigma$。在极限 $T \to \infty$ 下，积分周线 $\tilde{\mathcal{J}}_\sigma$ 会趋近 $\hat{\mathcal{J}}_\sigma$。类似文献 [61] 中的方法，我们可以利用 SA 流将近似 $\tilde{\mathcal{J}}_\sigma$ 作为逆过程求解。我们首先在临界点 $p_\sigma$ 处选取一个小的实 $n$ 维邻域 $V_\sigma$，再根据 SA 方程从 $V_\sigma$ 出发生成有限时间 $T$ 的升流。这些流的端点构成了实 $n$ 维流形 $\tilde{\mathcal{J}}_\sigma$ (图 9c)。由于流时间有限，该周线 $\tilde{\mathcal{J}}_\sigma$ 无法延伸到莱夫谢茨 thimble $\mathcal{J}_\sigma$ 的无穷远处，其大小取决于流时间 $T$ 的选取。

As a summary, the approximation of $\mathcal{J}_\sigma$ is illustrated in the following diagram:

综上所述，$\mathcal{J}_\sigma$ 的近似说明如下图所示:

$$\mathcal{J}_\sigma \xrightarrow{\mathrm{Fix}\, V_\sigma} \widehat{\mathcal{J}_\sigma} \xrightarrow{\mathrm{Fix}\, T} \tilde{\mathcal{J}}_\sigma$$

In the first step, we use the $\widehat{\mathcal{Y}_\sigma}$ as the union of all the SD paths falling to $V_\sigma$ to approximate $\mathcal{J}_\sigma$. The size of $V_\sigma$ can be set by a tolerance $\mathcal{E}$ of the fluctuation of the $\mathrm{Im}(\hat{S})$ around $\mathrm{Im}\left(S(\hat{p}_\sigma) \text{ on } \widehat{\mathcal{J}_\sigma}\right)$. In the second step, we use $\widehat{\mathcal{J}_\sigma}$ as the union of the finitely evolved SA paths with time $T$ starting from the points in $V_\sigma$ to approximate $\hat{\mathcal{J}}_\sigma$. The longer $T$ and smaller $V_\sigma$ are, the better approximation is achieved.

第一步，我们将 $\widehat{\mathcal{Y}_\sigma}$ 作为所有流向 $V_\sigma$ 的最速下降 (SD) 路径的并集，来近似 $\mathcal{J}_\sigma$。$V_\sigma$ 的范围可通过 $\mathrm{Im}\left(S(\hat{p}_\sigma) \text{ on } \widehat{\mathcal{J}_\sigma}\right)$ 附近 $\mathrm{Im}(\hat{S})$ 涨落的容差 $\mathcal{E}$ 设定。第二步，我们将 $\widehat{\mathcal{J}_\sigma}$ 作为从 $V_\sigma$ 内点出发、时长为 $T$ 的有限演化最陡上升 (SA) 路径的并集，来近似 $\hat{\mathcal{J}}_\sigma$。$T$ 越长、$V_\sigma$ 越小，近似效果越好。

Note that in the second step of the approximation, making $\tilde{\mathcal{J}}_\sigma$ very large (thus a very long $T$ ) is unnecessary. Recall that when computing (42), we sample the points on the thimble with the probability distribution $\mathrm{e}^{-\mathrm{Re}(S)}$ where $\mathrm{Re}(S)$ monotonically increases along the SA flow. Thus the contributions from points far away

from the critical point are exponentially suppressed. As a result, it is sufficient to choose flow time $T$, which provides $\widetilde{\mathcal{J}_\sigma}$ containing points that contribute dominantly to (42); thus increasing $T$ adds only negligible contributions. The result shall converge when further increasing $T$. In fact, existing results [15, 16, 63, 64] suggest $T < 1$ may already be sufficient for a good accuracy.

请注意，在近似的第二步中，无需将 $\mathcal{J}_\sigma$ 设置得非常大 (因此也不需要非常长的 $T$ )。回顾式 (42) 的计算过程，我们利用概率分布 $\mathrm{e}^{-\mathrm{Re}(S)}$ 对尖顶曲面上的点进行采样，其中 $\mathrm{Re}(S)$ 沿 SA 流单调递增。因此，远离临界点的点的贡献会被指数抑制。因此，只需选择合适的流时间 $T$，所得的 $\widetilde{\mathcal{J}_\sigma}$ 就已经包含了对式 (42) 贡献占主导的所有点；进一步增大 $T$ 只会增加可忽略的贡献。当继续增大 $T$ 时，结果将收敛。事实上，已有结果 [15, 16, 63, 64] 表明，$T < 1$ 就足以获得良好的精度。

The choice of real $n$-dimensional $V_\sigma$ depends on the local behavior of the SA equations (40) around the critical point $p_\sigma$. Consider a small holomorphic variation $\omega^k = \delta z^k$; we can linearize (40) around $p_\sigma$:

实 $n$ 维 $V_\sigma$ 的选择取决于临界点 $p_\sigma$ 附近 SA 方程 (40) 的局部行为。考虑一个微小全纯变分 $\omega^k = \delta z^k$，我们可以在 $p_\sigma$ 附近对 (40) 进行线性化:

$$\frac{\mathrm{d}\omega^k}{\mathrm{d}t} = \overline{\mathbf{H} \cdot \omega^l}, \tag{43}$$

where $\mathbf{H} = \left.\frac{\partial^2 \hat{S}}{\partial z_k \partial z_l}\right|_{z=p_\sigma}$ of $\hat{S}(\mathbf{z})$ is the Hessian matrix at $p_\sigma$. The solution of (43) is

其中 $\mathbf{H} = \left.\frac{\partial^2 \hat{S}}{\partial z_k \partial z_l}\right|_{z=p_\sigma}$ 在 $\hat{S}(\mathbf{z})$ 处是临界点 $p_\sigma$ 的黑塞矩阵。式 (43) 的解为

$$\omega = \sum_{a=1}^{2n} \mathrm{e}^{t\lambda^a} \omega_a$$

where $\lambda^a$ and $\omega_a$ are the eigenvalues and corresponding eigenvectors of the generalized eigenvalue equation:

其中 $\lambda^a$ 和 $\omega_a$ 分别是下述广义特征值方程的特征值与对应的特征向量:

$$\mathbf{H}\omega = \overline{\lambda\omega}. \tag{44}$$

(44) is a real $2n$-dimensional eigenvalue equation with the Takagi factorization [65]:

式 (44) 是一个实 $2n$ 维特征值方程，通过高木因式分解 [65] 可得:

$$\begin{bmatrix} \mathbf{H}_\mathbb{R} & -\mathbf{H}_\mathbb{I} \\ -\mathbf{H}_\mathbb{I} & -\mathbf{H}_\mathbb{R} \end{bmatrix} \begin{bmatrix} \omega_\mathbb{R} \\ \omega_\mathbb{I} \end{bmatrix} = \lambda \begin{bmatrix} \omega_\mathbb{R} \\ \omega_\mathbb{I} \end{bmatrix}, \tag{45}$$

where $\mathbf{H}_\mathbb{R}$ and $\mathbf{H}_\mathbb{I}$ are the real and imaginary parts of the Hessian $\mathbf{H}$. The eigenvalues of this matrix are real and appear in pairs $(-\lambda, \lambda)$. The complex eigenvectors $\{\omega_a\}$ can be reconstructed from the real eigenvectors $(\omega_{a\mathbb{R}}, \omega_{a\mathbb{I}})$ by

其中 $\mathbf{H}_{\mathbb{R}}$ 和 $\mathbf{H}_{\mathbb{I}}$ 分别是黑塞矩阵 $\mathbf{H}$ 的实部和虚部。该矩阵的特征值为实数，且成对出现 $(-\lambda, \lambda)$。复特征向量 $\{\omega_a\}$ 可由实特征向量 $(\omega_{a\mathbb{R}}, \omega_{a\mathbb{I}})$ 通过下式重构

$$\omega_a = \omega_a \mathbb{R} + i\omega_a \mathbb{I}.$$

The flow given by (40) is repulsive along the eigenvectors $\omega_a$ with positive eigenvalues and is attractive with negative eigenvalues. The paths along the attractive directions converge to the critical point $p_\sigma$, so they can not form $\widetilde{\mathcal{J}}_\sigma$. Only the paths along the repulsive directions form the $\widetilde{\mathcal{J}}_\sigma$. The space $\widehat{V}_\sigma$ at $p_\sigma$ in the $\mathbf{z}$-coordinate chart can be expressed as

由式 (40) 给出的流，沿特征值为正的特征向量 $\omega_a$ 方向是排斥的，沿特征值为负的方向是吸引的。沿吸引方向的路径收敛于临界点 $p_\sigma$，因此无法构成 $\widetilde{\mathcal{J}}_\sigma$。只有沿排斥方向的路径才能构成 $\widetilde{\mathcal{J}}_\sigma$。在 $\mathbf{z}$ 坐标卡中，$p_\sigma$ 处的空间 $\widehat{V}_\sigma$ 可表示为

$$\widehat{V}_\sigma = \left\{ \mathbf{z} \mid \mathbf{z} = \sum_{a=1}^{n} \widehat{\omega}_a x^a + p_\sigma, \text{ each } x^a \in \mathbb{R} \text{ is small} \right\}, \tag{46}$$

where $\widehat{\omega}_a$ is the normalized eigenvectors with positive eigenvalues.

其中 $\widehat{\omega}_a$ 是对应正特征值的单位特征向量。

In the active point of view, every point in $\widehat{V}_\sigma$ flows upward to $\widetilde{\mathcal{J}}_\sigma$ according to the SA equation (40) with a fixed time $T$. There exists a local diffeomorphism $\mathcal{C}_T : \widehat{V}_\sigma \to \widetilde{\mathcal{J}}_\sigma$ that maps the initial point $p \in \widehat{V}_\sigma$ to the endpoint $\mathcal{C}_T(p) \in \widetilde{\mathcal{J}}_\sigma$.

在主动视角下，$\widehat{V}_\sigma$ 中的每一点都按照 SA 方程 (40) 向上流动到 $\widetilde{\mathcal{J}}_\sigma$，流动时间固定为 $T$。存在局部微分同胚 $\mathcal{C}_T : \widehat{V}_\sigma \to \widetilde{\mathcal{J}}_\sigma$，将初始点 $p \in \widehat{V}_\sigma$ 映射为终点 $\mathcal{C}_T(p) \in \widetilde{\mathcal{J}}_\sigma$。

The change from $\{x^i\}$ to $\{z^i\}$ is induced by $\mathcal{C}_T$. The Jacobian matrix $J_i^k \equiv \partial z^k / \partial x^i$ for the change is determined by the flow equation

从 $\{x^i\}$ 到 $\{z^i\}$ 的变换由 $\mathcal{C}_T$ 诱导。该变换的雅可比矩阵 $J_i^k \equiv \partial z^k / \partial x^i$ 由流方程确定

$$\frac{\mathrm{d}\left(J_i^k\right)_t}{\mathrm{d}t} = \sum_{l=1}^{n} \overline{\frac{\partial^2 \hat{S}(\mathbf{z})}{\partial z_k \partial z_l}} \overline{\left(J_i^l\right)_t}. \tag{47}$$

The initial condition $J_0$ is formed by column vectors $\widehat{\omega}_a$. Note that $\det(J)$ here is a complex number.

初始条件 $J_0$ 由列向量 $\widehat{\omega}_a$ 构成。请注意此处 $\det(J)$ 是一个复数。

As a result, for any given observable $f$, its expectation value can be computed by

因此，对任意给定可观测量 $f$，其期望值可通过下式计算

$$\langle f\rangle \simeq \frac{\int_{\hat{\mathcal{J}}_\sigma} \mathrm{d}^n z \widehat{f}(z)\, \mathrm{e}^{-\widehat{S}(z)}}{\int_{\hat{\mathcal{J}}_\sigma} \mathrm{d}^n z \mathrm{e}^{-\widehat{S}(z)}} = \frac{\int_{\widehat{V}_\sigma} \mathrm{d}^n x \det(J(x))\, \widehat{f}(\mathcal{C}_T(x))\, \mathrm{e}^{-\widehat{S}(\mathcal{C}_T(x))}}{\int_{\widehat{V}_\sigma} \mathrm{d}^n x \det(J(x))\, \mathrm{e}^{-\widehat{S}(\mathcal{C}_T(x))}} \tag{48}$$
$$= \frac{\int_{\widehat{V}_\sigma} \mathrm{d}^n x \mathrm{e}^{i\left(\arg(\det(J)) - \mathrm{Im}\left(\widehat{S}\right)\right)} \widehat{f} \mathrm{e}^{-\mathrm{Re}\left(\widehat{S}\right) + \log(|\det(J)|)}}{\int_{\widehat{V}_\sigma} \mathrm{d}^n x \mathrm{e}^{i\left(\arg(\det(J)) - \mathrm{Im}\left(\widehat{S}\right)\right)} \mathrm{e}^{-\mathrm{Re}\left(\widehat{S}\right) + \log(|\det(J)|)}},$$

For any observable $f$, we define its expectation with respect to a real effective action $S_{\text{eff}}$ as

对任意可观测量 $f$，我们将它关于实有效作用量 $S_{\text{eff}}$ 的期望值定义为

$$\langle f\rangle_{\text{eff}} = \frac{\int_{\widehat{V}_\sigma} \mathrm{d}^n x f \mathrm{e}^{-S_{\text{eff}}}}{\int_{\widehat{V}_\sigma} \mathrm{d}^n x \mathrm{e}^{-S_{\text{eff}}}}. \tag{49}$$

(48) can be rewritten as

式 (48) 可改写为

$$\langle f\rangle \simeq \frac{\int_{\widehat{V}_\sigma} \mathrm{d}^n x \widehat{f} \mathrm{e}^{i\theta_{res}} \mathrm{e}^{-S_{\text{eff}}}}{\int_{\widehat{V}_\sigma} \mathrm{d}^n x \mathrm{e}^{-S_{\text{eff}}}} \times \frac{\int_{\widehat{V}_\sigma} \mathrm{d}^n x \mathrm{e}^{-S_{\text{eff}}}}{\int_{\widehat{V}_\sigma} \mathrm{d}^n x \mathrm{e}^{i\theta_{res}} \mathrm{e}^{-S_{\text{eff}}}} = \frac{\langle \mathrm{e}^{i\theta_{res}} \widehat{f}\rangle_{\text{eff}}}{\langle \mathrm{e}^{i\theta_{res}}\rangle_{\text{eff}}}. \tag{50}$$

with $S_{\text{eff}} \equiv \mathrm{Re}\left(\hat{S}\right) - \log(\det(J))$ as the purely real effective action and $\theta_{\text{res}} \equiv \arg(\det(J)) - \mathrm{Im}\left(\hat{S}\right)$ is the residual phase. Note that the efficacy of MCMC method in computing both $\left\langle \mathrm{e}^{i\theta_{\text{res}}} \widehat{f}\right\rangle_{\text{eff}}$ and $\left\langle \mathrm{e}^{i\theta_{\text{res}}}\right\rangle_{\text{eff}}$ relies on the little fluctuating residue phase $\theta_{\text{res}}$. The $\arg(\det(J))$ term usually does not have strong fluctuations, e.g., in the spinfoam calculations. The fluctuations coming from $\mathrm{Im}\left(\hat{S}(\mathbf{z})\right)$ in $\widehat{V}_\sigma$ can be bounded by a maximal tolerance $\mathcal{E}$. The tolerance determines the size of $\widehat{V}_\sigma$, s.t. at any point $p \in \widehat{V}_\sigma$, $\left|\mathrm{Im}\left(\hat{S}(p)\right) - \mathrm{Im}\left(\hat{S}(p_\sigma)\right)\right| \leq \mathcal{E}$.

其中 $S_{\text{eff}} \equiv \mathrm{Re}\left(\hat{S}\right) - \log(\det(J))$ 为纯实有效作用量，$\theta_{\text{res}} \equiv \arg(\det(J)) - \mathrm{Im}\left(\hat{S}\right)$ 为残余相位。需要注意的是，MCMC 方法计算 $\left\langle \mathrm{e}^{i\theta_{\text{res}}} \widehat{f}\right\rangle_{\text{eff}}$ 和 $\left\langle \mathrm{e}^{i\theta_{\text{res}}}\right\rangle_{\text{eff}}$ 的效率依赖于残余相位 $\theta_{\text{res}}$ 涨落较小。在例如自旋泡沫计算中，$\arg(\det(J))$ 项通常不存在强涨落。$\widehat{V}_\sigma$ 中来自 $\mathrm{Im}\left(\hat{S}(\mathbf{z})\right)$ 的涨落可由最大容差 $\mathcal{E}$ 界定，该容差决定了 $\widehat{V}_\sigma$ 的大小，使得在任意点 $p \in \widehat{V}_\sigma$, $\left|\mathrm{Im}\left(\hat{S}(p)\right) - \mathrm{Im}\left(\hat{S}(p_\sigma)\right)\right| \leq \mathcal{E}$ 都满足条件。

## Spinfoam on a Lefschetz Thimble

## 莱夫谢茨 thimble 上的自旋泡沫

In the previous section, we have described the general algorithm of integrals on Lefschetz thimbles. Here, we apply the Lefschetz thimble to spinfoam model.

上一节中，我们已经介绍了莱夫谢茨 thimble 上积分的通用算法。本文中，我们将莱夫谢茨 thimble 方法应用到自旋泡沫模型。

First, we complexify the spinfoam variables $j_{ab}, g_a, z_{ab}$ and analytically continue the integrand in (20). As described in, the analytic continuation makes $g_{ve}^\dagger$ and ${z_{vf}}^\dagger$ independent of $g_{ve}$ and $z_{vf}$. The spin variables $j_h$ are also complexified, and the integrands are holomorphic in $j_h$. The real scaling parameter $\lambda$ is kept

real. For spinfoam vertex amplitude, the analytic continuation renders the integrand and the action, denoted by $\tilde{S}$ , holomorphic functions of 54 complex variables. The thimbles are real 54-dimensional sub-manifolds in the space of complexified spinfoam variables. The detailed discussion of the analytic continuation of the spinfoam integrands is given in [12] (see also [66]).

首先，我们对自旋泡沫变量 $j_{ab}, g_a, z_{ab}$ 复化，并对式 (20) 中的被积函数做解析延拓。正如文献所述，解析延拓使得 $g_{ve}^{\dagger}$ 和 $z_{vf}{}^{\dagger}$ 独立于 $g_{ve}$ 和 $z_{vf}$ 。自旋变量 $j_h$ 也被复化，被积函数在 $j_h$ 上是全纯的。实标度参数 $\lambda$ 保持为实数。对于自旋泡沫顶点振幅，解析延拓使得被积函数和作用量 (记为 $\tilde{S}$ ) 成为 54 个复变量的全纯函数。Thimble 是复化自旋泡沫变量空间中的 54 维实子流形。自旋泡沫被积函数解析延拓的详细讨论参见文献 [12](也可参见 [66])。

As shown in Section "Complex Critical Points," after analytic continuation, $\tilde{S}$ may have more critical points than $S$ does: complex critical points may exist in addition to the real critical points discussed above. The spinfoam integrals admit decompositions as in (36), where $\{p_\sigma\}$ contains both real and complex critical points in the complex domain. Complex critical points $p_{\tilde{\sigma}}$ contribute to the integrals if $n_{\tilde{\sigma}} \neq 0$ , namely, there exist SA paths approaching $p_{\tilde{\sigma}}$ from the real variables. Thus, $n_{\tilde{\sigma}} \neq 0$ for a complex critical point $p_{\tilde{\sigma}}$ implies that $\mathrm{Re}\left(\tilde{S}\left(p_{\tilde{\sigma}}\right)\right) > 0$ since $\mathrm{Re}\left(\tilde{S}\right) = \mathrm{Re}\left(S\right) \geq 0$ in the real domain. Strictly positive $\mathrm{Re}\left(\tilde{S}\left(p_{\tilde{\sigma}}\right)\right)$ implies that when the spinfoam integrals are decomposed as in Eq. (36), the thimbles $\mathcal{J}_{\tilde{\sigma}}$ associated to complex critical points contribute exponentially small at large $\lambda$ .

如 "复临界点" 一节所述，解析延拓后，$\tilde{S}$ 的临界点可能比 $S$ 更多: 除了上文讨论的实临界点，还可能存在复临界点。自旋泡沫积分可分解为式 (36) 的形式，其中 $\{p_\sigma\}$ 同时包含复域中的实临界点和复临界点。若满足 $n_{\tilde{\sigma}} \neq 0$ ，即存在从实变量出发逼近 $p_{\tilde{\sigma}}$ 的最陡下降路径，则复临界点 $p_{\tilde{\sigma}}$ 会对积分产生贡献。因此，复临界点 $p_{\tilde{\sigma}}$ 满足 $n_{\tilde{\sigma}} \neq 0$ 意味着 $\mathrm{Re}\left(\tilde{S}\left(p_{\tilde{\sigma}}\right)\right) > 0$ ，这是因为实域中 $\mathrm{Re}\left(\tilde{S}\right) = \mathrm{Re}\left(S\right) \geq 0$ 。严格为正的 $\mathrm{Re}\left(\tilde{S}\left(p_{\tilde{\sigma}}\right)\right)$ 表明，当自旋泡沫积分分解为式 (36) 的形式时，关联到复临界点的 thimble $\mathcal{J}_{\tilde{\sigma}}$ 的贡献在大 $\lambda$ 下是指数小的。

As discussed in Section "Complex Critical Points," at large $\lambda$ , there exists a single geometrical critical point $p_{geo} = (k_0, j_0, g_0, z_0)$ dominating the spinfoam integrals (20) with geometrical boundary data. Hence, the single Lefschetz thimble $\mathcal{J}_{\text{geo}}$ associated to $p_{geo}$ dominates the decomposition (36) of the spinfoam integrals. Therefore, (41) is applicable to the partition function and expectation values at large $\lambda$ . As a result, the expectation value of spinfoam observables is given by

如 "复临界点" 一节讨论，在大 $\lambda$ 下，带有几何边界数据的自旋泡沫积分 (20) 存在唯一的几何临界点 $p_{geo} = (k_0, j_0, g_0, z_0)$ 主导积分。因此，关联到 $p_{geo}$ 的单个莱夫谢茨 thimble $\mathcal{J}_{\text{geo}}$ 主导自旋泡沫积分的分解式 (36)。因此，式 (41) 可用于大 $\lambda$ 下的配分函数和期望值。由此，自旋泡沫可观测量的期望值为

$$\langle O(j,g,z)\rangle := \frac{\langle W | O(j,g,z) | \Psi_0 \rangle}{\langle W | \Psi_0 \rangle} \tag{51}$$

$$\simeq \frac{\int_{\mathcal{J}_{\text{geo}}} \prod_h \mathrm{d}j_h \prod_h 2\lambda \tau_{[-\varepsilon, \lambda j^{\max}+\varepsilon]}(\lambda j_h) \int [\mathrm{dg}\, \mathrm{dz}]\, O(j,g,z)\, e^{\lambda S(k_0)}}{\int_{\mathcal{J}_{\text{geo}}} \prod_h \mathrm{d}j_h \prod_h 2\lambda \tau_{[-\varepsilon, \lambda j^{\max}+\varepsilon]}(\lambda j_h) \int [\mathrm{dg}\, \mathrm{dz}]\, e^{\lambda S(k_0)}},$$

for given boundary states $\Psi_0$ . Equations (51) capture the contributions of the dominant critical point $p_{\text{geo}}$ and include all orders of perturbative $1/\lambda$ corrections.

对应给定边界态 $\Psi_0$ 。式 (51) 捕获了主导临界点 $p_{\text{geo}}$ 的贡献，并包含了所有阶的微扰 $1/\lambda$ 修正。

The approximation leading to (51) neglects the exponentially suppressed contributions at large $\lambda$ . These contributions are (1) integrals with $k \neq 0$ in (19),(2) extending some integrals to infinite such as $\int \mathrm{d}j_h$ on the cover space, and (3) the complex critical points and associated Lefschetz thimbles.

推导式 (51) 的近似忽略了大 $\lambda$ 下被指数压低的贡献。这些贡献包括:(1) 式 (19) 中带有 $k \neq 0$ 的积分，(2) 延拓至无穷的积分，例如覆盖空间上的 $\int \mathrm{d}j_h$ ，以及 (3) 复临界点及其关联的莱夫谢茨 thimble。

We have shown that each quantity in the spinfoam partition function and observables can be expressed as the power series $\sum_S a_s\left(\frac{1}{\lambda}\right)^S$ plus contributions exponentially suppressed (viz., suppressed faster than $O\left(1/\lambda^N\right)$ for any integer $N$ ) at large $\lambda$ . Equation (51) captures the power series containing all the perturbative quantum corrections while neglecting the exponentially suppressed contributions.

我们已经证明，在大 $\lambda$ 极限下，自旋泡沫配分函数与可观测量中的每个物理量都可以表示为幂级数 $\sum_S a_s\left(\frac{1}{\lambda}\right)^S$ 加上指数压制的贡献 (即，比任意整数 $N$ 对应的 $O\left(1/\lambda^N\right)$ 压制得更快)。式 (51) 涵盖了包含所有微扰量子修正的幂级数，同时忽略了指数压制的贡献。

The exponentially suppressed contributions may be called non-perturbative corrections, as they contain the sub-dominant thimbles associated with the complex critical points generated by the analytic continuation. In this sense, Eq. (51) captures all perturbative quantum corrections while neglecting non-perturbative corrections.

这些指数压制的贡献可称为非微扰修正, 因为它们包含了与解析延拓产生的复临界点相关的次占优奶嘴。在此意义上，式 (51) 涵盖了所有微扰量子修正，同时忽略了非微扰修正。

It is known that in the traditional stationary phase expansion, the computational complexity grows exponentially when computing the coefficient of higher-order $O\left(1/\lambda^s\right)$ corrections with larger $s$ . In this sense, our method with the Lefschetz thimble is a powerful way to compute the spinfoam observables containing perturbative quantum corrections to all orders.

我们知道，在传统稳相近展开中，当计算更大 $s$ 对应的高阶 $O\left(1/\lambda^s\right)$ 修正系数时，计算复杂度会呈指数增长。在此意义上，我们采用莱夫谢茨奶嘴的方法是计算包含任意阶微扰量子修正的自旋泡沫可观测量的有力方法。

Besides, similar to the idea in [67, 68] , we can consider the integral with the Lefschetz thimble as a new definition of the spinfoam model. When generalizing to arbitrary simplicial complex $\Delta$ , we define the spinfoam model on the Lefschetz thimble by

此外，类似 [67, 68] 中的思路，我们可以将采用莱夫谢茨奶嘴的积分定义为新的自旋泡沫模型。推广到任意单纯复形 $\Delta$ 时，我们通过下式定义莱夫谢茨奶嘴上的自旋泡沫模型:

$$Z_{\mathcal{J}} = \int_{\mathcal{A}} \mathrm{d}j_h \left[\, \mathrm{d}g\, \mathrm{d}z\right] e^{-\lambda \hat{S}_\Delta}, \tag{52}$$

where $\hat{S}_\Delta$ is the analytic continuation of the spinfoam action on $\Delta$ [12]. Here, $\int \mathrm{d}j_h$ integrates all internal spins, and $\mathcal{J}$ is the Lefschetz thimble associated with a single critical point. Applying the Lefschetz thimble to the spinfoam model has been proposed earlier in the context of coupling to cosmological constant [69-71]. Equation (52) has the advantage of focusing on the contributions from a single critical point and excluding other critical points. In particular, when $\mathcal{J}$ is the thimble of the critical point corresponding to the Lorentzian Regge geometry, it excludes contributions from vector geometries and the geometries with flipping orientations (see [33, 34, 51, 52] for the classification of critical points). In addition, Eq. (52) is a better formulation from the computational point of view.

其中 $\hat{S}_\Delta$ 是自旋泡沫作用量在 $\Delta$ 上的解析延拓 [12]。此处 $\int \mathrm{d}j_h$ 对所有内部自旋积分，$\mathcal{J}$ 是单个临界点对应的莱夫谢茨奶嘴。将莱夫谢茨奶嘴应用到自旋泡沫模型的思路最早是在耦合宇宙学常数的研究背景下提出的 [69-71]。式 (52) 的优势在于只关注单个临界点的贡献，排除了其他临界点的贡献。特别地，当 $\mathcal{J}$ 是对应洛伦兹雷格几何的临界点的奶嘴时，它排除了矢量几何和翻转取向几何的贡献 (临界点的分类参见 [33, 34, 51, 52] )。此外，从计算角度来看，式 (52) 是更好的表述。

Given the dominant geometric critical point, the spinfoam model on the Lef-schetz thimble has the same perturbative $1/\lambda$ expansion as the usual definition of the spinfoam amplitude and, in particular, has the same semi-classical limit as the standard spinfoam amplitude, as shown in the numerical results in Section "Applications: Spinfoam Propagator as an Example." The small $\lambda$ behavior of (52) is different than the usual spinfoam amplitude because non-perturbative corrections are not negligible at small $\lambda$ .

给定占优的几何临界点，如“应用举例: 自旋泡沫传播子”一节的数值结果所示，莱夫谢茨奶嘴上的自旋泡沫模型与自旋泡沫振幅的通常定义具有相同的微扰 $1/\lambda$ 展开，尤其和标准自旋泡沫振幅具有相同的半经典极限。由于非微扰修正小 $\lambda$ 下不可忽略，式 (52) 在小 $\lambda$ 下的行为与常规自旋泡沫振幅不同。

## Applications: Spinfoam Propagator as an Example

## 应用: 以自旋泡沫传播子为例

In this section we will show the result of calculating the Lorentzian EPRL spinfoam propagator on a 4-simplex numerically with Lefschetz thimble MCMC method as a concrete example. From the connected two-point correlation function $G^{abcd}(x,y) = \left\langle q^{ab}(x)\, q^{c\hat{d}}(y)\right\rangle - \left\langle q^{ab}(x)\right\rangle \left\langle q^{ab}(x)\right\rangle$ , the spinfoam propagator is defined by

本节我们将以具体实例展示，利用莱夫谢茨纤维丛 MCMC 方法对 4 单形上洛伦兹 EPRL 自旋泡沫传播子进行数值计算的结果。从连通两点关联函数 $G^{abcd}(x,y) = \left\langle q^{ab}(x)\, q^{c\hat{d}}(y)\right\rangle - \left\langle q^{ab}(x)\right\rangle \left\langle q^{ab}(x)\right\rangle$ 出发，自旋泡沫传播子定义为

$$G^{abcd}_{mn} = \left\langle E^a_n \cdot E^b_n E^c_m \cdot E^d_m \right\rangle - \left\langle E^a_n \cdot E^b_n \right\rangle \left\langle E^c_m \cdot E^d_m \right\rangle \tag{53}$$

where $E^a_n$ is the flux operator through a face $f_{an}$ dual to the triangle between the tetrahedra $a$ and $n$ . It is obtained by computing the expectation values $\left\langle E^a_n \cdot E^b_n E^c_m \cdot E^d_m \right\rangle$ and $\left\langle E^a_n \cdot E^b_n \right\rangle$ . As shown in [72-75], their definition is given by

其中 $E_n^a$ 是穿过面 $f_{an}$ 的流量算符，该面对偶于四面体 $a$ 与 $n$ 之间的三角形。它通过计算期望值 $\langle E_n^a \cdot E_n^b E_m^c \cdot E_m^d \rangle$ 和 $\langle E_n^a \cdot E_n^b \rangle$ 得到。如文献 [72-75] 所示，它们的定义为

$$\langle W \mid \Psi_0 \rangle \simeq \int_{-\infty}^{\infty} \mathrm{d}^{10} j \int [\mathrm{dg}\, \mathrm{d}\mathbf{z}]\, \mathrm{e}^{-\lambda S}, \tag{54}$$

$$\left\langle W \left| E_n^a \cdot E_n^b E_m^c \cdot E_m^d \right| \Psi_0 \right\rangle \simeq \int_{-\infty}^{\infty} \mathrm{d}^{10} j \int [\mathrm{dg}\, \mathrm{d}\mathbf{z}]\, \mathrm{e}^{-\lambda S} \left(A_{an} \cdot A_{bn}\right)\left(A_{cm} \cdot A_{dm}\right), \tag{55}$$

$$\left\langle W \left| E_n^a \cdot E_n^b \right| \Psi_0 \right\rangle \simeq \int_{-\infty}^{\infty} \mathrm{d}^{10} j \int [\mathrm{dg}\, \mathrm{d}\mathbf{z}]\, \mathrm{e}^{-\lambda S} \left(A_{an} \cdot A_{bn}\right), \tag{56}$$

$$\left\langle W \left| E_m^c \cdot E_m^d \right| \Psi_0 \right\rangle \simeq \int_{-\infty}^{\infty} \mathrm{d}^{10} j \int [\mathrm{dg}\, \mathrm{d}\mathbf{z}]\, \mathrm{e}^{-\lambda S} \left(A_{cm} \cdot A_{dm}\right), \tag{57}$$

with

其中

$$A_{ab}^i = \gamma\lambda j_{ab} \frac{\langle \sigma^i Z_{ba}, \xi_{ba} \rangle}{\langle Z_{ba}, \xi_{ba} \rangle}, A_{ba}^i = -\gamma\lambda j_{ab} \frac{\langle J\xi_{ba}, \sigma_i Z_{ba} \rangle}{\langle J\xi_{ba}, Z_{ba} \rangle}. \tag{58}$$

In this example, Differential Evolution Adaptive Metropolis (DREAM) algorithm, which is a multi-chain MCMC method [76], is used. The detailed algorithm and the boundary data used for the numerical computation can be found in [16, 77, 78] . The code can update $> 1000$ samples per thread per hour on $X64$ processors (tested on systems with AMD EPYCTM7742 and AMD EPYC ™ 7642). Here the Barbero-Immirzi parameter is fixed to $\gamma = -0.1$ and different $\lambda$ is chosen in the computation.

本示例采用差分进化自适应梅特波利斯 (DREAM) 算法，这是一种多链 MCMC 方法 [76]。数值计算所用的详细算法与边界数据可参见 [16, 77, 78] 。代码在 $X64$ 处理器上可达到每个线程每小时更新 $> 1000$ 个样本 (测试系统配置为 AMD EPYCTM7742 与 AMD EPYC ™ 7642)。本文将巴贝罗-伊米尔齐参数固定为 $\gamma = -0.1$ ，计算中选取了不同的 $\lambda$ 。

The expectation value of $\langle E_n^a \cdot E_n^b E_m^c \cdot E_m^d \rangle$ has 1275 non-zero components, and $\langle E_n^a \cdot E_n^b \rangle$ consists 50 non-zero components. As a result, the propagator $G_{mn}^{abcd}$ has 1275 non-zero components. These components are evaluated around $10^7$ of samples obtained by the multi-chain MCMC method on the Lefschetz thimble. As an example of the computation, Fig. 10 shows the relative difference between the numerical results and the leading order asymptotic results of the component $G_{14}^{2315}$ and corresponding metric expectation values $\langle E_1^2 \cdot E_1^3 E_4^1 \cdot E_4^5 \rangle, \langle E_1^2 \cdot E_1^3 \rangle$ , and $E_4^1 \cdot E_4^5$ ). The results show the convergence to the leading order asymptotic results in the large spin regime. Their differences become large when $\lambda$ decreases because of the nonnegligible contributions from the higher-order $1/\lambda$ corrections beyond the leading order asymptotics.

$\langle E_n^a \cdot E_n^b E_m^c \cdot E_m^d \rangle$ 的期望值有 1275 个非零分量，$\langle E_n^a \cdot E_n^b \rangle$ 有 50 个非零分量，因此传播子 $G_{mn}^{abcd}$ 共有 1275 个非零分量。这些分量是在莱夫谢茨纤维丛上通过多链 MCMC 方法得到的 $10^7$ 个样本附近计算得到的。作为计算示例，图 10 给出了分量 $G_{14}^{2315}$ 与对应度规期望值 $\langle E_1^2 \cdot E_1^3 E_4^1 \cdot E_4^5 \rangle, \langle E_1^2 \cdot E_1^3 \rangle$ 、$E_4^1 \cdot E_4^5$ 的数值结果与领头阶渐近结果的相对差。结果表明，在大自旋区域结果收敛于领头阶渐近结果。当 $\lambda$ 减小时，二者差异会变大，这是因为超出领头阶渐近的高阶 $1/\lambda$ 修正贡献不可忽略。

The comparison of the results for all of the 1275 components of the propagator $G_{mn}^{abcd}$ from multi-chain MCMC on the Lefschetz thimble with the results from asymptotic analysis derived in (26) is shown in Fig. 11. As shown in Fig. 11a, the percentage differences of these components tend to decrease when the number of samples increases, since increasing the number of samples will make the Markov chains closer to the desired distribution. Figure 11b compares the histogram of the percentage differences of the components with different $\lambda$ for $\lambda = 10^7$ and $\lambda = 10^6$ . This shows that the Markov chains converge to the desired distribution faster with larger $\lambda$ , and the numerical results for larger $\lambda$ are more consistent with the leading order asymptotic results. This fact might suggest that when $\lambda$ is becoming large, the less important $1/\lambda$ correction and the easier converging Markov chains are correlated.

图 11 展示了 Lefschetz 上纤维上多链马尔可夫链蒙特卡罗方法得到的传播子 $G_{mn}^{abcd}$ 全部 1275 个分量的结果，与式 (26) 导出的渐近分析结果的对比。如图 11a 所示，这些分量的百分比差会随样本量增加而减小，这是因为增加样本量会让马尔可夫链更接近目标分布。图 11b 对比了 $\lambda = 10^7$ 和 $\lambda = 10^6$ 在不同 $\lambda$ 下分量百分比差的直方图。结果显示，$\lambda$ 越大，马尔可夫链收敛到目标分布的速度越快，且更大 $\lambda$ 对应的数值结果与领头阶渐近结果更一致。这一事实或许说明，当 $\lambda$ 增大时，$1/\lambda$ 修正的占比降低与马尔可夫链更易收敛是相关的。

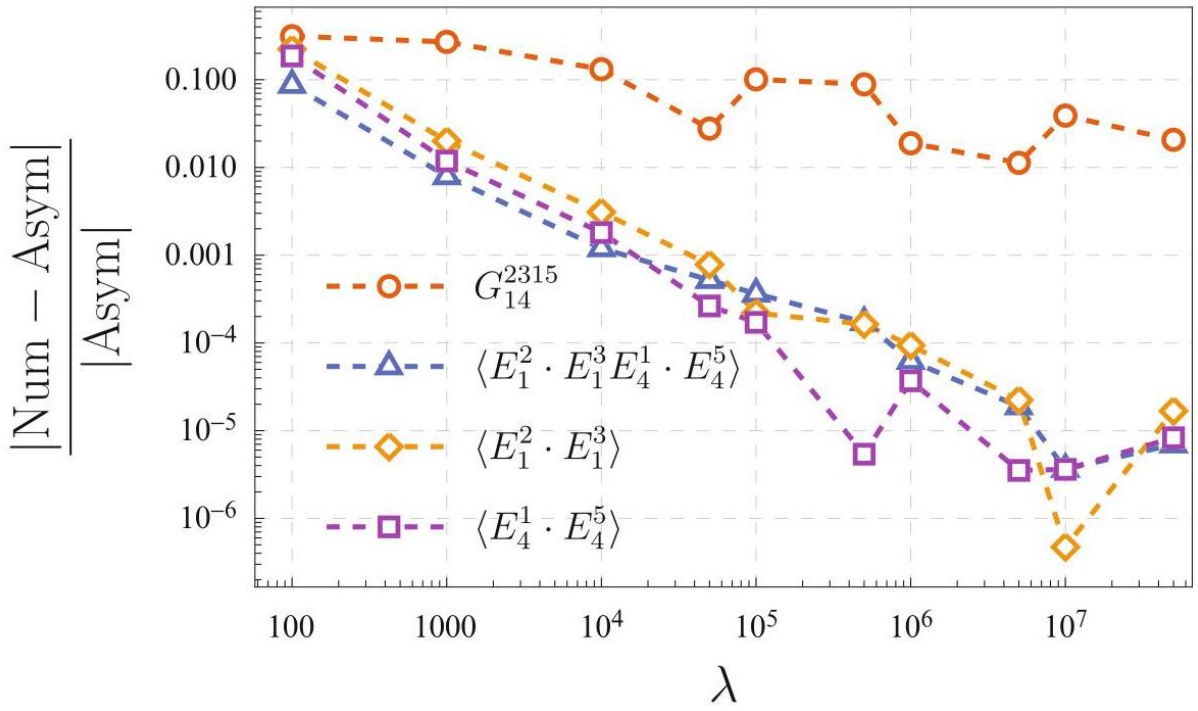


Fig. 10 Difference between the numerical results and the leading order asymptotic results of $G_{14}^{2315}, \langle E_1^2 \cdot E_1^3 E_4^1 \cdot E_4^5 \rangle, \langle E_1^2 \cdot E_1^3$ , and $\langle E_1^1 \cdot E_1^5 \rangle$

图 10 $G_{14}^{2315}, \langle E_1^2 \cdot E_1^3 E_4^1 \cdot E_4^5 \rangle, \langle E_1^2 \cdot E_1^3 \rangle$ 数值结果与领头阶渐近结果的差，以及 $\langle E_1^1 \cdot E_1^5 \rangle$

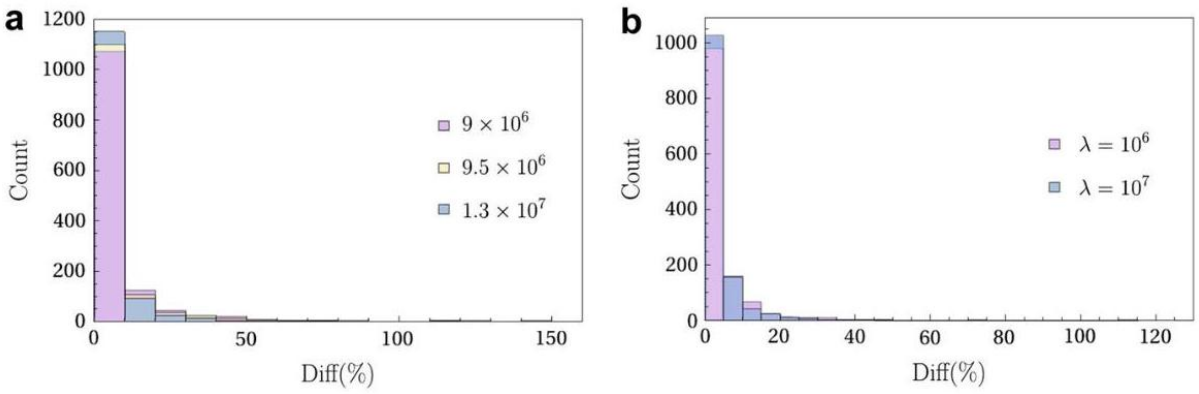


Fig. 11 Histogram of the percentage errors of the components of $G_{mn}^{abccd}$. (**a**) $\lambda = 10^6$ with different number of samples. (b) $\lambda = 10^6$ v.s. $\lambda = 10^7$

图 11 不同样本量下 $G_{mn}^{abccd}$. (**a**) $\lambda = 10^6$ 分量百分比误差的直方图。(b) $\lambda = 10^6$ 对 $\lambda = 10^7$

In summary, the algorithm based on Lefschetz thimble MCMC method is able to compute the expectation values of the metric operators as well as the propagators efficiently. The results show the compatibility with the asymptotic result in the large- $\lambda$ regime. As $\lambda$ is increasing, the compatibility with the asymptotic results tends to be improved. These results are consistent with the semi-classical behavior of the spinfoam propagator in the large- $\lambda$ regime, thus validating the algorithm. When $\lambda$ is not very large, we observe the non-negligible contributions from the higher-order $1/\lambda$ corrections beyond the leading order asymptotic results.

综上，基于 Lefschetz 上纤维 MCMC 的算法可以高效计算度规算子的期望值与传播子。结果表明，该算法在大 $\lambda$ 区域与渐近结果相容。随着 $\lambda$ 增大，与渐近结果的相容性会提升。这些结果与大 $\lambda$ 区域自旋泡沫传播子的半经典行为一致，因此验证了该算法的有效性。当 $\lambda$ 不是很大时，我们观测到，超出领头阶渐近结果的高阶 $1/\lambda$ 修正的贡献不可忽略。

# Conclusions

# 结论

Performing calculations has always been arduous in spinfoam theory due to its sheer complexity. In recent years the field has undergone a proper numerical revolution. Pulled by the fast developments in high-performance computing, the community developed many different codes and libraries to put a spinfoam in a computer. This chapter reviewed the major frameworks to perform calculations with the Lorentzian EPRL spinfoam model.

由于自旋泡沫理论本身十分复杂，计算工作向来十分艰巨。近年来该领域经历了一场真正的数值革命。在高性能计算快速发展的推动下，学界开发了多种不同的代码和库，将自旋泡沫模型搬上计算机。本章回顾了用于洛伦兹 EPRL 自旋泡沫模型计算的主要框架。

We reviewed first sl2cfoam-next a tool to calculate spinfoam amplitudes based on the booster decomposition of the EPRL vertex amplitude.

我们首先回顾了 sl2cfoam-next，这是一款基于 EPRL 顶点振幅的助推分解计算自旋泡沫振幅的工具。

The framework has many strengths. It provides all the tools to perform a vast amount of calculations. It has a fast and optimized structure to compute all the necessary building blocks (vertex, face, edge amplitudes, and coherent states). The user needs to compose writing minimal scripts. The framework is optimized to run calculations in parallel. Even if we can do small calculations on a personal laptop, most applications we presented require a cluster. The architecture of the library support also tensors contractions using GPUs. There are two main problems in the framework. First is the weak control over the truncation parameter, which is necessary to extract numbers from the amplitude with this technique. We do not have a way to prescribe a truncation to match a predetermined and desired error on the amplitude. We are limited to choosing it motivated by empirical arguments. Second is the large number of computational resources needed for extended transition amplitudes. These two aspects are currently being studied and improved. We are carrying out a systematical study of possible approximation techniques that would help us to go beyond truncations. Furthermore, we are experimenting with Monte Carlo techniques to overcome the impossible obstacle of the massive amount of resources necessary to sum over bulk degrees of freedom. We showcased the power of sl2cfoam-next with some applications. We explored the large spin regime of spinfoam amplitudes with a single and many vertices. We studied the divergences of the theory, and we are currently applying numerical techniques to physical applications like early-time cosmology or black hole tunneling.

该框架有诸多优势: 它提供了完成大量计算所需的全部工具，拥有快速优化的结构来计算所有必要的构造模块 (顶点、面、边振幅以及相干态)，用户只需编写极少的脚本即可组合使用；框架针对并行计算做了优化，虽然个人笔记本也可以运行小型计算，但我们展示的大多数应用都需要计算机集群；该库的架构还支持利用 GPU 进行张量收缩。框架目前存在两个主要问题: 第一是对截断参数的控制不足，而截断参数是该技术从振幅中提取数值的必要条件，我们目前没有办法规定截断来匹配振幅预设的目标误差，只能依靠经验论证来选择；第二是扩展跃迁振幅需要大量计算资源。目前我们正对这两方面开展研究与改进: 我们正在系统研究可行的近似技术，帮助我们突破截断的限制；此外我们还尝试用蒙特卡洛技术克服体自由度求和需要海量资源这一无法逾越的障碍。我们通过若干应用展示了 sl2cfoam-next 的能力: 我们探究了单顶点和多顶点自旋泡沫振幅的大自旋区域，研究了该理论的发散问题，目前我们正将数值技术应用于早期宇宙学、黑洞隧穿等物理场景。

Then we reviewed the numerical analysis of the curved Regge geometries from the four-dimensional Lorentzian EPRL spinfoam amplitude.

随后我们回顾了对四维洛伦兹 EPRL 自旋泡沫振幅导出弯曲里奇几何的数值分析。

The results resolve the flatness problem by explicitly finding the curved Regge geometries emergent from the EPRL spinfoam amplitudes. The curved geometries correspond to the complex critical points away from the real integration domain. They give non-suppressed $e^{\lambda\,\mathrm{Re}(\mathcal{S})}$ and satisfy the bound $\mathrm{Re}\left(a_2\left(\gamma\right)\right)\delta_h^2 \lesssim 1/\lambda$ , if we neglect high-order terms $O\left(\delta_h^3\right)$ in dihedral angle $\delta_h$ , in the examples we showed. This bound is consistent with the earlier proposal [55] and the result in the effective spinfoam model [18, 19, 58] , although now this bound should be corrected when taking into account $O\left(\delta_h^3\right)$ corrections. All resulting curved geometries have small deficit angles. The large- $j$ spinfoam amplitude is still suppressed for geometries with larger $\delta_h$ . This is not a problem for the semiclassical analysis. Indeed, the non-singular classical spacetime geometries are smooth with vanishing $\delta_h$ . To well-approximating smooth geometries by Regge geometries, the triangulation

must be sufficiently refined, and all deficit angles must be small. We showed the example with the method applying to triangulations of the 3-3 ($\Delta_3$) and 1-5 Pachner move. The 1-5 move is one of the elementary moves for the triangulation refinement. Our results provide a new method for analyzing the triangulation dependence in the spinfoam model (see, e.g., [79] for an earlier attempt). This may relate to the spinfoam renormalization [80,81], to address the issue of triangulation dependence of the spinfoam theory.

研究结果通过明确找到从 EPRL 自旋泡沫振幅演生出来的弯曲里奇几何，解决了平坦性问题。弯曲几何对应远离实积分域的复临界点。在我们展示的例子中，若忽略二面角 $\delta_h$ 中的高阶项 $O\left(\delta_h^3\right)$，它们会给出未被压制的 $e^{\lambda \operatorname{Re}(S)}$，并且满足界 $\operatorname{Re}\left(a_2(\gamma)\right) \delta_h^2 \lesssim 1/\lambda$。该界与早期文献 [55] 的提议以及有效自旋泡沫模型 [18, 19, 58] 的结果一致，不过现在考虑 $O\left(\delta_h^3\right)$ 修正后，该界需要修正。所有得到的弯曲几何都具有小亏缺角。对于二面角 $\delta_h$ 更大的几何，大 $j$ 自旋泡沫振幅仍然会被压制。这对半经典分析并不成问题，因为非奇异经典时空几何本身是光滑的，其 $\delta_h$ 为零。要想用里奇几何良好逼近光滑几何，三角剖分必须足够精细，且所有亏缺角都必须很小。我们展示了该方法应用于 3-3 ($\Delta_3$) 和 1-5 帕克纳移动三角剖分的例子。其中 1-5 移动是三角剖分细化的基本移动之一。我们的结果为分析自旋泡沫模型中的三角剖分依赖性提供了新方法 (早期尝试参见例如文献 [79])，这可能与自旋泡沫重整化 [80,81] 相关，有助于解决自旋泡沫理论的三角剖分依赖性问题。

Lastly, we reviewed the numerical method for computing the expectation value of any observable based on the Lefschetz thimble and MCMC methods.

最后，我们回顾了基于莱夫谢茨 thimble 和 MCMC 方法计算任意可观测量期望值的数值方法。

The method applies to all types of spinfoam models and graphs, independently of the choice of model (spacetime signature, $Y$ -map, etc.). The framework efficiently numerically computes observables in spinfoam models with relatively large spins. It captures perturbative quantum corrections to all orders. The multiple-chain MCMC method used in the framework runs in parallel and supports GPU boost. One of the main problems in the framework is the generalization to the small spins regime, as we neglect non-perturbative corrections that are exponentially small for large spins in the calculation. Unlike in the asymptotic regime, in the small spin regime, multiple thimbles will contribute to the partition function instead of only one dominant. This requires us to identify all thimbles associated with complex critical points and calculate their weight. Identifying all complex critical points is hard, even in the single simplex case, as the critical equations form a high-order polynomial system with 54 variables. A possible solution to this problem is the world-volume and globally adaptive sampling methods [82]. We are currently exploring the possibility of using these methods, and some preliminary results are available [17]. We showcased the power and efficiency of this framework with the application in calculating the spinfoam propagator as an example. Other exciting applications contain, e.g., the evaluation of geometrical observables in cosmology and black holes, exploring the continuum limit, and the renormalization group flow. In the meantime, we are currently working on improving the framework by choosing a more suitable ODE solver and by applying different Markov chain Monte Carlo techniques, like Hamiltonian Monte Carlo, to sample the amplitudes efficiently.

该方法适用于所有类型的自旋泡沫模型和图，与模型的具体选择 (时空符号、$Y$ 映射等) 无关。该框架可对带较大自旋的自旋泡沫模型中的可观测量进行高效数值计算，能够捕获任意阶的微扰量子修正。框架采用的多链马尔可夫链蒙特卡洛方法可并行运行，且支持 GPU 加速。框架的一个主要问题是向小自旋区域的推广: 我们在计算中忽略了对大自旋来说呈指数小的非微扰修正。与渐近区域不同，在小自旋区域，不止一个最陡下降 thimble 会对配分函数有贡献。这要求我们找出所有与复临界点关联的 thimble 并计算它们的权重。找出所有复临界点非常困难，即使是在单单纯形的情况下，因为临界方程构成了一个含 54 个变量的高阶多项式方程组。该问题的一个可行解决方案是世界体积和全局自适应采样方法 [82]。我们目前正在探索使用这些方法的可能性，且已经得到了一些初步结果 [17]。我们以计算自旋泡沫传播子为例，展示了该框架的性能与效率。其他值得关注的应用包括: 计算宇宙学与黑洞中的几何可观测量、探索连续极限以及重整化群流。同时，我们目前正在改进该框架: 选择更合适的常微分方程求解器，应用不同的马尔可夫链蒙特卡洛技术 (如哈密顿蒙特卡洛) 来高效对振幅采样。

## Cross-References

## 交叉引用

Emergence of Riemannian Quantum Geometry

黎曼量子几何的涌现

Spin Foams, Refinement Limit, and Renormalization

自旋泡沫、精化极限与重整化

Spin Foams: Foundations

自旋泡沫: 基础

Acknowledgments The work of P.D. was made possible through the support of the ID# 61466 and ID# 62312 grants from the John Templeton Foundation, as part of the https://www.templeton.org/grant/the-quantum-information-structure-of-spacetime-qiss-second-phase.The opinions expressed in this work are those of the authors and do not necessarily reflect the views of the John Templeton Foundation. P. D. also personally thanks Francesco Gozzini and Pietropaolo Frisoni for sharing some of the data used in section "Booster Functions and SU(2) Invariants: sl2cfoam." M.H. receives support from the National Science Foundation through grants PHY-1912278 and PHY-2207763 and the sponsorship provided by the Alexander von Humboldt Foundation. M.H. acknowledges IQG at FAU Erlangen-Nürnberg, IGC at Penn State University, and Perimeter Institute for Theoretical Institute for the hospitality during his visits.

致谢 P.D. 的研究工作得益于约翰·邓普顿基金会 ID# 61466 和 ID# 62312 项目资助，项目属于 https://www.templeton.org/grant/the-quantum-information-structure-of-spacetime-qiss-second-phase。本文表达的观点仅代表作者，不一定反映约翰·邓普顿基金会的立场。P.D. 还个人感谢 Francesco Gozzini 和 Pietropaolo Frisoni 分享了“助推函数与 SU(2) 不变量:sl2cfoam”小节所用的部分数据。M.H. 得到美国国家科学基金会 PHY-1912278 和 PHY-2207763 项目资助，以及亚历山大·冯·洪堡基金会资助。M.H. 对来访期间埃尔兰根-纽伦堡大学 IQG、宾夕法尼亚州立大学 IGC 以及圆周理论物理研究所的款待表示感谢。

## References

## 参考文献

1. J. Engle, E. Livine, R. Pereira, C. Rovelli, LQG vertex with finite Immirzi parameter. Nucl. Phys. B799, 136-149 (2008). http://arxiv.org/abs/0711.0146, arXiv:0711.0146

2. L. Freidel, K. Krasnov, A new spinfoam model for 4d gravity. Class. Quant. Grav. 25, 125018 (2008). http://arxiv.org/abs/0708.1595, arXiv:0708.1595

3. C. Rovelli, F. Vidotto, Covariant Loop Quantum Gravity: An Elementary Introduction to Quantum Gravity and Spinfoam Theory. Cambridge Monographs on Mathematical Physics (Cambridge University Press, Cambridge, 2014)

4. A. Perez, The spinfoam approach to quantum gravity. Liv. Rev. Rel. 16, 3 (2013). http://arxiv.org/abs/1205.2019, arXiv:1205.2019

5. P. Dona, G. Sarno, Numerical methods for EPRL spinfoam transition amplitudes and Lorentzian recoupling theory. Gen. Rel. Grav. 50, 127 (2018). http://arxiv.org/abs/1807.03066, arXiv:1807.03066

6. F. Gozzini, A high-performance code for EPRL spinfoam amplitudes. Class. Quant. Grav. 38(22), 225010 (2021). http://arxiv.org/abs/2107.13952, arXiv:2107.13952

7. J.S. Engle, W. Kaminski, J.R. Oliveira, Addendum to EPRL/FK asymptotics and the flatness problem. Class. Quant. Grav. 38, 119401 (2021). http://arxiv.org/abs/2012.14822, arXiv:2012.14822

8. F. Hellmann, W. Kaminski, Geometric asymptotics for spinfoam lattice gauge gravity on arbitrary triangulations. http://arxiv.org/abs/1210.5276, arXiv:1210.5276

9. V. Bonzom, Spinfoam models for quantum gravity from lattice path integrals. Phys. Rev. D 80, 064028 (2009). http://arxiv.org/abs/0905.1501, arXiv:0905.1501

10. C. Perini, Holonomy-flux spinfoam amplitude. http://arxiv.org/abs/1211.4807, arXiv:1211.4807

11. M. Han, Covariant loop quantum gravity, low energy perturbation theory, and Einstein gravity with high curvature UV corrections. Phys.Rev. D89, 124001 (2014). http://arxiv.org/abs/1308.4063, arXiv:1308.4063

12. M. Han, On spinfoam models in large spin regime. Class. Quant. Grav. 31, 015004 (2014). http://arxiv.org/abs/1304.562 arXiv:1304.5627

13. M. Han, Semiclassical analysis of spinfoam model with a small Barbero-Immirzi parameter. Phys. Rev. D88, 044051 (2013). http://arxiv.org/abs/1304.5628, arXiv:1304.5628

14. M. Han, Z. Huang, H. Liu, D. Qu, Numerical computations of next-to-leading order corrections in spinfoam large- $j$ asymptotics. Phys. Rev. D 102(12),124010 (2020). http://arxiv.org/abs/ 2007.01998, arXiv:2007.01998

15. A. Alexandru, G. Basar, P.F. Bedaque, N.C. Warrington, Complex Paths Around the Sign Problem. http://arxiv.org/abs/2007.05436, arXiv:2007.05436

16. M. Han, Z. Huang, H. Liu, D. Qu, Y. Wan, Spinfoam on a Lefschetz thimble: Markov chain Monte Carlo computation of a Lorentzian spinfoam propagator. Phys. Rev. D 103(8), 084026 (2021). http://arxiv.org/abs/2012.11515, arXiv:2012.11515

17. Z. Huang, S. Huang, Y. Wan, A saddle-point finder and its application to the spinfoam model. http://arxiv.org/abs/2206.11874, arXiv:2206.11874

18. S.K. Asante, B. Dittrich, H.M. Haggard, Discrete gravity dynamics from effective spinfoams. Class. Quant. Grav. 38(14), 145023 (2021). http://arxiv.org/abs/2011.14468, arXiv:2011.14468

19. S.K. Asante, B. Dittrich, J. Padua-Arguelles, Effective spinfoam models for Lorentzian quantum gravity. Class. Quant. Grav. 38(19), 195002 (2021). http://arxiv.org/abs/2104.00485, arXiv:2104.00485

20. B. Bahr, S. Steinhaus, Hypercuboidal renormalization in spinfoam quantum gravity. Phys. Rev. D95(12), 126006 (2017). http://arxiv.org/abs/1701.02311, arXiv:1701.02311

21. P. Donà, P. Frisoni, How-to compute EPRL spinfoam amplitudes. Universe 8(4), 208 (2022)

22. A. Perez, The spinfoam approach to quantum gravity. Liv. Rev. Rel. 16, 3 (2013). http://arxiv.org/abs/1205.2019, arXiv:1205.2019

23. E. Bianchi, D. Regoli, C. Rovelli, Face amplitude of spinfoam quantum gravity, Class. Quant. Grav. 27, 185009 (2010). http://arxiv.org/abs/1005.0764, arXiv:1005.0764

24. J. Engle, R. Pereira, Regularization and finiteness of the Lorentzian LQG vertices. Phys. Rev. D79, 084034 (2009). http://arxiv.org/abs/0805.4696, arXiv:0805.4696

25. S. Speziale, Boosting Wigner's NJ-symbols. J. Math. Phys. 58(3), 032501 (2017). http://arxiv.org/abs/1609.01632, arXiv:1609.01632

26. W. Rühl, The Lorentz Group and Harmonic Analysis. Mathematical Physics Monograph Series (W.A. Benjamin, New York, 1970)

27. R.L. Anderson, R. Raczka, M.A. Rashid, P. Winternitz, Clebsch-gordan coefficients for the coupling of sl(2, c) principal-series representations. J. Math. Phys. 11, 1050-1058 (1970)

28. G.A. Kerimov, I.A. Verdiev, Clebsch-Gordan coefficients of the SL(2, c) group. Rept. Math. Phys. 13, 315-326 (1978)

29. P. Dona, M. Fanizza, P. Martin-Dussaud, S. Speziale, Asymptotics of SL(2, C) coherent invariant tensors. http://arxiv.org/abs/2011.13909, arXiv:2011.13909

30. A.P. Yutsis, I.B. Levinson, V.V. Vanagas, Mathematical Apparatus of the Theory of Angular Momentum (Israel Program for Scientific Translation, Jerusalem, Israel, 1962)

31. H.T. Johansson, C. Forssén, Fast and accurate evaluation of wigner $3j, 6j$ , and $9j$ symbols using prime factorization and multiword integer arithmetic. SIAM J. Sci. Comput. 38, A376- A384 (2016)

32. P. Frisoni, F. Gozzini, F. Vidotto, Numerical analysis of the self-energy in covariant loop quantum gravity. Phys. Rev. D 105(10), 106018 (2022). http://arxiv.org/abs/2112.14781, arXiv:2112.14781

33. J.W. Barrett, R. Dowdall, W.J. Fairbairn, F. Hellmann, R. Pereira, Lorentzian spinfoam amplitudes: graphical calculus and asymptotics. Class. Quant. Grav. 27, 165009 (2010). http:// arxiv.org/abs/0907.2440, arXiv:0907.2440

34. M. Han, M. Zhang, Asymptotics of spinfoam amplitude on simplicial manifold: Lorentzian theory. Class. Quant. Grav. 30, 165012 (2013). http://arxiv.org/abs/1109.0499, arXiv:1109.0499

35. P. Donà, M. Fanizza, G. Sarno, S. Speziale, Numerical study of the Lorentzian EPRL spinfoam amplitude. http://arxiv.org/abs/1903.12624, arXiv:1903.12624

36. E.R. Livine, S. Speziale, A new spinfoam vertex for quantum gravity. Phys. Rev. D76, 084028 (2007). http://arxiv.org/abs/0705.0674, arXiv:0705.0674

37. M. Han, Einstein equation from covariant loop quantum gravity in semiclassical continuum limit. Phys. Rev. D96(2), 024047 (2017). http://arxiv.org/abs/1705.09030, arXiv:1705.09030

38. J. Engle, C. Rovelli, The accidental flatness constraint does not mean a wrong classical limit. http://arxiv.org/abs/2111.0
arXiv:2111.03166

39. F. Conrady, L. Freidel, On the semiclassical limit of 4d spinfoam models, Phys.Rev. D78, 104023 (2008). http://arxiv.org/abs/0809.2280, arXiv:0809.2280

40. F. Hellmann, W. Kaminski, Holonomy spinfoam models: asymptotic geometry of the partition function. JHEP 10, 165 (2013). http://arxiv.org/abs/1307.1679, arXiv:1307.1679

41. P. Dona, F. Gozzini, G. Sarno, Numerical analysis of spinfoam dynamics and the flatness problem. http://arxiv.org/abs/2004.12911, arXiv:2004.12911

42. A. Riello, Self-energy of the Lorentzian Engle-Pereira-Rovelli-Livine and Freidel-Krasnov model of quantum gravity. Phys. Rev. D88(2), 024011 (2013). http://arxiv.org/abs/1302.1781, arXiv:1302.1781

43. P. Donà, Infrared divergences in the EPRL-FK SpinFoam model. Class. Quant. Grav. 35(17), 175019 (2018). http://arxiv.org/abs/1803.00835, arXiv:1803.00835

44. P. Donà, P. Frisoni, E. Wilson-Ewing, Radiative corrections to the Lorentzian EPRL spinfoam propagator. http://arxiv.org/abs/2206.14755, arXiv:2206.14755

45. F. Gozzini, F. Vidotto, Primordial fluctuations from quantum gravity. Front. Astron. Space Sci. 7, 629466 (2021). http://arxiv.org/abs/1906.02211, arXiv:1906.02211

46. P. Frisoni, F. Gozzini, F. Vidotto, Markov Chain Monte Carlo methods for graph refinement in covariant Loop Quantum Gravity. http://arxiv.org/abs/2207.02881, arXiv:2207.02881

47. M. Han, Z. Huang, H. Liu, D. Qu, Complex critical points and curved geometries in four-dimensional Lorentzian spinfoam quantum gravity. Phys. Rev. D 106, 044005 (2022). http:// arxiv.org/abs/2110.10670, arXiv:2110.10670

48. F. Conrady, L. Freidel, On the semiclassical limit of 4d spinfoam models. Phys. Rev. D78, 104023 (2008). http://arxiv.org/abs/0809.2280, arXiv:0809.2280

49. M. Han, M. Zhang, Asymptotics of spinfoam amplitude on simplicial manifold: Lorentzian theory. Class. Quant. Grav. 30, 165012 (2013). http://arxiv.org/abs/1109.0499, arXiv:1109.0499

50. M. Han, T. Krajewski, Path integral representation of Lorentzian spinfoam model, asymptotics, and simplicial geometries. Class. Quant. Grav. 31, 015009 (2014). http://arxiv.org/abs/1304.5626, arXiv:1304.5626

51. W. Kaminski, M. Kisielowski, H. Sahlmann, Asymptotic analysis of the EPRL model with timelike tetrahedra. Class. Quant. Grav. 35(13), 135012 (2018). http://arxiv.org/abs/1705.02862, arXiv:1705.02862

52. H. Liu, M. Han, Asymptotic analysis of spinfoam amplitude with timelike triangles. Phys. Rev. D 99(8), 084040 (2019). http://arxiv.org/abs/1810.09042, arXiv:1810.09042

53. J.D. Simão, S. Steinhaus, Asymptotic analysis of spinfoams with time-like faces in a new parameterisation. http://arxiv.org/abs/2106.15635, arXiv:2106.15635

54. P. Dona, S. Speziale, Asymptotics of lowest unitary SL(2, C) invariants on graphs. Phys. Rev. D 102(8), 086016 (2020). http://arxiv.org/abs/2007.09089, arXiv:2007.09089

55. M. Han, On spinfoam models in large spin regime. Class. Quant. Grav. 31, 015004 (2014). http://arxiv.org/abs/1304.562
arXiv:1304.5627

56. A. Melin, J. Sjöstrand, Fourier Integral Operators with Complex-Valued Phase Functions, in Fourier Integral Operators and Partial Differential Equations, ed. by J. Chazarain (Springer, Berlin/Heidelberg, 1975), pp. 120-223

57. L. Hormander, The Analysis of Linear Partial Differential Operators I. (Springer, Berlin, 1983)

58. S.K. Asante, B. Dittrich, H.M. Haggard, Effective spinfoam models for four-dimensional quantum gravity. Phys. Rev. Lett. 125(23), 231301 (2020). http://arxiv.org/abs/2004.07013, arXiv:2004.07013

59. E. Witten, Analytic continuation Of Chern-Simons theory. AMS/IP Stud. Adv. Math. 50, 347- 446 (2011). http://arxiv.org/abs/1001.2933, arXiv:1001.2933

60. L. Scorzato, The Lefschetz thimble and the sign problem. PoS LATTICE2015, 016 (2016). http://arxiv.org/abs/1512.080
arXiv:1512.08039

61. P.F. Bedaque, A complex path around the sign problem. EPJ Web Conf. 175, 01020 (2018). http://arxiv.org/abs/1711.058
arXiv:1711.05868

62. S. Bluecher, J.M. Pawlowski, M. Scherzer, M. Schlosser, I.-O. Stamatescu, S. Syrkowski, F.P. Ziegler, Reweighting Lefschetz Thimbles. Sci. Post Phys. 5(5), 044 (2018). http://arxiv.org/ abs/1803.08418, arXiv:1803.08418

63. A. Alexandru, G. Basar, P.F. Bedaque, G.W. Ridgway, N.C. Warrington, Sign problem and Monte Carlo calculations beyond Lefschetz thimbles. JHEP, 05, 053 (2016). http://arxiv.org/ abs/1512.08764, arXiv:1512.08764

64. A. Alexandru, G. Basar, P. Bedaque, Monte Carlo algorithm for simulating fermions on Lefschetz thimbles. Phys. Rev. D 93(1), 014504 (2016). http://arxiv.org/abs/1510.03258, arXiv:1510.03258

65. T. Takagi, On an algebraic problem reluted to an analytic theorem of Carathéodory and Fejér and on an allied theorem of Landau. Japanese J. Math.: Trans. Abstr. 1, 83-93 (1924)

66. M. Han, H. Liu, Analytic Continuation of SpinFoam Models. Phys. Rev. D 105, 024012 (2020). https://doi.org/10.1103/PhysRevD.105.024012

67. E. Witten, A New Look At The Path Integral Of Quantum Mechanics. http://arxiv.org/abs/1009.6032, arXiv:1009.6032

68. AuroraScience Collaboration, M. Cristoforetti, F. Di Renzo, L. Scorzato, New approach to the sign problem in quantum field theories: high density QCD on a Lefschetz thimble. Phys. Rev. D86, 074506 (2012). http://arxiv.org/abs/1205.3996, arXiv:1205.3996

69. H.M. Haggard, M. Han, W. Kamiński, A. Riello, Four-dimensional quantum gravity with a cosmological constant from three-dimensional holomorphic blocks. Phys. Lett. B752, 258- 262 (2016). http://arxiv.org/abs/1509.00458, arXiv:1509.00458

70. H.M. Haggard, M. Han, W. Kaminski, A. Riello, SL(2, C) Chern-Simons theory, flat connections, and four-dimensional quantum geometry. http://arxiv.org/abs/1512.07690, arXiv:1512.07690

71. M. Han, 4d quantum geometry from 3d supersymmetric gauge theory and holomorphic block. JHEP 01, 065 (2016). http://arxiv.org/abs/1509.00466, arXiv:1509.00466

72. C. Rovelli, Graviton propagator from background-independent quantum gravity. Phys. Rev. Lett. 97, 151301 (2006). http://arxiv.org/abs/gr-qc/0508124, gr-qc/0508124

73. E. Bianchi, L. Modesto, C. Rovelli, S. Speziale, Graviton propagator in loop quantum gravity. Class. Quant. Grav. 23, 6989-7028 (2006). http://arxiv.org/abs/gr-qc/0604044, gr-qc/0604044

74. E. Bianchi, E. Magliaro, C. Perini, LQG propagator from the new spin foams. Nucl. Phys. B822, 245-269 (2009). http://arxiv.org/abs/0905.4082, arXiv:0905.4082

75. E. Bianchi, Y. Ding, Lorentzian spinfoam propagator. Phys. Rev. D86, 104040 (2012). http://arxiv.org/abs/1109.6538, arXiv:1109.6538

76. J.A. Vrugt, Markov chain monte carlo simulation using the dream software package: theory, concepts, and matlab implementation. Environ. Model. Softw. 75, 273-316 (2016)

77. H. Liu. https://github.com/LQG-Florida-Atlantic-University/spinfoam-propagator

78. H. Zichang, Spinfoam propagator code. October, 2020. https://gitee.com/ZCHuang1126/ spinfoam-propagator.git,

79. A. Banburski, L.-Q. Chen, L. Freidel, J. Hnybida, Pachner moves in a 4d Riemannian holomorphic SpinFoam model. http://arxiv.org/abs/1412.8247, arXiv:1412.8247

80. B. Bahr, S. Steinhaus, Numerical evidence for a phase transition in 4d spinfoam quantum gravity. Phys. Rev. Lett. 117(14), 141302 (2016). http://arxiv.org/abs/1605.07649, arXiv:1605.07649

81. C. Delcamp, B. Dittrich, Towards a phase diagram for spinfoams. http://arxiv.org/abs/1612.04506, arXiv:1612.04506

82. M. Fukuma, N. Matsumoto, Worldvolume Approach to the Tempered Lefschetz Thimble Method. Progress of Theoretical and Experimental Physics. 2021(2) (2021). https://doi.org/ 10.1093/ptep/ptab010